DOCTORATE THESIS

# Fluctuating superconductivity and pair-density wave order in the cuprate superconductors

JONATAN WÅRDH

Department of Physics
University of Gothenburg
Göteborg, Sweden 2020

*Fluctuating superconductivity and pair-density wave order in the cuprate superconductors*
Jonatan Wårdh

ISBN 978-91-7833-936-5 (PRINT)
ISBN 978-91-7833-937-2 (PDF)

This thesis is electronically published, available at
http://hdl.handle.net/2077/64092
Department of Physics
University of Gothenburg
SE-412 96 Göteborg
Sweden
Telephone: +46 (0)31-786 00 00

Front cover: A suggestive phase diagram based on the PDW instability discussed in this thesis. The pseudogap is imagined to consist of a fluctuating PDW state with possible vestigial orders, including loop-current (LC) and nematic order. Above the transition temperature on the underdoped side, we expect to find anisotropic fluctuations.

Printed by Stema specialtryck AB
Göteborg, Sweden 2020

# ABSTRACT

High-temperature superconductors are some of nature's most enigmatic materials. Besides carrying a supercurrent, these materials manifest a range of electronic and structural orders. A state of modulated superconductivity, called a pair-density wave (PDW), has been suggested to occur in copper-based (cuprate) high-temperature superconductors, with the possibility of explaining these various orders, and perhaps even superconductivity itself. This thesis is based upon four appended papers and concerns the nature of the PDW state and the cuprate superconductors.

In the first two papers, we consider a so-called pair-hopping interaction that can stabilize a (mean-field) PDW state. In the first paper, we use this interaction to study the supercurrent carried by a PDW state, which, due to it being a multiple-component order, can lead to phase-separation and additional symmetry breaking. In the second paper, we study the competition between a PDW state and an ordinary uniform superconducting state in the context of a BCS-BEC crossover. We find a suppressed superfluid stiffness in the vicinity of a PDW instability, with implications on the nature of the underdoped cuprates.

The third paper includes an experimental study on thin films of $La_{2-x}Sr_xCuO_4$, which above $T_c$ develops a highly anisotropic resistive response, especially pronounced for underdoped samples, pointing towards an exotic pseudogap phase in the underdoped cuprates with quasi-1D phase superfluid stiffness. We interpret these results in terms of nematic order manifested in the superconducting fluctuations. In the last paper of this thesis, we consider a scenario where the cuprate pseudogap phase consists of a thermally disorder PDW state with vestigial order. We show that a vestigial PDW nematic order coexisting with a uniform superconducting order yields an anisotropic superconductor on a form consistent with the fluctuations seen in $La_{2-x}Sr_xCuO_4$.

Finally, in addition to providing background for the appended papers, this thesis contains an introduction to the general phenomenology of the cuprate superconductors.

# SAMMANFATTNING

Högtemperatursupraledare är några av naturens mest gåtfulla material. Förutom att leda en superström så uppvisar dessa material en rad olika elektroniska och strukturella ordningar. En så kallad pardensitetsvåg (PDW), ett tillstånd av modulerad supraledning, har föreslagits som en möjlig förklaring till olika observerade ordningar i kopparbaserade supraledare (kallade kuprater). Denna avhandling är baserad på fyra artiklar som behandlar olika aspekter av ett PDW-tillstånd, samt dess möjliga förekomst i kuprater.

I de två första artiklarna betraktas en parhoppningsinteraktion som kan stabilisera ett PDW-tillstånd. I första artikeln används denna växelverkan till att studera hur en superström leds i ett PDW-tillstånd. På grund av tillståndets flerkomponentskaraktär så kan en ström ge upphov till fasseparation, samt ytterligare symmetribrott. I den andra artikeln avhandlas tävlan mellan ett PDW-tillstånd och ett homogent supraledande tillstånd. I närheten av en PDW-instabilitet så undertrycks den supraledande fasstyvheten. Detta medför en ny möjlig tolkning av den enigmatiska underdopade delen av kupratfasdiagrammet.

Den tredje artikeln innefattar en experimentell studie av $La_{2-x}Sr_xCuO_4$ som över $T_c$ uppvisar en högst anisotrop resistivitet. Denna anisotropi är mest framträdande i underdopade kuprater vilket tyder på en exotisk pseudogap-fas. Dessa resultat tolkas i termer av en nematisk ordning i de supraledande fluktuationerna. I avhandlingens fjärde och sista artikeln betraktas ett scenario där pseudogap-fasen består av ett termiskt oordnat PDW-tillstånd. Detta tillstånd kan uppvisa en rudimentär ordning med brutna kristallsymmetrier, trots avsaknad av supraledande ordning. Det visar sig att en rudimentär nematisk PDW-ordning som samexisterar med en homogen supraledande ordning kan ge upphov till den typ av anisotropt supraledande tillstånd som observerats i $La_{2-x}Sr_xCuO_4$.

Denna avhandling innehåller, förutom bakgrund till de bifogade artiklarna, även en introduktion till kopparbaserade högtemperatursupraledare.

## List of papers

This thesis is based on four appended papers:

### Paper A

Wårdh, J. & Granath, M. 2017 Effective model for a supercurrent in a pair-density wave *Physical Review B* **96**, 224503.

### Paper B

Wårdh, J., Andersen, B.M. & Granath, M. 2018 Suppression of superfluid stiffness near a Lifshitz-point instability to finite-momentum superconductivity *Physical Review B* **98**, 224501.

### Paper C

Wårdh, J., Granath, M., Wu, J., Bolliinger, A.T., He, Xi. & Božović, I. 2020 Nematic superconducting phase fluctuations in a copper oxide *Under review*

### Paper D

Wårdh, J. & Granath, M. 2020 Nematic single-component superconductivity and loop-current order from pair-density wave instability *Manuscript, to be submitted, pending review process of paper C*

## My contribution

I performed all calculations, simulations, and the analysis contained in Paper A-D, with the aid of my supervisor Mats Granath (MG). The work contained in Paper B was done in collaboration with Brian Møller Andersen (BA). The experimental work contained in Paper C was done by Ivan Božović's (IB) group at Brookhaven National Laboratory, which I did not take part in; all data-processing was, however, done by me. The written work in Paper A, B, and D was done by me together with MG, and BA in Paper B. The written work of Paper C, was a joint effort of me, MG and IB.

# ACKNOWLEDGEMENTS

First and foremost, I would like to thank my supervisor Mats Granath who has guided me through these years. For the endless hours of discussion and numerous messages, I am forever indebted.

Of particular importance for this work is Ivan Božović and co-workers at Brookhaven National Laboratory, to whom I am thoroughly grateful. I would also like to thank Brian Møller Andersen for the time I spend at Niels Bohr Institute and for his collaboration.

I thank my office mates Oleksandr, Lorenzo, and Yoran, who made the working days much more enjoyable. A special thanks to my friend and semi colleague Magnus, who took the time proof-reading the thesis. Still, I assume full responsibility for all remaining typos.

Finally, a shout-out to family and friends who I expect, in particular, will enjoy this thesis.

“So it begins”
- Gandalf
*Lord of the Rings*

# CONTENTS

# PART I
# INTRODUCTION

A system consisting of a large number of particles can not simply be understood from studying its single-particle components. Instead, the manifested phenomena are typically emergent from the vast number of degrees of freedoms in a way that is fundamentally different from any microscopic description of its constituents. In the words of P. W. Anderson, "More is different" [1]. Perhaps one of the most enchanting emergent phenomena of a many-body system is the superconducting state where a persistent flow, or current, can exist without decay. It is safe to say that the understanding of superconductivity in conventional metals is one of the greatest achievements of modern physics. Nevertheless, ever since the discovery of high-temperature superconductivity in $La_{2-x}Ba_xCuO_4$ [2] in 1986, the general understanding of superconductivity has remained one of the most daunting problems in physics to this date.

In this thesis, we are interested in ceramic compounds based on layers of oxygen and copper, so-called cuprates. These materials have turned out to be a monumental challenge for the theoretician. Not only are cuprates strongly coupled, manifested by superconductivity developing from a correlated insulator, but they also show a range of different orders. Best demonstrating this diversity is the complexity of the cuprate phase diagram, including (but not limited to) charge and spin-order, as well as electronic nematic orders. A cornerstone in the phase diagram is the pseudogap phase, a mysterious phase which seems to correlate with the onset of various electronic orders and unique spectroscopic features.

It is not well understood to what extent superconductivity in cuprates is dependent on the various other phases and orders present [3, 4, 5, 6, 7, 8]. Thus, it is perhaps not surprising that the general problem about the nature of high-temperature superconductivity still, even after more than 30 years after its discovery, remains largely an open problem.

## 1.1 What is this thesis about?

One major question about the cuprate superconductor is the nature of the pseudogap state and its relation to different electronic orders, including superconductivity. An exciting possibility is that of a parent state with the possibility of setting up subleading orders through partial melting and disordering, generally referred to as vestigial orders. A suggestion for such a "mother state" is a state with a spatially modulated superconducting order around a mean of zero, called a pair-density wave (PDW) state [9, 10, 11, 12]. Originally in the context of cuprates, PDW was suggested to account for the anomalous suppression of superconductivity at $x = 1/8$ doping in $La_{2-x}Ba_xCuO_4$ [13, 6, 14, 11]. However, recently there have been more direct experimental findings [15, 16], and the relevance of the PDW state has become more apparent.

This thesis will focus on questions concerning the nature of the suggested PDW state. We consider the stability of a PDW state, and its competition with a homogeneous superconducting state, from a specific form of interaction, coined a pair-hopping interaction. Also, we consider the superconducting properties of a PDW state through the study of the supercurrent.

Regardless of microscopic origin, quite a lot can be said about a PDW order, as well as other orders, using phenomenological Ginzburg-Landau theories. Such models have been used extensively in the study of the phenomenology of electronic orders in the cuprate system [17, 18, 19, 20, 21, 22]. Specific implications of an underlying PDW state has also been explored in some detail [17, 18, 19]. This thesis continues the exploration of the PDW as a possible "mother state" of the cuprate system. Specifically, we consider a PDW with broken time-reversal symmetry with the possibility of setting up magnetoelectric (ME) loop-current (LC) orders, as well as nematic orders, suggested to occur in cuprates. These theories are extended to include a homogeneous superconducting order, showing the emergence of an effectively anisotropic superconductor in the presence of vestigial nematic PDW order. Included in this thesis is a study on thin films of $La_{2-x}Sr_xCuO_4$, which develops a transverse resistivity [23] consistent with an electronic nematic order of the form described by the above-mentioned effective anisotropic superconducting action.

## 1.2 Structure of the thesis

The main work of this thesis is contained in four appended papers A-D. The body of the thesis aims to provide a background to, commenting on, and developing some of the ideas presented in the papers further.

The thesis is divided into five parts. Part I gives an introduction to some of the basic aspects of superconductivity in general, as well as cuprate superconductors in particular. Part II contains the main body of the thesis and includes both theoretical background and considerations of the work in the appended papers. Part III contains an outlook and conclusions of the presented work. Part IV contains an Appendix with additional, more technical notes in order to unburden the main text. Finally, Part V contains the appended papers.

# 2 Superconductivity

Being the first to liquefy Helium successfully, Kamerlingh Onnes observed that below 4.2 K mercury transitions into a state where electricity flows without any resistance [24]. This was the discovery of superconductivity and the starting point for one of the most significant scientific inquires ever undertaken, which continues to this very day. Following Onnes pioneering work was the discovery of the Meissner effect, where a magnetic field gets expelled from a superconductor [25], an effect later explained by London who suggested that the quantum mechanical many-body wave-function of the superconducting state somehow acquire a rigidity against an applied field [26]. In 1957, 46 years later than the original discovery, Bardeen, Cooper, and Schrieffer (BCS) finally put forward a successful microscopic theory of superconductivity [27].

In 1986 superconductivity was discovered in the cuprate $La_{2-x}Ba_xCuO_4$ (LBCO) [2] with a substantially higher transition temperature, of 35 K, than the old "conventional" superconducting metals. This discovery of high-temperature superconductivity (HTC) marked a new era in condensed matter physics and since then numerous other compounds with even higher transition temperatures have been discovered (e.g. $HgBa_2Ca_2Cu_3O_8$ with $T_c = 134\,\mathrm{K}$ [28]). These compounds have proven to be immensely hard to understand theoretically. Even though the basic features of the superconducting state can be classified in terms of a Bardeen Cooper Schrieffer (BCS) type ground state, there is, unlike for conventional metals, no successful theory able to describe the cause of superconductivity or to predict the transition temperature in these materials.

## 2.1 The superconducting state

The basic idea of a superconducting state is to consider the emergence of a macroscopic wave function, describing a condensate, the superconducting entity of a superconductor. This idea dates back to London [26] and was put forth in a more complete form by Ginzburg and Landau [29] who considered a free energy-functional of a complex-valued superconducting order

parameter, $\Delta$, in the presence of a magnetic field $\mathbf{B} = \nabla \times \mathbf{A}$

$$F = F_N + \int_{\mathbf{x}} \frac{1}{2m^*}|(-i\hbar\nabla - e^*\mathbf{A})\Delta(\mathbf{x})|^2 + r|\Delta(\mathbf{x})|^2 + \frac{u}{2}|\Delta(\mathbf{x})|^4 + \frac{B^2}{2\mu_0}, \quad (2.1)$$

here with gauge field $\mathbf{A}$, mass $m^*$, charge $e^*$, and the normal state free energy $F_N$. The parameter $r$ is a function of temperature, $r = r_0(T - T_c)$, and $u > 0$ describes a repulsive interaction[1]. For $T > T_c$ the free energy (2.1) is minimized by a zero superconducting order parameter, $\Delta = 0$, describing the normal, non-superconducting state. For $T < T_c$, $r < 0$, the free energy minimum is given by a finite (uniform) superconducting order, $\Delta = \Delta_0 e^{i\phi}$, $\Delta_0 = \frac{|r|}{u}$ where $\phi$ is an arbitrary phase, signaling broken $U(1)$ gauge symmetry. The current is found[2] by minimizing (2.1) with regard to $\mathbf{A}$

$$\mathbf{J} = \frac{e^*\hbar}{m^*}|\Delta_0|^2(\nabla\phi - \frac{e^*}{\hbar}\mathbf{A}). \quad (2.2)$$

Thus, a finite expectation values of the superconducting order, $\Delta_0 \neq 0$, implies a supercurrent on the form considered by London.

The microscopic realization of a condensate is in principle given by a Bose-Einstein condensate, which describes the macroscopic occupation of the lowest energy state of bosonic particles. In order to get electrons, which are fermions, to condense they have to pair-up into a bosonic entity. BCS theory was founded on the realization by Cooper that a pair of electrons, subsequently called a Cooper pair, will form a bound state on top of a filled Fermi sea for an *arbitrarily weak* electron-electron attraction [30]. By adding more Cooper pairs the Fermi surface (FS) gets destabilized. The BCS ground state can be considered a coherent state of such bound states $|GS\rangle = e^{\hat{\lambda}^\dagger}|0\rangle$ where $\hat{\lambda}^\dagger = \int_{\mathbf{r},\mathbf{r}'} \Phi(\mathbf{r},\mathbf{r}')\hat{\psi}^\dagger_\uparrow(\mathbf{r})\hat{\psi}^\dagger_\downarrow(\mathbf{r}')$, with $\Phi(\mathbf{r},\mathbf{r}')$ being the Cooper pair-wave function [31]. This state acquire an anomalous expectation value

$$\langle GS|\hat{\psi}_\uparrow(\mathbf{r})\hat{\psi}_\downarrow(\mathbf{r}')|GS\rangle \propto \Phi(\mathbf{r},\mathbf{r}'), \quad (2.3)$$

[1] We will use the notation $\int_{\mathbf{x}} = \int \mathrm{d}^d\mathbf{x}$, where $d$ is the spatial dimension. Henceforth we will set the reduced Planck's and Boltzmann's constant to one, $\hbar = k_B = 1$. For other conventions, see Appendix A.

[2] The current is identified from the Ampère-Maxwell formula $\mu_0\mathbf{J} = \nabla \times \mathbf{B}$. The contribution to the current from $F_N$ is not included in (2.2).

and we identify the coherent state of paired-up electrons with the development of the phenomenological condensate $\Delta \sim \Phi$. Dropping conversion factors, we write the condensate order parameter as a $2e$ charged field

$$\Delta(\mathbf{r},\mathbf{r}') = \langle \hat{\psi}_\uparrow(\mathbf{r})\hat{\psi}_\downarrow(\mathbf{r}')\rangle = f(\mathbf{r}-\mathbf{r}')\Delta(\mathbf{R}) \tag{2.4}$$

where $\mathbf{R} = \frac{\mathbf{r}+\mathbf{r}'}{2}$ is the center of mass coordinate and $f(\mathbf{r}-\mathbf{r}')$ the symmetry function describing the relative coordinate of the electrons. Here we have assumed that the Cooper pairs form a singlet state, pairing one spin up and one spin down electron. Since fermions are antisymmetric under exchange $f(\mathbf{r}-\mathbf{r}')$ must be an even function[3]. Conventional superconductors have an s-wave symmetry function, meaning that the wave function is even under a 90 degree rotation. Unconventional superconductors, like cuprates, are d-wave, with an order parameter that changes sign under 90 degree rotation. After Fourier transforming (2.4) into momentum space we find

$$\langle \hat{c}_{\uparrow,\mathbf{k}+\mathbf{Q}/2}\hat{c}_{\downarrow,-\mathbf{k}+\mathbf{Q}/2}\rangle = f(\mathbf{k})\Delta_{\mathbf{Q}}\,. \tag{2.5}$$

Ordinary BCS theory considers a uniform condensate $\mathbf{Q} = 0$, where electrons of opposite momenta pair together. But in general, we can expand $\Delta(\mathbf{R})$ into a series of modes

$$\Delta(\mathbf{R}) = \Delta_0 + \Delta_{\mathbf{Q}}e^{i\mathbf{Q}\cdot\mathbf{R}} + \Delta_{-\mathbf{Q}}e^{-i\mathbf{Q}\cdot\mathbf{R}} + ... \tag{2.6}$$

with $\Delta_0 \neq 0, \Delta_{\pm\mathbf{Q}} = 0...$ being the ordinary homogeneous superconductor. In this work, we are interested in exploring the consequences and the signatures of a superconducting state with finite-momentum modes.

### 2.1.1 Type I and II superconductors

From the Ginzburg-Landau (GL) theory (2.1) two length scales can be formed, the correlation length, and the penetration depth

$$\xi = \sqrt{\frac{\hbar^2}{2m^*|r|}} = \xi_0\left(1-\frac{T}{T_c}\right)^{-1/2}, \quad \lambda = \sqrt{\frac{m^*}{(e^*)^2|\Delta_0|^2\mu}}. \tag{2.7}$$

[3]A singlet state is odd under spin exchange $|\uparrow\rangle|\downarrow\rangle - |\downarrow\rangle|\uparrow\rangle$, while a triplet state form a multicomponent order parameter that is symmetric under spin exchange $|\uparrow\rangle|\uparrow\rangle, |\uparrow\rangle|\downarrow\rangle + |\downarrow\rangle|\uparrow\rangle, |\downarrow\rangle|\downarrow\rangle$.

Here $\xi_0$ is the coherence length, $e^* = 2e$, and $m^*$ the effective pair mass[4]. The correlation length sets the length over which the condensate is anticipated to vary, while the penetration depth sets the scale for electromagnetic variation. The relative size of these length-scales implies two important kinds of superconductors, type I for $\xi \gtrsim \lambda$ and type II for $\lambda \gtrsim \xi$. In the presence of a strong enough magnetic field, it is energetically favorable for a type II superconductor to let the magnetic field penetrate in the form of vortices. This defines the lower critical field $B_{c1}$, where the Meissner state[5] is destroyed. However, the superconducting state is first destroyed at the upper critical field $B_{c2}$. For a type I superconductor, such vortex penetration is unfavorable, and there is only one critical field strength given by the destruction of the condensate.

## 2.2 Homogeneous and finite-momentum superconductivity, the FFLO/PDW-state

Perhaps the biggest surprise about the BCS theory is that it predicts a weak-coupling instability of the Fermi surface (FS). For any finite attraction, the Fermi sea will succumb to a BCS ground state at low enough temperatures; this is the essence of the Cooper instability. This instability can be seen as a result of pairing up electrons with opposite momenta and spin such that the FS is perfectly nested, yielding a divergent susceptibility (see section 6.2). Therefore, a state of finite-momentum superconducting, which will not nest the FS, is expected to be unfavorable compared to the zero-momentum state. This is the basic reason why ordinary BCS theory only considers the zero momentum mode in (2.6).

Nevertheless, in the presence of a time-reversal breaking magnetic (Zeeman) field, the spin up and down FSs are split, and the perfect nesting is destroyed regardless of the momentum of the order parameter. It was realized more or less simultaneously by Fulde, Ferrell [33], and Larkin, Ovchinnikov [34] that in this case, a finite-momentum condensate would better match the two FSs (see Figure 2.1). Fulde-Ferrell and Larkin-Ovchinnikov considered two different versions of the jointly called FFLO state: The Larkin-Ovchinnikov (LO) state [34], having two pair-fields $\Delta_{\mathbf{Q}} = \Delta_{-\mathbf{Q}}$, such that $\Delta(\mathbf{R}) = 2\Delta_{\mathbf{Q}} \cos(\mathbf{Q}\cdot\mathbf{R})$, breaking translational symmetry while preserving time-

[4] For the GL free energy functional the normalization of effective mass is arbitrary [32].

[5] The state where a magnetic field is fully repelled out of the superconductor.

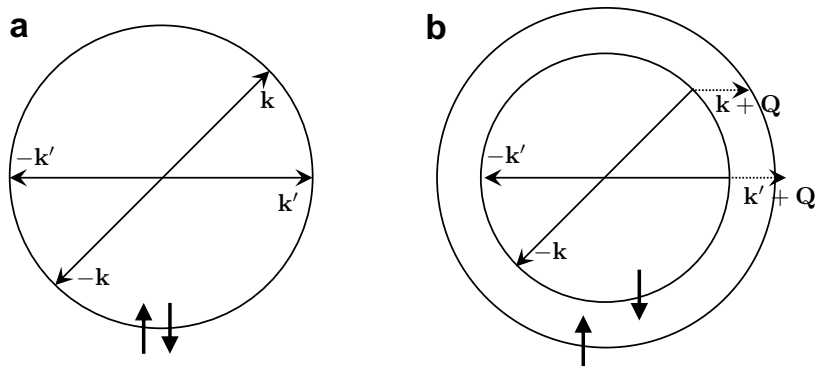


**Figure 2.1:** Nesting of a spherical Fermi surface (FS). **a** For an equal spin-up and spin-down occupation, a zero momenta condensate, $\mathbf{Q} = 0$, perfectly nests the two FSs. **b** For an unequal spin-up and spin-down occupation, the perfect nesting is inevitably lost. However, a finite $\mathbf{Q} \neq 0$ leads to a better match.

reversal, and the Fulde-Ferrell (FF) state [33], with one pair-field $\Delta_{-\mathbf{Q}} = 0$, such that $\Delta(\mathbf{R}) = \Delta_{\mathbf{Q}} e^{i\mathbf{Q}\cdot\mathbf{R}}$, breaking time-reversal and parity but preserving translational invariance.

A similar state of finite-momentum superconductivity is suggested to appear cuprates (see Section 3.4.1). Here there is no explicit time-reversal symmetry breaking with an unbalanced population of spins, so the mechanism is not that of the FFLO state. Instead, for cuprates, the finite-momentum superconducting state is referred to as a pair-density wave (PDW). However, it is convenient to use the notation FF and LO to refer to the different possible symmetries of the state. Since a PDW state does not result from a weak-coupling instability, it makes sense to assume that both homogeneous and modulated superconducting orders are admissible in a strongly-coupled system. This motivates the study of the PDW state as a part of the general phenomenology of a strongly-coupled superconductor.

# 3 Cuprate superconductors

The BCS theory has proven successful in describing the superconducting state of a conventional superconductor, a pure metals with a Fermi liquid normal state. The source of attraction in metals is due to phonons, in the form

of the Bardeen-Pines effective interaction [35]. This attraction overcomes the (instantaneous) Coulomb repulsion by being heavily retarded; the electron leaves a distortion in the underlying crystal, which attracts another electron at later times. However, in principle, any attraction can be set-up within the BCS framework.

Several key features distinguishing the cuprates from the conventional superconductors were realized shortly after their discovery [36, 37]. The cuprates are quasi-two-dimensional, made up of $CuO_2$ planes with weak inter-planar coupling, and the interaction between electrons is not believed to be phonon mediated. But, establishing the source of attraction only solves half the problem (or less) of cuprate superconductivity. The BCS theory is based on the assumption of weak interaction, while cuprates show strongly-coupled behavior and large fluctuations. Thus, there are many reasons to believe that the BCS framework is inherently inapt for describing the superconductivity of cuprates. However, BCS theory might still provide some valuable insights.

## 3.1 The cuprate compound

Of particular importance for this work and serving as a generic cuprate, we consider the lanthanum (La) based compounds with the chemical composition $La_2CuO_4$ in its un-doped form (see Figure 3.1**a**). The electrons are distributed into $La^{3+}$, $Cu^{2+}$ and $O^{2-}$ ions. Other cuprate families do differ in the specific structure, but they all share the $CuO_2$ planes where superconductivity is believed to emerge [38, 39]. Electrons in the $CuO_2$ layers belongs to the 3d orbitals of $Cu^{2+}$ and 2p orbitals of $O^{2-}$. Modeling of cuprates often focuses on these layers alone, with only a small inter-plane coupling. In the simplest, one-band model, one could consider hopping between localized d orbitals of the $Cu^{2+}$ ions. Band-theory predicts metallic behavior, with one electron per site (half-filling). However, in order to conduct current, two electrons must be able to reside on the same site. Due to strong on-site Coulomb repulsion, $U$, an insulating (correlation) gap opens up in the d-band, and the system becomes insulating. A well-studied model describing this is the Hubbard model [40]. The Hubbard model is hypothesized to capture the basic physics of HTC compounds in general, and cuprates in particular. At half-filling, even though pairs cannot reside on the same site, a virtual ex-

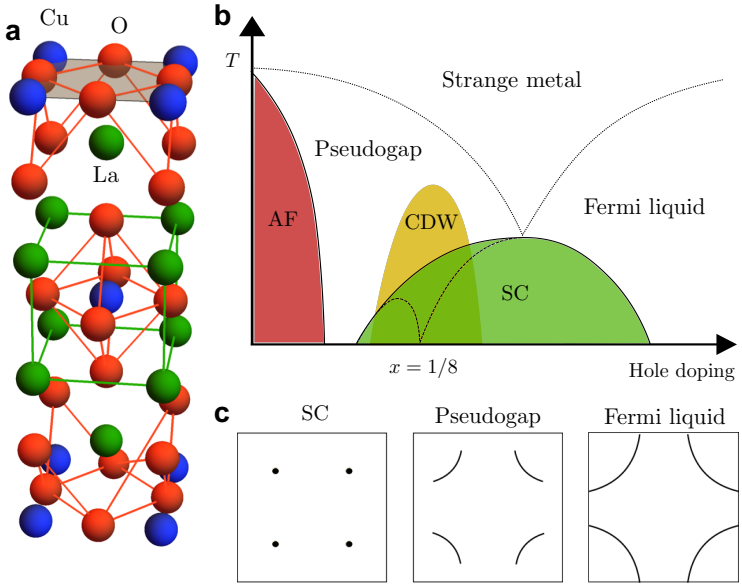


**Figure 3.1:** **a** Crystal structure of the cuprate parent compound $La_2CuO_4$ with La (green), Cu (blue) and O (red). One $CuO_2$ plane is marked in gray. **b** A conceptual phase diagram of the cuprate-family with anti-ferromagnetic (AF), charge-density wave (CDW), and superconducting (SC) order. The dashed line in the SC dome corresponds to the enhanced suppression at $x = 1/8$ observed in LBCO. **c** Schematic Fermi surface in different states of the cuprate phase diagram.

change, called super-exchange, between neighboring sites is allowed [41]. Super-exchange leads to an effective coupling between neighboring spins $J = 4t^2/U$ (where $t$ is the hopping parameter). The exchange favors an anti-ferromagnetic (AF) ground state, a state which is indeed observed in all cuprates. In order for a cuprate to become superconducting, it has to be chemically doped away from half-filling. Substituting La with, for instance, Sr, which has two valence electrons instead of three, introduces a hole in the copper-oxide layer [39]. Away from half-filling, including hopping, yields the well-studied $t-J$ model, which can be considered a low energy effective model of the Hubbard model [42].

Early after the discovery of superconductivity in cuprates, Anderson [37] put forward a quite compelling theory of superconductivity based on the

emergence of superconductivity from a Mott insulator. The idea, known as resonating valence bond (RVB), is that the ground state is a superposition of states where neighboring pairs forms a singlet similar to the Cooper pair. When moving away from half-filling, these pairs should be able to move, and superconductivity would emerge. This state would constitute a spin liquid. However, after investigations by, e.g., neutron spectroscopy, a commensurate AF (Néel order) pattern was observed even for finite doping [36]. This state has gapless spin excitations not consistent with the RVB scenario. Nevertheless, pairing from local singlet correlations in a more general sense is considered as a possible pairing mechanism [3].

## 3.2 Phase diagram

The complicated nature of the cuprates is perhaps best described by its phase diagram as a function of temperature and doping (see Figure 3.1**b**). At zero doping, we have a correlated insulator with AF order, which gets gradually suppressed as doping increases and eventually substituted for the superconducting (SC) "dome". Overarching these two phases is the enigmatic *pseduogap* phase, ending near the optimum doped superconductor state (the state with maximum $T_c$). On the underdoped side of the superconducting dome, the pseudogap constitutes the normal state of the superconductor. At the same time, at higher doping, it is believed to be Fermi liquid like[1]. Fanning out between the pseudogap and Fermi liquid is the strange metal phase with linear in temperature resistivity, $\rho \propto T$ [44, 45].

The defining feature of the pseudogap is its incomplete FS, which is gapped at the anti-nodal point but with so-called Fermi arcs present at the nodal points (see Figure 3.1**c**). This structure remains at temperatures significantly higher than the superconducting transition temperature. The nature of the pseudogap is highly debated [3], and since it constitutes the phase from which superconductivity emerges, it is essential for understanding the cuprate superconductivity itself. For instance, the incomplete FS implies deviation from Fermi liquid theory upon which BCS theory is based. Additionally, the pseudogap phase contains a range of anomalous correlations and signs of broken symmetries [44], including charge- and spin-density

[1] There is, however, evidence that even overdoped cuprates show signs of non-Fermi liquid like behavior [43].

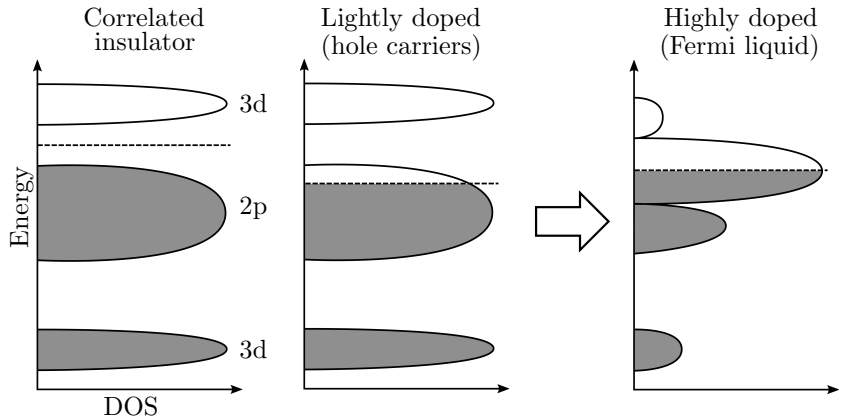


**Figure 3.2:** Development of the effective band structure when increasing doping. Adapted from [53]. The dashed line indicate the Fermi level.

waves [3], time-reversal breaking [46], diamagnetic response [47], nematic order [48, 49, 23] and quantum oscillations [50, 51]. It seems evident that the inter-dependency between these electronic orders and superconductivity is essential to sort out [52, 49].

## 3.3 Band structure, Fermi surface and pseudogap

A complementary view to the phase diagram is the evolution of the band structure, and FS as doping is increased. It turns out that the insulation gap of the $CuO_2$ planes is not directly associated with a $d_i^n d_j^n \rightarrow d_i^{n-1} d_j^{n+1}$ excitation of the Cu-atoms ($i$, $j$ are neighboring sites, $n$ the electron occupation), suggested by the one-band Hubbard model. Instead, the p bands of the oxygen ions will reside within the gap [53] (see Figure 3.2). The gap should therefore be considered a charge-transfer gap [54], associated with the $d_i^n p_k^n \rightarrow d_i^{n+1} p_k^{n-1}$ excitation between neighboring O and Cu ($k$ a neighboring bond)[2].

At zero doping, the Fermi level lies in the correlated gap, moving down into

[2]Accounting for the hybridization of the p and d orbitals is referred to as the p-d model, or Emery model [55]. To justify taking only the Cu-site into account, as is done in the Hubbard model, when it is rather the O-sites that contribute with a hole [56, 57], one can consider the formation of a bound state with the $Cu^{2+}$ site, known as a Zhang-Rice singlet [58].

the p-band for finite doping. We expect that the numbers of hole carriers equal the chemical doping $p = x$, a picture which agrees with transport measurements of Hall conductivity [59] (see also [38] and references therein) for underdoped samples. However, for overdoped samples we eventually end up at a Fermi liquid like metal [53] with $n \sim 1-x$. This implies a quite complex development of the spectral weight, including a vanishing correlated gap, which is mirrored in the evolution of the FS.

Starting in the superconducting state, the order parameter is known to have d-wave symmetry [60], $\Delta(\mathbf{k}) = \Delta_0(\cos(a\,k_x) + \cos(a\,k_y))$ (where $\mathbf{k}$ is the relative momenta of Cooper pairs and $a$ the lattice spacing) with a superconducting gap closing at the four nodal points of the FS (see Figure 3.1**c**). Raising the temperature on the overdoped side, we end up in a Fermi liquid state with a closed FS. However, on the underdoped side, after raising the temperature, we end up in the pseudogap phase with only a partial FS, which remains gapped at the anti-nodal points but with Fermi arcs left at the nodal points. Again, we see that the pseudogap is key to understanding the evolution of a correlated insulator into a Fermi liquid, as well as into a superconductor.

## 3.4 Stripes

A common feature of models considering doped Mott insulators, like the Hubbard model and $t-J$ models, is that holes tend to be repelled from regions of AF order, setting up incommensurate unidirectional charge-density wave (CDW) and spin-density wave (SDW) orders [61, 62, 3]

Such combined spin and charge order, often called stripes [63], has been found in $La_{2-x}Ba_xCuO_4$ and related compounds [6, 64, 38]. Neutron diffraction experiments reveal a Bragg peak $\mathbf{Q}_B = \frac{2\pi}{a}(n,m)$, with $n,m \in \mathbb{Z}$, and the Néel peak $\mathbf{Q} = \frac{2\pi}{a}(\pm 1/2, \pm 1/2)$ in the AF undoped case. Upon doping, these peaks start to split. The Bragg peak splits into $\mathbf{Q}_B \pm 2\mathbf{d}$ because of CDW order, and the Néel peak split into $\mathbf{Q} \pm \mathbf{d}$ ($|\mathbf{d}| \approx \frac{2\pi}{a}x$) [64]. These results can be understood from introducing holes in a striped pattern on an AF background (see Figure 3.3)) [6]. Putting one hole for every two sites in the charged stripes results in a stripe period of $a/2x$. If the charged stripes act as anti-phase boundaries the spin-order period would be twice that, $a/x$, consistent with the observed SDW and CDW. These stripe patterns are particularly enhanced

at and around $x = 1/8$ [65].

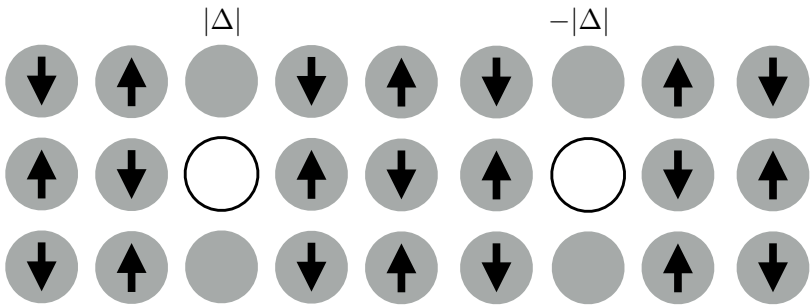


**Figure 3.3:** Stripe ordering at $x = 1/8$. Arrows indicate spin, while the filled circles indicate electron occupation. The SDW with period $8a$ which is twice that of the CDW period of $4a$. The superconducting order is non-vanishing at the charge stripes, but with alternating sign, yielding a PDW with period $8a$.

### 3.4.1 PDW and stripes

At $x = 1/8$ doping in $La_{2-x}Ba_xCuO_4$ (LBCO), where stripes are pronounced, there is a significant suppression of the superconducting critical temperature down to $T_c \approx 4\,\mathrm{K}$ [13] (see Figure 3.1**b**), known as the "1/8-anomaly". Thus, stripes seem to compete with superconductivity [65]; however, the full scenario turns out to be more complicated than that [14]. Transport and magnetic susceptibility measurements suggest that the superconducting correlations are highly two-dimensional [14, 66], and the emerging scenario is that the stripe order decouples the $CuO_2$ layers [9, 11]. In 2D, long-range order cannot be established due to the proliferation of fluctuations; this is known as the Mermin-Wagner theorem [67]. Instead, a state of quasi-long-range order (with algebraically decaying correlations) is established, which goes through a topological Kosterlitz-Thouless (KT) transition to the disordered state [68]. The 2D superconducting state does not show a full Meissner effect but has a residual diamagnetic response. Further, the in-plane resistance is finite below the KT-transition [69], vanishing only for zero current. These signatures are consistent with the stripe phase of LBCO, which sets in at $T_{KT} \approx 16\,\mathrm{K}$. It is only the full 3D Meisner state that is suppressed down to $T_c \approx 4\,\mathrm{K}$ [14, 11].

In explaining the emergent 2D superconductivity at the onset of stripe

order, the existence of a striped superconducting state was proposed in the form of a spatially modulated superconducting order without any homogeneous superconducting component. This state shares the symmetry properties of the FFLO state discussed in the presence of a spin-population imbalance due to a Zeeman field. However, in cuprates, where no such symmetry breaking field exist, this state is referred to as a pair-density wave (PDW) state [9, 11, 10]. The superconducting order is imagined to live on the charged stripes, but with an alternating sign and zero weight at the spin-stripes (see Figure 3.3). Due to the alternating direction of stripes in the layers of LBCO, the Josephson-coupling between layers vanishes, causing the observed 2D superconducting state [11].

## 3.5 PDW, vestigial orders, and the pseudogap

The phenomenology of stripes can be fitted into the larger scheme of electronic liquid crystal phases developed in analogy to classical liquid crystalline phases [52, 3]. A smectic phase, which breaks translational symmetry in one direction, corresponding to CDW, can melt into a nematic phase which only breaks lattice rotational symmetry, but with restored translational invariance [52, 3]. Indeed, nematic order is a ubiquitous phenomena in cuprates [70, 71, 72], as well as in related compounds [3, 49]. Correspondingly CDW has also shown to be an omnipresent order in cuprates; most notably, it has been detected in $YBa_2Cu_3O_{6+x}$ (YBCO) [73, 74], that is outside the lanthanum cuprate family.

The establishment of the stripe phenomenology throughout the cuprate family (although somewhat revised) has motivated suggestions of PDW as a general feature of the cuprate superconductors [10, 3], most notably as the pseudogap itself [12]. PDW has the possibility of unifying many of the features seen in the pseudogap state, as well as the abundance of orders. The reason for these possibilities are the transformation properties of PDW under symmetry

$$\begin{array}{ll} \text{U(1) gauge :} & \Delta_{\mathbf{Q}} \to \Delta_{\mathbf{Q}} e^{i\phi} \\ \text{Translation:} & \Delta_{\mathbf{Q}} \to \Delta_{\mathbf{Q}} e^{i\mathbf{Q}\cdot\mathbf{R}} \\ \text{Parity:} & \Delta_{\mathbf{Q}} \to \Delta_{-\mathbf{Q}} \\ \text{Time-reversal:} & \Delta_{\mathbf{Q}} \to \Delta^*_{-\mathbf{Q}} \\ \text{Point-group, e.g. } \pi/2 \text{ rotation:} & \Delta_{\mathbf{Q}} \to \pm\Delta_{\overline{\mathbf{Q}}}. \end{array} \tag{3.1}$$

The last row is meant to illustrate general transformation under lattice symmetries, which depends on what point-group is realized. Here we exemplified with a $\pi/2$ rotation in a tetragonal symmetry where $\overline{\mathbf{Q}}$ and $\mathbf{Q}$ is related by the transformation. The difference in sign corresponds to an s-wave or d-wave symmetry of the PDW order. Many features of superconductivity are the direct result of an order parameter transforming under U(1) gauge symmetry. This includes the Meisner effect, zero-resistance, flux quantization as well as the occurrence of a supercurrent. (It should be noted, however, that PDW is sensitive to disorder [10].) Thus we expect many of these properties in a state of long-range PDW order $\langle\Delta_{\mathbf{Q}}\rangle \neq 0$. Indeed there are signs of residual superconductivity in the pseudogap, like the prevalence of diamagnetic response [47]. Also, the quasiparticles of a PDW state quite naturally give rise to Fermi arcs [75, 12] (see Figure 6.3). Further, PDW may be able to account for the anomalous quantum oscillations seen at large magnetic fields [50, 51].

### 3.5.1 Vestigial orders

Perhaps more interesting is the possibility of setting composite orders transforming only under a subset of the operations in (3.1). Assuming the existence of a homogeneous superconducting order, $\Delta_0$, as well as four PDW orders $\vec{\Delta} = (\Delta_{\mathbf{Q}_x}, \Delta_{-\mathbf{Q}_x}, \Delta_{\mathbf{Q}_y}, \Delta_{-\mathbf{Q}_y})$ we find, in a tetragonal symmetry,

$$\begin{array}{ll} 2\mathbf{Q}\text{ CDW}: & \rho_{2\mathbf{Q}_i} = \Delta_{\mathbf{Q}_i}\Delta^*_{-\mathbf{Q}_i} \\ \mathbf{Q}\text{ CDW}: & \rho_{\mathbf{Q}_i} = \Delta_0\Delta^*_{-\mathbf{Q}_i} \\ \text{4e SC}: & \Delta_{4e,i} = \Delta_{\mathbf{Q}_i}\Delta^*_{\mathbf{Q}_i} \\ \text{Nematic}: & N = |\Delta_{\mathbf{Q}_x}|^2 + |\Delta_{-\mathbf{Q}_x}|^2 - |\Delta_{\mathbf{Q}_y}|^2 - |\Delta_{-\mathbf{Q}_y}|^2 \\ \text{Loop-current}: & \vec{l} = (|\Delta_{\mathbf{Q}_x}|^2 - |\Delta_{-\mathbf{Q}_x}|^2, |\Delta_{\mathbf{Q}_y}|^2 - |\Delta_{-\mathbf{Q}_y}|^2). \end{array} \tag{3.2}$$

A state of long-range PDW order $\vec{\Delta} \neq 0$ will naturally have expectation values on the composite orders in (3.2) (according to the broken symmetry). However, there are situations under which the PDW melts such that not all broken symmetries are restored simultaneously [17, 19, 3, 20]. In this way a PDW can, for instance, generate a CDW phase with $\langle\vec{\Delta}\rangle = 0, \langle\Delta_0\rangle = 0$ but $\langle\rho_{2\mathbf{Q}_i}\rangle \neq 0$, and similarly for other phases. This is in general referred to as vestigial ordering [76].

The last order in (3.2) represents a so called loop-current (LC) order which is odd under parity and time-reversal, but invariant under the product. Classically such an order can be imagined as a result of circulating currents

$\mathbf{L} \propto \int d\mathbf{r}\, \mathbf{M} \times \mathbf{r}$, with $\mathbf{M} \propto \mathbf{r} \times \mathbf{p}$ the magnetic moment [77]. Originally such order was considered by Varma as a proposal for the pseudogap [78, 79]. Evidence of time-reversal breaking intra-unit cell magnetic order present in the pseudogap phase [80, 81, 82, 83, 84, 85] has further spurred the suggestion of different ME orders, specifically the above mentioned LC orders [86, 87, 88, 89]. An LC order arising from underlying (ME) PDW of the form presented in (3.2) was suggested in [20]. Clearly there is much to explore about the plethora of orders possibly set up by PDW.

### 3.5.2 Evidence for PDW

Besides the suggestion for PDW in LBCO, there are more direct measurements made in $Bi_2Sr_2CaCu_2O_{8+x}$ (BSCCO). Through the use of a Josephson STM tip, a $4a$ PDW was observed [15]. However, as we just have seen, in the presence of homogeneous superconducting order, $\Delta_0$, there is out of necessity a (trivial) PDW of period $4a$ if there is an underlying $4a$ CDW (the periodicity results from the $x = 1/8$ stripe pattern). Instead, following the striped scenario in Figure 3.3, the non-trivial PDW state would be of period $8a$. Intriguingly such an $8a$ PDW state was indirectly observed in vortex halos of BSCCO [16] through the detection of an additional $8a$ CDW (which in the presence of homogeneous superconducting order indicates an $8a$ PDW). There is a notable difference between the PDW seen in BSCCO compared to the one suggested for LBCO. In LBCO, the homogeneous SC is subleading to PDW, prevailing only under 4K, whereas in BSCCO, PDW is subleading to superconducting (SC), first visible when SC is sufficiently suppressed, like in the presence of a vortex core.

# 4 Outlook — My work

We have described some of the most fundamental problems concerning cuprate superconductivity as well as the experimental status. There are several questions to be answered about the PDW. The most fundamental ones regard the mechanism of such a state. What drives the pairing? And what are the observable consequences of a PDW state? The work of this thesis, contained in the appended Paper A-D, considers aspects of these questions. In this chapter, I would like to introduce the reader to some key points about

the work before embarking on the full theoretical development. Let us start by discussing the methods used and other theoretical considerations worth keeping in mind.

## 4.1 Methods and considerations

One way to interpret the question of cuprate superconductivity is to ask what happens when doping a Mott insulator [90]. This question has turned out to be a very hard one, and so far, progress has only been made in a limited set of systems (see [3]). However, it is highly probable that cuprates are more than just doped Mott insulators. Therefore, an important complementary view is a phenomenological approach, which is taken in this thesis. The goal here is to try to sort out what phenomena encountered in experiments are connected and which ones are (more or less) independent. Essentially, this is the appealing possibility of the proposed PDW order; it has the possibility of explaining the occurrence of many features seen in cuprates. An important task is to sort out to what extent this holds true.

The way we will go about modeling cuprates is to start with a Hamiltonian describing the interaction between electrons and then expand the action in collective degrees of freedom (Chapter 5). Our underlying assumption here is that a PDW state, i.e., an expansion of superconducting correlations with multiple modes, will constitute the most important set of freedoms[1]. We will consider two formulations. The first one, which is BCS theory (Chapter 6), is to assume there is a well condensed superconducting mode (generically with a finite momentum) and study the fermionic (Bogoliubov) quasiparticles. The second formulation is Ginzburg-Landau (GL) theory (Chapter 5). Here the action is expressed solely in terms of the bosonic superconducting freedoms by integrating out the electrons. The GL theory is an expansion in the superconducting order parameter, which means that the theory will hold if we are close to the transition temperatures of the orders involved. The upside is that this assumption holds regardless of the strength of the interaction. The downside is that we cannot study physics deep within an ordered state, in contrast to BCS theory. Nevertheless, the often overwhelming importance of symmetry makes these theories interesting to study more generally.

[1] Anti-ferromagnetic ordering is likely an instability of its own.

### 4.1.1 Fluctuations and vestigial orders

BCS theory assumes a constant static superconducting order parameter. It is a mean-field theory, expected to hold when fluctuations of the order parameter are small. For conventional superconductor this assumption holds extremely well (see Section 10.1). In cuprates however, the fluctuations are important which can be seen by comparing coherence lengths, which in conventional superconductors are on the order of $\xi_0 \sim 1000\,\text{nm}$ (1600 nm for aluminum [91]) while much shorter in cuprates $\xi_0 \sim 1\,\text{nm}$ [92]. Also, the superconducting transition temperature for underdoped cuprates are believed to be determined by fluctuations [93] rather than the BCS instability. The existence of fluctuating superconductivity is perhaps most clear above the superconducting transition, where fluctuations lead to a residual superconducting response. For instance, there will be a contribution to conductivity above the critical temperature, called paraconductivity. We will study this in Chapter 8.

GL theories are well suited to take fluctuations into account. The breakdown of mean-field theory and the presence of fluctuations alters the physics of symmetry breaking fundamentally. One is the possibility of vestigial orders, i.e., splitting of a (mean-field) transition where a composite order parameter form before the primary one. We will discuss this in Chapter 10 and 11.

### 4.1.2 Weak and strong-coupled superconductors — BCS to BEC crossover

A superconducting state can be associated with an emergent boson undergoing condensation. Before BCS, a heavily discussed topic was that of electrons pairing into hardbound bosons[2] forming a Bose-Einstein condensate (BEC) [95, 96, 97]. This pairing idea might seem similar to that of BCS theory; however, the concept is, in fact, quite distinct.

In the BEC picture, the bosons are in a tightly bound state of fermions, where the pair size is typically much smaller than the average distance between particles ($\xi_{\text{pair}} \ll k_F^{-1}$). This idea hinges on there being a two-particle bound state, which (in 3D) requires a finite interaction strength. BCS, on the other hand, is a weak-coupling scenario that relies on the Cooper instability; pairs keep together because of the underlying Fermi sea, and the pair

[2] For a historical review see [94].

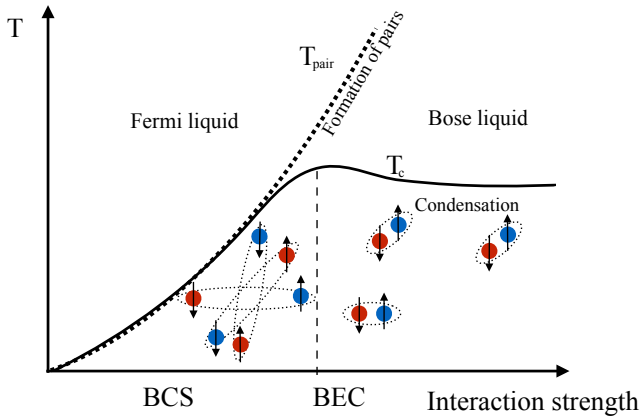


**Figure 4.1:** The BCS-BEC crossover with loosely bound and overlapping pairs on the BCS side and tightly bound non-overlapping pairs on the BEC side. The normal state of the condensate evolves from a Fermi liquid in the BCS limit to a Bose liquid in the BEC limit.

size is typically much bigger than the average distance between particles ($\xi_{\text{pair}} \gg k_F^{-1}$). The difference in physics is perhaps most easily understood in terms of the low energy excitations. For the loosely bound, highly overlapping Cooper pairs, the low energy excitations are fermionic and come from breaking the pairs while the condensate stiffness is comparably high. Contrary to this, in the BEC scenario, the bosons are tightly bound, and the breaking of pairs can be considered a frozen out high-energy excitation. Instead, the non-overlapping pairs lead to a small condensate stiffness, and the collective bosonic excitations make up the low energy physics.

From this picture, we understand that both the density and the interaction strength are important parameters to control the nature of the condensate. Perhaps surprising, the ground state of both the BCS case and the BEC case is qualitatively the same [96, 97], and one talks about a BCS-BEC crossover rather than a transition (see Figure 4.1). When it was discovered that cuprates had a very short coherence length, which can be roughly identified with the size of the Cooper pair, suggestions were made that these compounds might be more of a BEC than conventional superconductors, and the BCS-BEC scenario was revisited [98, 99, 100, 101]. An intriguing property of the BEC limit is that the critical temperature, $T_c$, is set by the condensation of bosons,

while the dissociation of pairs does not occur until higher temperatures, $T_{\text{pair}} > T_c$. This leads to a state made up of pre-formed pairs, which has been discussed as a candidate for the pseudogap state.

We will consider the BCS-BEC crossover for a finite-momentum condensate in Chapter 7. We will formulate it in terms of a GL theory, which in principle holds both for strong and weak coupling, and study the propagator of pairs. In the weak-coupling limit, where BCS theory is expected to hold, the propagator will describe a damped propagation of pairs, due to them breaking up into electrons. In the opposite strong-coupling limit, the pair propagator will describe a coherent propagation, since the pairs are essentially a robust entity.

## 4.2 Key results

I find it useful to describe the main findings of the work contained in Paper A–D already at this point. Both as an aid to understanding the development of the thesis and to comment on how the papers are related.

- **Stabilizing a PDW.** A critical question regarding the PDW state is to what extent it is a good superconductor. In order to study the supercurrent of a PDW state, we considered a *pair-hopping interaction*, which we introduced in Paper A. In Paper B, we continued the exploration of this interaction and its relation to homogeneous superconductivity. We find that a homogeneous superconducting component becomes unstable towards a PDW state either through a Lifshitz point, where the superconducting stiffness vanishes and the pairing momenta develops from zero, or through a metastable PDW state occurring at finite paring momenta. This simple phenomenology was also used as a starting point in Paper D.

  - **Bloch's theorem on vanishing ground state current.** According to a theorem attributed to Bloch, a ground state cannot carry a finite current. This theorem has implications on the stability of a single PDW mode $\Delta_{\mathbf{Q}}$, which in general is expected to carry a finite current since it breaks time-reversal symmetry. The pair-hopping interaction circumvents this by inducing an anomalous

pair-hopping current, similar to a Josephson current. This is discussed in Paper A.

- **PDW as the pseudogap.** In Paper D, we continue to explore the possibility of PDW as the source for the pseudogap by focusing on a ME-PDW exploring its preemptive transitions into phases with loop-current (LC) as well as nematic order. Here we find the possibility for an LC state which decouples from the underlying lattice yielding approximate rotational freedom. Relation to the cuprate phase diagram is discussed.

- **Nematic superconducting fluctuations in LSCO.** Paper C is the result of a collaboration with Ivan Božović's group at Brookhaven National Laboratory. Based on previous transport measurements on thin films of $La_{2-x}Sr_xCuO_4$ (LSCO) [23] indicating the presence of electronic nematic order, we show that this can be attributed to a highly anisotropic fluctuating response. At the same time, the normal component remains more or less isotropic—additional measurements were done under the influence of a magnetic field, showing the expected suppression of the fluctuating response.

- **The single-component nematic superconductor.** Paper D also contains a theory for the superconducting state observed in Paper C. Nematicity is known to develop in, e.g., triplet superconductors through vestigial ordering, with a corresponding nematic response in fluctuations [102]. A surprising aspect of the findings in Paper C is that a nematic response shows up in a single-component (d-wave) superconductor. Vestigial ordering relies on composite orders transforming under a subgroup of symmetry operations of the primary order. For a single component, in the trivial representation, such ordering is not possible. In Paper D, we show instead that the rotational symmetry can be broken in the dynamical response of a single-component superconductor if it couples to a PDW, which develops nematic order. Interestingly for the scenario of the PDW in cuprates, we show that the homogeneous to PDW instability, described in Paper A and Paper B, implies high susceptibility towards such nematic fluctuating superconductivity. Thus the observation in Paper C would be consistent with an underlying PDW instability in the cuprate system.

# PART II
# FLUCTUATING SUPERCONDUCTIVITY AND PAIR-DENSITY WAVE ORDER IN THE CUPRATE SUPERCONDUCTORS

## 5 Effective theory for finite-momentum superconductivity

In this chapter, we will describe the derivation of an effective theory in terms of a finite-momentum superconducting order parameter. We will start by describing the fermionic Hamiltonian and then go on to expand in the collective superconducting degrees of freedom, which will lead us both to a formulation of a finite-momentum BCS theory, as well as a finite-momentum Ginzburg-Landau theory. (For conventions, see Appendix A.)

### 5.1 Fermionic Hamiltonian

A valuable, yet highly simplified, microscopic description for cuprate superconductivity is to study a one-band tight-binding Hamiltonian on a square lattice

$$\hat{H} = \sum_{\mathbf{k}} \varepsilon(\mathbf{k}) \hat{c}^{\dagger}_{\mathbf{k}} \hat{c}_{\mathbf{k}} + \hat{H}_{\text{int}} \tag{5.1}$$

with an attractive interaction described by $\hat{H}_{\text{int}}$. A common interaction to study which gives rise to d-wave superconductivity is a nearest-neighbor

interaction[1]

$$\hat{H}_{\text{int}} = -g_0 \sum_{\langle ij\rangle,\sigma,\sigma'} \hat{c}^\dagger_{\sigma,i}\hat{c}_{\sigma,i}\hat{c}^\dagger_{\sigma',j}\hat{c}_{\sigma',j}\,. \tag{5.2}$$

This interaction can be seen as a limit of the more general attractive interaction which respects translational invariance

$$\hat{H}_{\text{int}} = -g_0 \sum_{ijkl}\sum_{\sigma,\sigma'} T(\mathbf{r}^+_{ij}-\mathbf{r}^+_{kl})t(\mathbf{r}^-_{ij},\mathbf{r}^-_{kl})\hat{c}^\dagger_{\sigma,i}\hat{c}^\dagger_{\sigma',j}\hat{c}_{\sigma',l}\hat{c}_{\sigma,k}\,, \tag{5.3}$$

where $\mathbf{r}^\pm_{ij} = (\mathbf{r}_i \pm \mathbf{r}_j)/2$. Here $t(\mathbf{r}^-_{ij},\mathbf{r}^-_{kl})$ describes the electron-electron attraction and $T(\mathbf{r}^+_{ij}-\mathbf{r}^+_{kl})$ represents the possibility of a correlated jump of an electron pair. The form (5.2), which only contains density-density interaction, is obtained for $T(\mathbf{r}_1-\mathbf{r}_2)=\delta(\mathbf{r}_1-\mathbf{r}_2)$ and $t(\mathbf{r}^-_{ij},\mathbf{r}^-_{kl}) = t(\mathbf{r}^-_{ij},\mathbf{r}^-_{ij})\delta_{\mathbf{r}^-_{ij},\mathbf{r}^-_{kl}}$ where $t(\mathbf{r}^-_{ij},\mathbf{r}^-_{ij})=\delta_{\mathbf{r}^-_{ij},\hat{x}/2}+(\hat{x}\to-\hat{x},\pm\hat{y})$ is the nearest-neighbor interaction.

### 5.1.1 Pair-hopping interaction

A weak-coupling scenario is not expected to generate a PDW. It is still unexpected for a finite-momentum superconducting state to be energetically preferable over a zero-momentum state for stronger coupling, since portions of the FS will be ungapped. However, for an interaction that promotes d-wave pairing, the nodal points of the FS are already ungapped. Thus, one might imagine that a reduced nodal gap could conspire with a finite-momentum condensate to form an effectively less gapped FS. Such a result was reported by Loder et al. [103], who found that for sufficiently strong nearest-neighbor attraction, finite-momentum pairing triumphs over zero-momentum (with d-wave symmetry). When trying to use this result in order to explore the depairing current in a PDW state (Paper A), we found that a substantially higher interaction strength than previously reported was needed ($g_0 \gtrsim 6t$ where $t$ is the hopping strength)[2]. Instead, we considered a finite range

[1] These attractive interactions should be viewed as low-energy effective Hamiltonians. In general, one can consider different sources for attractive interactions; however, the repulsive Coulomb repulsion has to be overcome. In the BCS model, the total interaction can become attractive due to the highly retarded phonon-mediated attraction. Relevant for the cuprates is a nearest-neighbor attraction that can be realized by a residual AF interaction, which in the d-wave channel is orthogonal to an on-site Coulomb repulsion [31].

[2] See Appendix A of Paper A. Here $V$ is used to indicate interaction strength, not $g_0$.

pair-hopping term of the form

$$T(\mathbf{r}^+_{ij}-\mathbf{r}^+_{kl}) = \frac{\kappa_y\kappa_x}{2\pi} e^{-\sum_\mu \kappa_\mu^2 \frac{(r^+_{ij,\mu}-r^+_{kl,\mu})^2}{2}} \cos\frac{2\pi}{\lambda}(r^+_{ij,x}-r^+_{kl,x}) \tag{5.4}$$

(still with a nearest neighbor attraction $t(\mathbf{r}^-_{ij},\mathbf{r}^-_{kl}) = \delta_{\mathbf{r}^-_{ij},\hat{x}/2}\delta_{\mathbf{r}^-_{kl},\hat{x}/2} + (\hat{x} \to -\hat{x},\pm\hat{y})$). Here $\kappa_\mu, \mu = x, y$ sets the range of the hopping and for $\kappa_{x,y} \to \infty$ (5.4) reduces to an ordinary nearest-neighbor interaction. In order to have a negligible zero-momentum pairing the modulation needs to be well resolved by the hopping range, thus[3] $\kappa_x \lesssim \frac{2}{\lambda}$. Using this interaction we were able to find stable PDW solutions for a significantly smaller interaction strength $g_0 \gtrsim 1.5t$.

In Paper B we wanted to generalize the assumptions and instead considered a continuous field theory

$$\hat{H}_{\text{int}} = -\frac{g_0}{2}\sum_{\sigma,\sigma'}\int_{\mathbf{r}_1,\mathbf{r}_2} T(\mathbf{r}_1-\mathbf{r}_2)\hat{\psi}^\dagger_\sigma(\mathbf{r}_1)\hat{\psi}^\dagger_{\sigma'}(\mathbf{r}_1)\hat{\psi}_{\sigma'}(\mathbf{r}_2)\hat{\psi}_\sigma(\mathbf{r}_2) \tag{5.5}$$

with local attraction $t(\mathbf{r}^-_{ij},\mathbf{r}^-_{kl}) = \delta_{\mathbf{r}^-_{ij},0}\delta_{\mathbf{r}^-_{kl},0}$, and repulsive pair-hopping of the form

$$T(\mathbf{r}_1-\mathbf{r}_2) = \delta(\mathbf{r}_1-\mathbf{r}_2) - \alpha\delta\left(\mathbf{r}_1-\mathbf{r}_2 \pm \begin{Bmatrix}\hat{x}\\ \hat{y}\end{Bmatrix}\frac{\lambda}{2}\right) \tag{5.6}$$

with $\alpha > 0$ and hopping length $\lambda$. Simultaneously having a pair at position $x$ and $x+\lambda$ is energetically unfavorable, which leads to a staggered distribution of pairs. This effect is perhaps most easily understood in the reciprocal space where $T(\mathbf{p}) = 1-2\alpha\cos(\frac{\lambda}{2}p_x)-2\alpha\cos(\frac{\lambda}{2}p_y)$ can be thought of as the dispersion of the pairs. The reason for considering two different kinds of pair-hopping is that in Paper A we were interested in a strong tendency towards forming a PDW (small $\kappa$ in (5.4)). In Paper B we rather wanted to explore what happens for a very weak pair-hopping modulations ($\alpha \ll 1$ in (5.6)). Alternatively (5.4) can be considered a smoothened version of (5.6).

Similar sorts of pair-hopping interactions have been suggested to arise from off-diagonal terms of the microscopic Coulomb interaction [40, 104, 105, 106]. The original idea of PDW arising from stripe order is that the stripe domains act as Josephson $\pi$-junction, yielding an alternating sign of the

[3] We also included a possible finite hopping range along the $y$-direction.

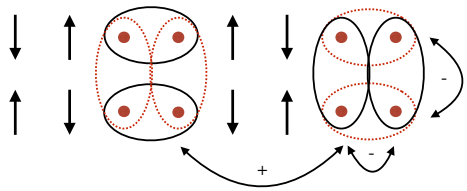


**Figure 5.1:** Sketch of the interaction (5.6) and (5.4) with local attraction and longer range pair-hopping. Solid (dashed) rings indicate positive (negative) pair-amplitudes of a commensurate PDW. This depicts a d-wave order, relevant for Paper A.

superconducting order [10](see Figure 3.3). The pair-hopping presented here can be considered a microscopic version of the same idea.

There are other possible sources for a PDW state as well. The original suggestion of PDW comes from a variational Monte Carlo study of the 2D t-t'-J model [9]. Suggested from tensor networks, a striped PDW is near-degenerate with the uniform d-wave superconductor [107]. However, from DMRG studies on t-J ladders, clear evidence for a PDW order is lacking [108]. Interestingly, in Paper B, we find that even a small pair-hopping can stabilize a PDW state.

## 5.2 Path-integral formulation

To derive both the BCS formulation and the Ginzburg-Landau effective action of a PDW state we will consider the coherent state path-integral formulation of the many-body Hamiltonian. A coherent state is defined as an eigenstate of the annihilation operator, $\hat{\psi}_\pm(x)|\psi_\pm\rangle = \psi_\pm(x)|\psi_\pm\rangle$, $|\psi_\pm\rangle = e^{\pm\int \mathrm{d}x\psi_\pm(x)\hat{\psi}^\dagger_\pm(x)}|0\rangle$ where we use $+,-$ to refer to bosons and fermions respectively. We can label the coherent state by the field $\psi_\pm$, which is then no longer an operator. For bosons these fields are ordinary commuting numbers, but for fermions they are the anti-commuting Grassmann numbers.

We can express the many-body partition function for a fermionic Hamiltonian ($\psi = \psi_-$) in terms of a functional integral over all coherent states

$$Z = \mathrm{Tr}\, e^{-\beta(\hat{H}-\mu\hat{N})} = \int \mathscr{D}\psi^*\mathscr{D}\psi\, e^{-\psi^*\psi}\langle -\psi|\, e^{-\beta(\hat{H}-\mu\hat{N})}|\psi\rangle\,. \tag{5.7}$$

(With $\beta = 1/T$.) We want to utilize that acting with a normal ordered operator[4] on a coherent state replaces the $\hat{\psi}$ operators with their Grassman number equivalents $\psi$. To do this, we split up the argument of the exponential in $N$ small slices of width $\Delta\tau = \beta/N$, which then becomes normal-ordered to first order in $\Delta\tau$. Inserting the resolution of identity for every slice we obtain[5] [31]

$$Z = \int \mathscr{D}\psi\, e^{-S(\psi)},\ S(\psi) = \int_0^\beta \mathrm{d}\tau \int_{\mathbf{k}} \psi^*_{\mathbf{k}} \partial_\tau \psi_{\mathbf{k}} + H(\tau) - \mu N(\tau)\,, \tag{5.8}$$

where $\tau$ is a continuous label of each slice. We can use this partition function to calculate imaginary time-ordered Greens functions

$$G(\tau,\tau') = -\langle T\hat{\psi}(\tau)\hat{\psi}^\dagger(\tau')\rangle = -\frac{1}{Z}\mathrm{Tr}\left[e^{-\beta(H-\mu N)} T\hat{\psi}(\tau)\hat{\psi}^\dagger(\tau')\right] \tag{5.9}$$

using

$$\langle T\hat{\psi}(\tau)\hat{\psi}^\dagger(\tau')\rangle = \langle \psi(\tau)\psi^*(\tau')\rangle = \frac{1}{Z}\int \mathscr{D}\psi\, \psi(\tau)\psi^*(\tau') e^{-S(\tau)}, \tag{5.10}$$

where $\hat{\psi}(\tau) = e^{\tau\hat{H}}\hat{\psi}e^{-\tau\hat{H}}$ are Heisenberg operators in imaginary time $\tau = it$.

Considering the $s$-wave pairing interaction in (5.5) the action can be written as

$$S(\Psi) = \int_0^\beta \mathrm{d}\tau \int_{\mathbf{k}} \Psi^\dagger_{\mathbf{k}} \partial_\tau \Psi_{\mathbf{k}} + H(\tau) - \mu N(\tau), \tag{5.11}$$

in reciprocal space with

$$H = \int_{\mathbf{k}} \Psi^\dagger_{\mathbf{k}} \varepsilon(\tau_3 \mathbf{k})\tau_3 \Psi_{\mathbf{k}} - g_0 \int_{\mathbf{k},\mathbf{k}',\mathbf{p}} T(\mathbf{p}) \Psi^\dagger_{\mathbf{k}+\frac{\mathbf{p}}{2}} \tau_+ \Psi_{\mathbf{k}-\frac{\mathbf{p}}{2}} \Psi^\dagger_{\mathbf{k}'-\frac{\mathbf{p}}{2}} \tau_- \Psi_{\mathbf{k}'+\frac{\mathbf{p}}{2}}\,, \tag{5.12}$$

where $T(\mathbf{p}) = 1 - 2\alpha\cos(\frac{\lambda}{2}p_x) - 2\alpha\cos(\frac{\lambda}{2}p_y)$. We have introduced the Nambu-spinors $\Psi^\dagger_{\mathbf{k}} = [\psi^*_{\uparrow,\mathbf{k}}\ \psi_{\downarrow,-\mathbf{k}}]$ and $\tau_\pm = \frac{\tau_1 \pm i\tau_2}{2}$, where $\tau_i$ are the Pauli-matrices[6].

[4] An operator with all creation operators to the left of annihilation operators.

[5] We will use $\mathscr{D}\psi$ as a short-hand notation for $\mathscr{D}\psi\mathscr{D}\psi^*$.

[6]
$$\tau_1 = \begin{bmatrix} 0 & 1 \\ 1 & 0 \end{bmatrix} \quad \tau_2 = \begin{bmatrix} 0 & -i \\ i & 0 \end{bmatrix} \quad \tau_3 = \begin{bmatrix} 1 & 0 \\ 0 & -1 \end{bmatrix}. \tag{5.13}$$

### 5.2.1 Hubbard-Stratonovich transformation

The action (5.11) describes an interacting system. In order to treat the interaction, we will utilize the Hubbard-Stratonovich (HS) transformation to decouple the interaction in (5.12) in the superconducting channel. Formally we do this by the replacement[7]

$$\begin{aligned} -g_0 \int_{\mathbf{k},\mathbf{k}',\mathbf{p}} T(\mathbf{p}) \Psi^\dagger_{\mathbf{k}+\frac{\mathbf{p}}{2}} \tau_+ \Psi_{\mathbf{k}-\frac{\mathbf{p}}{2}} \Psi^\dagger_{\mathbf{k}'-\frac{\mathbf{p}}{2}} \tau_- \Psi_{\mathbf{k}'+\frac{\mathbf{p}}{2}} \longrightarrow \frac{1}{g_0} \int_{\mathbf{p}} \Delta^*(\mathbf{p},\tau) T^{-1}(\mathbf{p}) \Delta(\mathbf{p},\tau) \\ - \int_{\mathbf{k},\mathbf{p}} \Delta(\mathbf{p},\tau) \Psi^\dagger_{\mathbf{k}+\frac{\mathbf{p}}{2}} \tau_+ \Psi_{\mathbf{k}-\frac{\mathbf{p}}{2}} - \int_{\mathbf{k},\mathbf{p}} \Delta^*(\mathbf{p},\tau) \Psi^\dagger_{\mathbf{k}-\frac{\mathbf{p}}{2}} \tau_- \Psi_{\mathbf{k}+\frac{\mathbf{p}}{2}} \end{aligned} \tag{5.15}$$

in (5.12). Simultaneously the partition function should be evaluated over all configurations of the *bosonic* (superconducting) field $\Delta$

$$Z = \int \mathscr{D}\Psi \mathscr{D}\Delta \, e^{-S(\Psi,\Delta)}. \tag{5.16}$$

The HS transformation is central to this thesis and some more technical aspects are discussed in Appendix B. In reciprocal space the action takes the form

$$\begin{aligned} S(\Psi,\Delta) &= \int_{k,k'} \Psi^\dagger_k \mathscr{G}^{-1}_{k,k'} \Psi_{k'} + \frac{1}{g_0} \int_p |\Delta(p)|^2 T^{-1}(\mathbf{p}), \\ \mathscr{G}^{-1}_{k,k'} &= \mathscr{G}^{-1}_{0,k} \delta_{k-k'} - \Sigma_{k,k'}, \quad \mathscr{G}^{-1}_{0,k} = -i\omega + \tau_3 \xi(\tau_3 \mathbf{k}), \\ \Sigma_{k,k'} &= \Delta(k-k')\tau_+ + \Delta^*(-k+k')\tau_-, \end{aligned} \tag{5.17}$$

where $\xi(\mathbf{k}) = \varepsilon(\mathbf{k}) - \mu$ and $k = (\mathbf{k}, i\omega)$ and $p = (\mathbf{p}, i\Omega)$ for the bosonic and fermionic modes respectively. $\Omega = \frac{2n\pi}{\beta}, \omega = \frac{(2n+1)\pi}{\beta}$ are the bosonic and fermionic Matsubara frequencies (corresponding to a periodic and an anti-periodic Greens function) and $\delta_{k-k'} = \delta(\mathbf{k}-\mathbf{k}')\beta\delta_{n,n'}$.

[7] The HS transformation utilizes the identity

$$\int \mathrm{d}z \, \mathrm{d}z^* e^{-z^* M z + j^* z + z^* j} = \text{constant} \, e^{j^* M^{-1} j} \tag{5.14}$$

where we identify $j \sim \Psi^\dagger_{\mathbf{k}-\frac{\mathbf{p}}{2}} \tau_- \Psi_{\mathbf{k}+\frac{\mathbf{p}}{2}} = \psi_{\downarrow,\mathbf{k}-\frac{\mathbf{p}}{2}} \psi_{\uparrow,\mathbf{k}+\frac{\mathbf{p}}{2}}$ and $z \sim \Delta$ (see Appendix B).

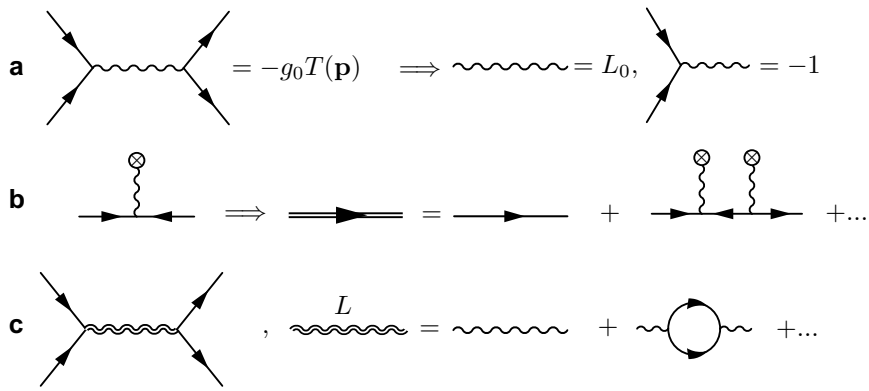


**Figure 5.2:** Illustration of the HS transformation in terms of Feynman diagrams. **a** The interaction is decoupled by the introduction of a new (propagating) field $\Delta$, and a vertex. **b** BCS theory is obtained by letting $\Delta$ acquire an expectation value. **c** Dressing $L_0$ with loops of electrons introduces dynamics and is equivalent to the RPA approximation.

A nice physical way to understand the HS transformation is to appeal to the corresponding Feynman diagrams of the interaction described by the left and right-hand side of (5.15); this is illustrated in Figure 5.2. The left-hand side describes a theory with an interaction term equal to $-g_0 T(\mathbf{p})$. In contrast, the right-hand side, after the HS transformation, replaces this interaction with an additional field, $\Delta$, with the bare propagator $L_0 = -\langle \Delta\Delta^* \rangle = -g_0 T(\mathbf{p})$, and a vertex (see Figure 5.2**a**). Diagrams with only external fermionic legs will be given by the same expression in both representations.

The theory with the bosonic superconducting field has several advantages as a starting point for approximations. Since the theory is quadratic in the electronic field, we can evaluate it for specific field configurations of $\Delta$. If a finite expectation value well approximates $\Delta$, we can write down a corresponding mean-field theory and study the fermionic excitations; this will be the BCS theory (see Figure 5.2**b**). Furthermore, we can also study dynamics of $\Delta$ by including screening by the electron fields. Note that dressing the superconducting propagator (one-loop correction) will equal the random phase approximation (RPA) of the electron-electron interaction; this is the starting point for considering fluctuations of the superconducting field (see Figure 5.2**c**).

We find the effective action in terms of the superconducting order param-

eter by integrating over the fermionic degrees of freedom[8]

$$Z = \int \mathscr{D}\Psi\mathscr{D}\Delta e^{-S} = \int \mathscr{D}\Delta e^{-\frac{1}{g_0}\int_p |\Delta(p)|^2 T^{-1}(\mathbf{p})} \mathrm{Det}(\mathscr{G}^{-1}_{k,k'}) \tag{5.18}$$

where the Grassmann integral yields the functional determinant spanning over all fermionic degrees of freedom [42]. After re-exponentiating the functional determinant by using ln(Det) = Tr(ln), we find

$$\begin{aligned} Z &= \int \mathscr{D}\Delta e^{-S_{\mathrm{eff}}(\Delta)} \\ S_{\mathrm{eff}}(\Delta) &= -\mathrm{Tr}\ln\mathscr{G}^{-1} + \frac{1}{g_0}\int_p |\Delta(p)|^2 T^{-1}(\mathbf{p}). \end{aligned} \tag{5.19}$$

## 5.3 BCS mean-field theory as a saddle-point approximation

BCS theory utilizes that we can calculate the fermionic spectra of $S(\Psi,\Delta)$ for specific configuration of the superconducting field $\Delta$. The configuration that best approximates the partition function is given by the configuration at the saddle-point $\Delta = \Delta_0$ that fulfills $\delta S_{\mathrm{eff}}/\delta\Delta = 0$

$$Z \approx Z_{\mathrm{BCS}} = e^{-S_{\mathrm{eff}}(\Delta_0)} = \int \mathscr{D}\Psi\, e^{-S(\Psi,\Delta_0)}. \tag{5.20}$$

The saddle-point equation implies

$$\langle\frac{\delta S}{\delta\Delta}\rangle_{\mathrm{BCS}} = 0 \Rightarrow \Delta(q) = g_0 T(\mathbf{q}) \int_k \langle\psi_{\downarrow,-k+q/2}\psi_{\uparrow,k+q/2}\rangle \tag{5.21}$$

where the average is taken with respect to $Z_{\mathrm{BCS}}$. This gives the well-known BCS self-consistency equation after evaluating the anomalous Greens function in (5.21). We will continue to discuss the mean-field in Section 6.2, where we develop the mean-field theory from a slightly different perspective, more suitable for introducing a supercurrent.

[8] Here we asserted the overall normalization factor 1, which can be confirmed by taking the free-electron limit $\mathscr{G}^{-1}_{k,k'} \to \mathscr{G}^{-1}_{0,k}\delta_{k,k'}$ where $\mathscr{G}^{-1}_{0,k} = -i\omega + \tau_3\xi(\mathbf{k})$.

## 5.4 Superconducting effective action

To make some headway with the effective action (5.19) we will assume that we are close to an ordering transition and expand the order parameter around $\Delta = 0$ (or $\Sigma = 0$)

$$-\mathrm{Tr}\ln\beta\mathscr{G}^{-1} = -\mathrm{Tr}\ln\beta\mathscr{G}_0^{-1} + \sum_n \frac{1}{n}\mathrm{Tr}(\mathscr{G}_0\Sigma)^n \tag{5.22}$$

and truncate to some finite order[9]. For weak enough ordering it suffices to truncate the series to fourth order in $\Delta$ for which the partition function can be written

$$Z \approx Z_0 Z_{\mathrm{GL}}, \quad Z_{\mathrm{GL}} = \int \mathscr{D}\Delta e^{-\beta F(\Delta)}, \tag{5.23}$$

with $Z_0 = \mathrm{Det}(\beta\mathscr{G}_0^{-1})$ being the free electron contribution and

$$F = \frac{1}{\beta}\left(\frac{1}{g_0}\int_p |\Delta(p)|^2 T^{-1}(\mathbf{p}) + \frac{1}{2}\mathrm{Tr}(\mathscr{G}_0\Sigma)^2 + \frac{1}{4}\mathrm{Tr}(\mathscr{G}_0\Sigma)^4\right) \tag{5.24}$$

the Ginzburg-Landau energy functional. Here we used that the series in (5.22) only involves pairs of $\Delta$ and $\Delta^*$ since $\mathrm{tr}(\tau_\pm) = 0, \tau_\pm^2 = 0$.

Studying weak ordering implies $T \approx T_c$, which is a limitation that does not arise in the BCS mean-field theory treatment. In contrast, the mean-field treatment is limited to consider weak interaction. The form of the GL theory, in principle, allows for arbitrary strong interaction, and we will use this formulation to study the BCS-BEC crossover in Chapter 7.

### 5.4.1 Multiple superconducting orders

The effective action (5.19) is formally exact, and the fluctuating bosonic field $\Delta$ takes all correlation effects into account. However, when expanding in $\Delta$, many correlation effects are lost. We could have considered another decomposition of the interaction by, for instance, letting CDW or SDW mediate the interaction. Ideally, we would like to include many possible orders simultaneously. While this is easy to do phenomenologically, by considering

[9] Tr indicates trace over all degrees of freedom while we let tr indicate trace over freedoms in "matrix" representation, like the Pauli matrices.

the appropriate symmetry respecting terms, an expansion as outlined above would, in general, lead to double-counting degrees of freedoms [109]. Our hypothesis for the cuprate system is, however, that the superconducting instability dominates, but with the possibility of developing finite-momentum orders. This hypothesis motivates us to consider the GL functional (5.24), where we expand in finite-momentum orders. This was the scenario considered in Paper B.

In the presence of a finite-momentum instability we include an expansion in anticipated modes[10]

$$\Delta(\mathbf{x}) = \Delta_{-\mathbf{Q}}(\mathbf{x})e^{-i\mathbf{Q}\cdot\mathbf{x}} + \Delta_0(\mathbf{x}) + \Delta_{\mathbf{Q}}(\mathbf{x})e^{i\mathbf{Q}\cdot\mathbf{x}} \tag{5.25}$$

in $Z_{\mathrm{GL}}$ (5.23). The functional measure should be written

$$\mathscr{D}\Delta(x) = \prod_{\mathbf{p}} \mathrm{d}\Delta_{\mathbf{p}} = \tilde{\mathscr{D}}\Delta_{-\mathbf{Q}}(x)\tilde{\mathscr{D}}\Delta_0(x)\tilde{\mathscr{D}}\Delta_{\mathbf{Q}}(x) \tag{5.26}$$

where $\tilde{\mathscr{D}}$ indicates that the function should only vary over lengths bigger than $2/|\mathbf{Q}|$ in order not to result in double counting of degrees of freedom. To clarify, terms like $\Delta_0(\mathbf{Q}+\mathbf{q})$ should be identified with $\Delta_{\mathbf{Q}}(\mathbf{q})$ in order not to take the same mode into account twice. Eventually, we are interested in a gradient expansion of the action, considering slow variations of $\Delta$. With $2/|\mathbf{Q}|$ typically on the order of a few lattice constants, this constraint will be automatically enforced, and the distinction between $\tilde{\mathscr{D}}$ and $\mathscr{D}$ can be dropped. The expansion (5.25) implies that $\Sigma$ in (5.17) splits into three parts

$$\Sigma = \Sigma_{-\mathbf{Q}} + \Sigma_0 + \Sigma_{\mathbf{Q}} \tag{5.27}$$

where

$$\begin{aligned}&\Sigma_{\mathbf{q}}(\mathbf{k},\mathbf{k}',i\omega - i\omega') = \\ &\Delta_{\mathbf{q}}(\mathbf{k}-\mathbf{k}'-\mathbf{q},i\omega-i\omega')\tau_+ + \Delta^*_{\mathbf{q}}(-\mathbf{k}+\mathbf{k}'-\mathbf{q},-i\omega+i\omega')\tau_-.\end{aligned} \tag{5.28}$$

Inserting this into (5.24) we can find the second and fourth-order terms for a theory with multiple modes of superconducting order.

[10] Here we only included three anticipated modes along one axis, possibly describing a unidirectional PDW. In Paper D and Chapter 11 we include a (more) complete set of ordering momenta, consistent with a tetragonal symmetry.

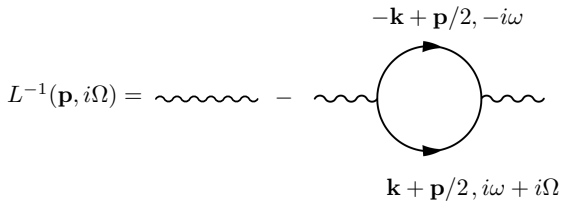


**Figure 5.3:** Diagrammatic representation of (5.31).

### 5.4.2 Second-order terms and the pair propagator

The second-order term in (5.24) takes the form

$$\frac{1}{2}\mathrm{Tr}(\mathscr{G}_0\Sigma)^2 = \frac{1}{2}\mathrm{Tr}(\mathscr{G}_0\Sigma_{-\mathbf{Q}})^2 + \frac{1}{2}\mathrm{Tr}(\mathscr{G}_0\Sigma_0)^2 + \frac{1}{2}\mathrm{Tr}(\mathscr{G}_0\Sigma_{\mathbf{Q}})^2 \tag{5.29}$$

where cross terms vanishes because of the restriction from double counting[11], similar for $\frac{1}{g_0}\int\limits_p |\Delta(p)|^2 T^{-1}(\mathbf{p})$. The zero-order momentum term yields

$$\begin{aligned}&\frac{1}{2}\mathrm{Tr}\mathscr{G}_0\Sigma_0\mathscr{G}_0\Sigma_0 = \\ &\frac{1}{2}\int \mathrm{tr}\,\mathscr{G}_0(\mathbf{p}, i\omega)\Sigma_0(\mathbf{p},\mathbf{p}', i\omega - i\omega')\mathscr{G}_0(\mathbf{p}', i\omega')\Sigma_0(\mathbf{p}',\mathbf{p}, i\omega' - i\omega).\end{aligned} \tag{5.30}$$

Performing the trace in Nambu space yields a factor of two and we find for the second order term of the free energy (5.24)

$$\begin{aligned}&-\int\limits_p L^{-1}(\mathbf{p}, i\Omega)|\Delta(\mathbf{p}, i\Omega)|^2\,, \\ &L^{-1}(\mathbf{p}, i\Omega) = \int\limits_k G_0(\mathbf{k}+\frac{\mathbf{p}}{2}, i\omega + i\Omega)G_0(-\mathbf{k}+\frac{\mathbf{p}}{2}, -i\omega) - \frac{T^{-1}(\mathbf{p})}{g_0}\end{aligned} \tag{5.31}$$

where $G_0(\mathbf{k}, i\omega) = (i\omega - \xi(\mathbf{k}))^{-1}$. Here we have defined the pair susceptibility, or pair propagator $L(\mathbf{p}, i\Omega)$, diagrammatically shown in Figure 5.3. The other terms in (5.29) are formally similar and can be obtained by shifting $L^{-1}(\mathbf{p}, i\Omega)$

[11] Alternatively, the cancellation of cross terms can be seen as a result of averaging over highly oscillatory terms like $\Delta_{\mathbf{Q}}\Delta^*_{-\mathbf{Q}}e^{2\mathbf{Q}\cdot\mathbf{R}}$.

to $L^{-1}(\mathbf{p}\pm\mathbf{Q}, i\Omega)$. The analytic structure of $L(\mathbf{p}, z)$ contains information about the excitation spectra of the pairs and is needed to determined the occupation number of bosonic excitations, which we will come back to in Section 7.2.

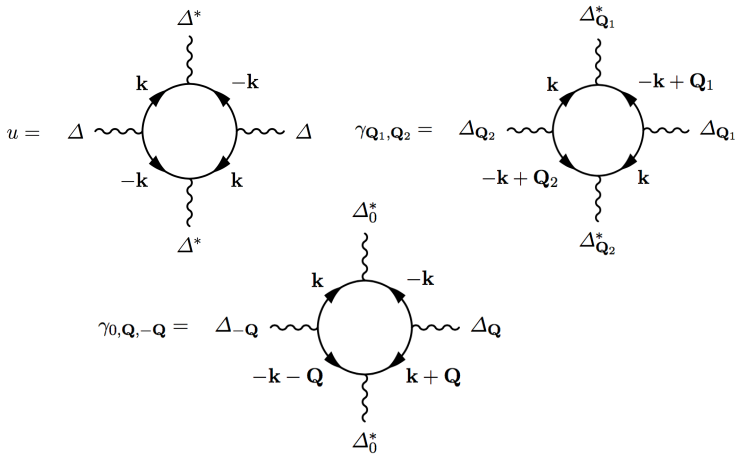


**Figure 5.4:** Diagrammatic representation of (5.35). A factor 2 arises for $u_{\mathbf{Q}}$ because of charge conjugation (CC). For the mixed term we get a factor of 4 from the cyclic property of the trace as well as a factor of 2 from CC for $\gamma_{\mathbf{Q}_1,\mathbf{Q}_2}$. ($\gamma_{0,\mathbf{Q},-\mathbf{Q}}$ is not invariant under CC which leads to two terms in (5.34).)

### 5.4.3 Fourth-order terms

Expanding the fourth-order terms around the different momenta yields

$$\begin{aligned}\frac{1}{4}\mathrm{Tr}(\mathscr{G}_0\Sigma)^4 &= \frac{1}{4}\mathrm{Tr}(\mathscr{G}_0\Sigma_{-\mathbf{Q}})^4 + \frac{1}{4}\mathrm{Tr}(\mathscr{G}_0\Sigma_0)^4 + \frac{1}{4}\mathrm{Tr}(\mathscr{G}_0\Sigma_Q)^4 \\ &+ \mathrm{Tr}(\mathscr{G}_0\Sigma_0)^2(\mathscr{G}_0\Sigma_{\mathbf{Q}})^2 + \mathrm{Tr}(\mathscr{G}_0\Sigma_0)^2(\mathscr{G}_0\Sigma_{-\mathbf{Q}})^2 + \mathrm{Tr}(\mathscr{G}_0\Sigma_{\mathbf{Q}})^2(\mathscr{G}_0\Sigma_{-\mathbf{Q}})^2 \\ &+ \mathrm{Tr}(\mathscr{G}_0\Sigma_0)(\mathscr{G}_0\Sigma_{\mathbf{Q}})(\mathscr{G}_0\Sigma_0)(\mathscr{G}_0\Sigma_{-\mathbf{Q}})\end{aligned} \tag{5.32}$$

where we used the non-double counting restriction and the cyclic property of the trace[12]. Explicitly in terms of $\Delta$ the un-mixed fourth order finite-

[12]One might have guessed that terms in the second row of (5.32) should come with a factor of 6/4 in front, however the two terms (related by cyclic transformation) of the form $\Delta_{\mathbf{Q}_1}\Delta^*_{\mathbf{Q}_2}\Delta_{\mathbf{Q}_1}\Delta^*_{\mathbf{Q}_2}$ leads to double counting and only four terms of the form $\Delta_{\mathbf{Q}_1}\Delta^*_{\mathbf{Q}_1}\Delta_{\mathbf{Q}_2}\Delta^*_{\mathbf{Q}_2}$

momentum term takes the form

$$\begin{aligned}\frac{1}{4}\mathrm{Tr}(\mathscr{G}_0\Sigma_0)^4 = \int\limits_{q_1,q_2,q_3} \frac{u(q_1,q_2,q_3)}{2}\Delta(q_1)\Delta^*(q_2)\Delta(q_3)\Delta^*(q_1-q_2+q_3) \approx \\ \frac{u_0}{2}\int\limits_{q_1,q_2,q_3}\Delta(q_1)\Delta^*(q_2)\Delta(q_3)\Delta^*(q_1-q_2+q_3) = \frac{u_0}{2}\int\limits_x |\Delta(x)|^4\end{aligned} \tag{5.33}$$

where we have only kept the $q=(\mathbf{q},i\Omega)$ independent part of $u_0=u(0,0,0)$, yielding a local term in real space and time (see Figure 5.4). This is in contrast to how we treated the second-order term, where the momentum dependence in $L$ was kept, see (5.31). This is a valid assumption if the time-dependence and spatial dependence of $\Delta$ are of much longer scale than the coherence time and coherence length of the pairs themselves (see discussion around (7.16) and (7.17)). Similar terms arise for finite-momentum orders with $u_{\mathbf{Q}}=u(\mathbf{Q},\mathbf{Q},\mathbf{Q})$ where we again assume small dependence of $u$ on additional variation of momentum. Similarly, we find from (5.32) the mixed terms

$$\gamma_{0,\mathbf{Q}}|\Delta_0|^2|\Delta_{\mathbf{Q}}|^2, \quad \gamma_{\mathbf{Q}_1,\mathbf{Q}_2}|\Delta_{\mathbf{Q}_1}|^2|\Delta_{\mathbf{Q}_2}|^2, \quad \gamma_{0,\mathbf{Q},-\mathbf{Q}}\Delta_0^2\Delta_{\mathbf{Q}}^*\Delta_{-\mathbf{Q}}^* + c.c. + ... \tag{5.34}$$

where

$$\begin{aligned}u_{\mathbf{Q}} &= \int\limits_k G_0^2(\mathbf{k}+\frac{\mathbf{Q}}{2},i\omega)G_0^2(-\mathbf{k}+\frac{\mathbf{Q}}{2},-i\omega),\\ \gamma_{0,\mathbf{q}} &= 2\int\limits_k G_0(\mathbf{k},i\omega)G_0(-\mathbf{k}+\mathbf{q},-i\omega)G_0(\mathbf{k},i\omega)G_0(-\mathbf{k},-i\omega),\\ \gamma_{\mathbf{Q}_1,\mathbf{Q}_2} &= 2\int\limits_k G(\mathbf{k},i\omega)G_0(-\mathbf{k}+\mathbf{Q}_1,-i\omega)G_0(\mathbf{k},i\omega)G_0(-\mathbf{k}+\mathbf{Q}_2,-i\omega),\\ \gamma_{0,\mathbf{Q},-\mathbf{Q}} &= \int\limits_k G_0(\mathbf{k},i\omega)G_0(-\mathbf{k},-i\omega)G_0(\mathbf{k}+\mathbf{Q},i\omega)G_0(-\mathbf{k}-\mathbf{Q},-i\omega).\end{aligned} \tag{5.35}$$

The diagrammatic representation of these terms is shown in Figure 5.4. The mixed terms determine how the superconducting orders interact.

remains. This, as well as the formation of the last term in (5.32), is most easily seen from the diagrammatic representation shown in Figure 5.4.

## 5.5 Ginzburg-Landau theory

For an effective Ginzburg-Landau (GL) free energy functional one usually neglects the Matsubara frequency dependence[13] and considers an expansion to second order in momenta $-L^{-1}(\mathbf{p},0) = r + \frac{a}{2}p^2$ with $a$ describing the stiffness to deformation. The onset of ordering occurs when the the uniform static susceptibility $1/r$ diverges and one typically finds $r \propto T - T_c$, with $T_c$ the ordering temperature[14].

In the presence of pair-hopping, $\alpha > 0$, we do expect that a finite momentum superconducting mode can be stable as well as the zero momentum one. The general expansion of $L^{-1}(\mathbf{p},0)$ around a finite momentum takes the form

$$-L^{-1}(\mathbf{Q}+\mathbf{p},0) = r_{\mathbf{Q}} + a'_{i,\mathbf{Q}} p_i + \frac{a_{i,\mathbf{Q}}}{2} p_i^2 \,. \tag{5.36}$$

where we, in general, have the possibility of the linear term $a'_{i,\mathbf{Q}}$, this term does, however, indicate that the finite-momentum $Q$ solution is unstable (since a shift of momentum can decrease the energy). Usually, when writing down phenomenological GL theories, this term is just assumed to be zero. However, the cancellation of this term for finite momenta is a subtle thing and is likely to put constraints on any model giving rise to finite-momentum superconductivity. For the pair-hopping interaction, this term will cancel due to the existence of a back-propagating Josephson like current arising since the interaction couples to the gauge field (see (6.13)). Importantly, note that the cancellation of the $a'_{i,\mathbf{Q}}$ term is a necessity for the stability of both FF, $\Delta_{\mathbf{Q}} \neq 0, \Delta_{\mathbf{Q}} = 0$, and LO, $\Delta_{\mathbf{Q}} = \Delta_{\mathbf{Q}} \neq 0$, type state. Assuming $a'_{i,\mathbf{Q}} = 0$ we write down the full GL energy functional ($F = S/\beta$)

$$\begin{aligned} F = \int_{\mathbf{p}} & r_0|\Delta_0|^2 + \frac{a_0 p^2}{2}|\Delta_0(\mathbf{p})|^2 + r_{\mathbf{Q}}|\Delta_{\mathbf{Q}}|^2 + \frac{a_{i,\mathbf{Q}} p_i^2}{2}|\Delta_{\mathbf{Q}}(\mathbf{p})|^2 + r_{-\mathbf{Q}}|\Delta_{-\mathbf{Q}}|^2 \\ & + \frac{a_{i,-\mathbf{Q}} p_i^2}{2}|\Delta_{-\mathbf{Q}}(\mathbf{p})|^2 + \int_{\mathbf{x}} \frac{u_0}{2}|\Delta_0|^4 + \frac{u_{\mathbf{Q}}}{2}|\Delta_{\mathbf{Q}}|^4 + \frac{u_{-\mathbf{Q}}}{2}|\Delta_{-\mathbf{Q}}|^4 + \gamma_{0,\mathbf{Q}}|\Delta_0|^2|\Delta_{\mathbf{Q}}|^2 \\ & + \gamma_{0,-\mathbf{Q}}|\Delta_0|^2|\Delta_{-\mathbf{Q}}|^2 + \gamma_{\mathbf{Q},-\mathbf{Q}}|\Delta_{\mathbf{Q}}|^2|\Delta_{-\mathbf{Q}}|^2 + \gamma_{0,\mathbf{Q},-\mathbf{Q}}|\Delta_{\mathbf{Q}}|^2|\Delta_{-\mathbf{Q}}|^2 \,. \end{aligned} \tag{5.37}$$

[13] This can be considered a classical limit with $T \to \infty$.

[14] For strong coupling $r$ is not determined by the temperature, but by the chemical potential, $\mu$ (see Section 7.1).

This is the basis of many phenomenological approaches and we will discuss this further in Paper D and Chapter 10.

## 5.6 The PDW instability

One of the results presented in Paper B is that (5.31) takes on a rather simple structure and that the GL theory can be characterized by a sixth order polynomial in $\mathbf{Q} = (Q_x, Q_y)$. I.e. for a given $(T, \mu, g, \alpha)$ $L^{-1}(\mathbf{Q}, 0)$ can be described by[15]

$$A(\mathbf{Q}) = r + \frac{a}{2}Q^2 + bQ_+^2Q_-^2 + \frac{c}{4}(Q_+^2 + Q_-^2)^2 + \frac{1}{6}Q^6 \tag{5.38}$$

such that the GL free energy for a finite-momentum mode[16] is given by

$$F_M = A(\mathbf{Q})|\Delta_{\mathbf{Q}}|^2 + \frac{u_{\mathbf{Q}}}{2}|\Delta_{\mathbf{Q}}|^4 \tag{5.39}$$

where $Q_\pm = \frac{Q_x \pm Q_y}{2}$. (The exact form of $L^{-1}(\mathbf{Q}, 0)$ is given, for a few examples, in Figure 4 in Appendix A of Paper B, which illustrates this behavior). Here the $Q_+ \longleftrightarrow Q_-$ symmetry is given by the specific form of $T(\mathbf{p})$, which ensures $b > 0$. We anticipate that an explicit band-structure with a high density of states directions along $p_x$ and $p_y$ may change the sign of $b$ (as a function of interaction strength) with $b < 0$ implying a "lattice-aligned" FF state. (This possibility is considered in Paper D.) Further $u > 0$, which results from the residual repulsive interaction between pairs due to the Pauli principle. However, it turns out that $r, a, c$ can have either sign, leading to a rather intricate phase diagram (see Figure 7.3**a**).

### 5.6.1 Lifshitz point

We recognize a transition from ordinary homogeneous SC to a modulated FF state through a so-called Lifshitz point [110], when $a$ changes sign and $c > 0$. In this case, the pairing momenta, $Q_+$ evolves continuously from zero. However, for $c < 0$, there is a region of coexisting minima at $Q_+ = 0$ and

[15] The term proportional to $c$ differs from what is erroneously reported in Paper B (5).

[16] Here we let GL free energy *functional* denote the situation where spatial modulations are included and GL free energy only considering uniform solutions.

$Q_+ = \pm Q_0$. The critical surfaces of these solutions meet at a line of bicritical[17] points $r = A(Q_0) = 0$ where $Q_+$ jumps.

### 5.6.2 Super-Lifshitz point

One key finding in Paper B is the possibility of a new kind of critical point, a point we call a *super-Lifshitz* point. This point occurs at the intersection between the bicritical line and the line of Lifshitz point, $a = c = 0$. The name of super Lifshitz (SL) refers to the simultaneous cancellation of higher orders in the dispersion, which leads to distinct mean-field exponents with even softer modes, $\varepsilon \sim q^6$. The correlation length mean-field exponents change from $\nu = 1/4$ to $\nu = 1/6$ when going from a Lifshitz point to a super-Lifshitz point. Correspondingly the critical exponent associated with $Q$, $Q \sim |a|^{\beta_k}$ is given by $\beta_k = 1/2$ for a Lifshitz point, and $\beta_k = 1/4$ for the SL point [111].

[17] To conclude the bicritical nature (instead of a possible tetracritical transition), one needs to consider the interaction between the homogeneous SC and finite-momentum FF solution. In general we expect a repulsive interaction between SC and FF, indicated by $\gamma(\mathbf{Q}, 0) > 0$. It turns out that the rise in interaction energy is higher than the sum of the condensation energies of the two orders ($\gamma(\mathbf{Q}, 0) > \sqrt{u(\mathbf{Q})u(0)}$). Thus there will be a first-order, bicritical transition. For details, see supplemental note of Paper B.

# 6 BCS theory and supercurrent

The defining feature of a superconductor is its ability to conduct a supercurrent, that is, a current without resistance. An important question when considering the possibility of more exotic superconducting states, like PDW, is how such a state would affect the overall phenomenology of superconducting properties. This was one main subject of Paper A.

The physics of supercurrents is a quite tricky subject with various limits and effects to take into consideration. Practically the critical current, $J_c$, is the most definitive measure of a superconductor's ability to superconduct. The critical current is the highest current a superconducting device can withstand without developing a voltage drop. However, this quantity is often dependent on the specific geometry of the device and resistance can develop in a device which is still formally a superconductor, meaning that it is still in a superconducting state (this can happen through, for instance, phase-slips and vortex drifts [92]). Furthermore, since a current induces a magnetic field, one, in general, has to consider the superconductor's resilience to a magnetic field in order to calculate the critical current. (For a discussion see Appendix D.)

A more robust quantity is the so-called *depairing* current, $J_d$. This is the current above which the condensate ceases to exist, i.e., the superconductor is forced into the normal state. Naturally, the critical current can never exceed the depairing current $J_c \leq J_d$, and we can consider it an upper estimate of the critical current. In general, we anticipate residual superconducting behavior for $J_c < J < J_d$ since local pairing correlations prevail.

## 6.1 Supercurrent and depairing current

The standard uniform current is given by the operator

$$\hat{\mathbf{J}} = \sum_{\mathbf{k}} \mathbf{v}_{\mathbf{k}} \hat{n}_{\mathbf{k}}, \quad \mathbf{v}_{\mathbf{k}} = \nabla_{\mathbf{k}} \varepsilon(\mathbf{k}). \tag{6.1}$$

where $\mathbf{v}_{\mathbf{k}}$ is the velocity of the electrons and $\hat{n}_{\mathbf{k}} = \sum_\sigma \hat{c}^\dagger_{\sigma,\mathbf{k}} \hat{c}_{\sigma,\mathbf{k}}$ the occupation operator. In a superconductor the electronic freedoms generally divide into a quasiparticle part and a condensate part, usually described by

the anomalous expectation value $\langle \hat{c}_{\downarrow,\mathbf{k}} \hat{c}_{\uparrow,-\mathbf{k}} \rangle$. With a condensate evenly distributed around zero momentum, the current will be zero. However, if the condensate acquires a finite velocity, the system will carry a supercurrent. In practice we study this by imposing a momentum shift, $\mathbf{q}_s$, of the condensate, $\langle \hat{c}_{\downarrow,\mathbf{k}} \hat{c}_{\uparrow,-\mathbf{k}} \rangle \rightarrow \langle \hat{c}_{\downarrow,\mathbf{k}+\frac{\mathbf{q}_s}{2}} \hat{c}_{\uparrow,-\mathbf{k}+\frac{\mathbf{q}_s}{2}} \rangle$, and calculate the quasiparticle spectra[1]. In general, we find a (Doppler) shifted dispersion, describing a spontaneous quasiparticle excitation current, $\mathbf{J}_e$, counter-propagating to the the condensate current, $\mathbf{J}_{co}$, such that the total current is given by $\mathbf{J} = \mathbf{J}_{co} - \mathbf{J}_e$. The existence of a finite supercurrent is a consequence of the condensate current being a quantity protected by a gap, while the quasiparticles are free to relax[2]. Increasing $\mathbf{q}_s$ eventually leads to the destruction of the supercurrent due to two separate effects; the increase of the counter-propagating quasiparticle current $\mathbf{J}_e$, and the depletion of the condensate, resulting in a smaller $\mathbf{J}_{co}$. The function $\mathbf{J}(\mathbf{q}_s)$ will therefore have a maximum, which one identifies with the depairing current $\mathbf{J}_d$ [113, 114].

## 6.2 BCS mean-field theory for finite-momentum superconductivity

Clearly, in order both to describe a supercurrent carrying homogeneous superconductor as well as PDW state, we need to be able to describe a finite-momentum state in BCS theory. To describe the propagation of electrons in the presence of a condensate is it useful to define the imaginary-time Nambu Gorkov Greens function

$$\begin{aligned} \bar{G}(\mathbf{k},\mathbf{q},\tau) &= -\langle T \hat{\Psi}_{\mathbf{k},\mathbf{q}}(\tau) \hat{\Psi}^{\dagger}_{\mathbf{k},\mathbf{q}}(0) \rangle = \\ &- \begin{bmatrix} \langle T\, \hat{c}_{\uparrow,\mathbf{k}+\mathbf{q}/2}(\tau) \hat{c}^{\dagger}_{\uparrow,\mathbf{k}+\mathbf{q}/2}(0) \rangle & \langle T\, \hat{c}_{\uparrow,\mathbf{k}+\mathbf{q}/2}(\tau) \hat{c}_{\downarrow,-\mathbf{k}+\mathbf{q}/2}(0) \rangle \\ \langle T\, \hat{c}^{\dagger}_{\downarrow,-\mathbf{k}+\mathbf{q}/2}(\tau) \hat{c}^{\dagger}_{\uparrow,\mathbf{k}+\mathbf{q}/2}(0) \rangle & \langle T\, \hat{c}^{\dagger}_{\downarrow,\mathbf{k}+\mathbf{q}/2}(\tau) \hat{c}_{\downarrow,\mathbf{k}+\mathbf{q}/2}(0) \rangle \end{bmatrix} \end{aligned} \tag{6.2}$$

where we introduced the finite-momentum Nambu-spinors

$$\hat{\Psi}^{\dagger}_{\mathbf{k},\mathbf{q}}(\tau) = [\hat{c}^{\dagger}_{\uparrow,\mathbf{k}+\mathbf{q}/2}\ \hat{c}_{\downarrow,-\mathbf{k}+\mathbf{q}/2}]. \tag{6.3}$$

[1] The current-carrying state of the superconductor is a metastable state. However, it would require a total reconstruction of the condensate to reach the ground state. This is what prevents the decay of current [112].

[2] In an ordinary metal, there is distinction between $\mathbf{J}_{co}$ and $\mathbf{J}_e$. Imposing a supercurrent is like boosting a limited part of the FS, which simply relax back to the ordinary configuration with zero current.

Assuming that $\Delta$ acquires a *single* finite expectation value for a mode with momentum $\mathbf{q}$, $\Delta(\mathbf{p},\tau)=\Delta_{\mathbf{q}}\delta(\mathbf{p}-\mathbf{q})$, i.e. an FF state or homogeneous superconducting state with current, we found the mean-field BCS action (5.20) as

$$S(\Psi,\Delta_{\mathbf{q}})=\int_0^\beta \mathrm{d}\tau\left(\sum_{\mathbf{k}}\Psi_{\mathbf{k}}^\dagger\partial_\tau\Psi_{\mathbf{k}}+H_{\mathrm{MF}}+\frac{V}{g_0T(\mathbf{q})}|\Delta_{\mathbf{q}}|^2\right) \tag{6.4}$$

with the mean-field Hamiltonian

$$\begin{aligned}\hat{H}_{\mathrm{MF}}&=\sum_{\mathbf{k}\sigma}\xi(\mathbf{k})\hat{c}^\dagger_{\mathbf{k}\sigma}\hat{c}_{\mathbf{k}\sigma}-\sum_{\mathbf{k}}\Delta_{\mathbf{q}}\hat{c}^\dagger_{\uparrow\mathbf{k}+\mathbf{q}/2}\hat{c}^\dagger_{\downarrow-\mathbf{k}+\mathbf{q}/2}+\sum_{\mathbf{k}}\Delta^*_{\mathbf{q}}\hat{c}_{\downarrow-\mathbf{k}+\mathbf{q}/2}\hat{c}_{\uparrow\mathbf{k}+\mathbf{q}/2}\\&=\sum_{\mathbf{k}}\hat{\Psi}^\dagger_{\mathbf{k},\mathbf{q}}h_{\mathbf{k},\mathbf{q}}\hat{\Psi}_{\mathbf{k},\mathbf{q}}\end{aligned} \tag{6.5}$$

where $\xi(\mathbf{k})=\varepsilon(\mathbf{k})-\mu$ and $h_{\mathbf{k},\mathbf{q}}=\tau_3\xi(\tau_3\mathbf{k}+\mathbf{q}/2)-\Delta_{\mathbf{q}}\tau_+-\Delta^*_{\mathbf{q}}\tau_-$. (Decomposition in finite-momentum Bogoliubov quasiparticles is shown i Appendix C.) Since the Hamiltonian is quadratic we can solve for the Nambu-Gorkov Greens-function exactly $\bar{G}(\mathbf{k},\mathbf{q},\tau)=-(\partial_\tau+h_{\mathbf{k},\mathbf{q}})^{-1}$,

$$\bar{G}^{-1}(\mathbf{k},\mathbf{q},i\omega)=\begin{bmatrix}i\omega-\xi(\mathbf{k}+\mathbf{q}/2) & \Delta_{\mathbf{q}}\\ \Delta^*_{\mathbf{q}} & i\omega+\xi(\mathbf{k}-\mathbf{q}/2)\end{bmatrix}. \tag{6.6}$$

We write down the (non-trivial) gap-equation (5.21) as

$$1=\frac{g_0T(\mathbf{q})}{V\beta}\sum_{\mathbf{k},i\omega}\frac{\tanh(\beta E^{(-)}_{\mathbf{k}}/2)+\tanh(\beta E^{(+)}_{\mathbf{k}}/2)}{4E_{\mathbf{k}}}, \tag{6.7}$$

where, introducing $\epsilon_\pm(\mathbf{k})=(\xi(\mathbf{k}+\mathbf{q}/2)\pm\xi(\mathbf{k}-\mathbf{q}/2))/2$,

$$E^{(\pm)}_{\mathbf{k}}=E_{\mathbf{k}}\pm\epsilon_-(\mathbf{k}),\quad E_{\mathbf{k}}=\sqrt{|\Delta_{\mathbf{q}}|+\epsilon_+(\mathbf{k})^2} \tag{6.8}$$

are the Doppler-shifted quasiparticle energies. After solving (6.7) for $\Delta_{\mathbf{q}}$, all electron correlators of the system can be written in terms of $\bar{G}$.

A finite interaction (6.7) admits solutions for a range of $\mathbf{q}$, however it is only for $\mathbf{q}=0$ that solutions exists for arbitrarily small $g_0$. This can be seen from the summand in (6.7) which diverges for $\mathbf{k}$ at the FS when $\Delta_{\mathbf{q}=0}\to 0$, since $\epsilon_+(\mathbf{k})=\xi(\mathbf{k})=0$ for $\mathbf{q}=0$. We refer to the latter as perfect nesting. This is the Cooper instability and yields a logarithmic divergence of the sum. Clearly perfect nesting is destroyed for $\mathbf{q}\neq 0$ and we need a finite $g_0$ to fulfill (6.7).

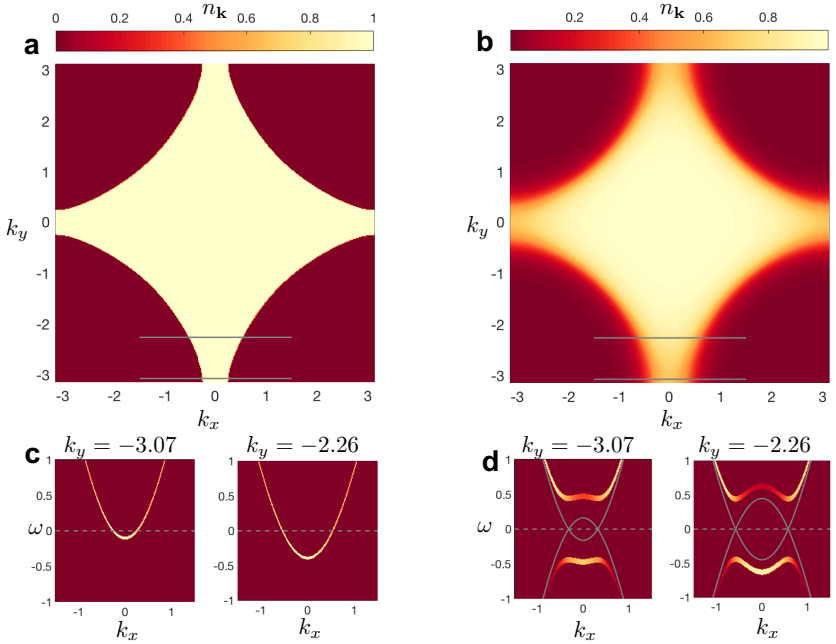


**Figure 6.1:** Electron occupation for the normal **a** and the superconducting state **b** at $T = 0$ and $n = 0.8$. The spectral function is shown in **c** (normal) and **d** (superconducting) where the latter shows a gap opening. We use the tight-binding dispersion $\xi(\mathbf{k}) = -2t(\cos(k_x) + \cos(k_y) - 4t'\cos(k_x)\cos(k_y) - \mu, t' = -0.3t, t = 1$. The gray lines in **b** and **d** shows the bare dispersions $\xi(\mathbf{k})$ and $-\xi(-\mathbf{k})$.

### 6.2.1 Generalized mean-field treatment

We have seen how to construct a BCS mean-field theory for a single-component superconducting order parameter as a saddle-point approximation of the effective superconducting action. However, the construction of a mean-field Hamiltonian can be considered more generally as a treatment to find approximate solutions to an interacting system. This view helps address the stability of the LO state (which has two order parameters) as well as imposing supercurrent in such state.

In order to find solutions to a given *full* interacting Hamiltonian, $H$, we choose to address another non-interacting mean-field (MF) Hamiltonian.

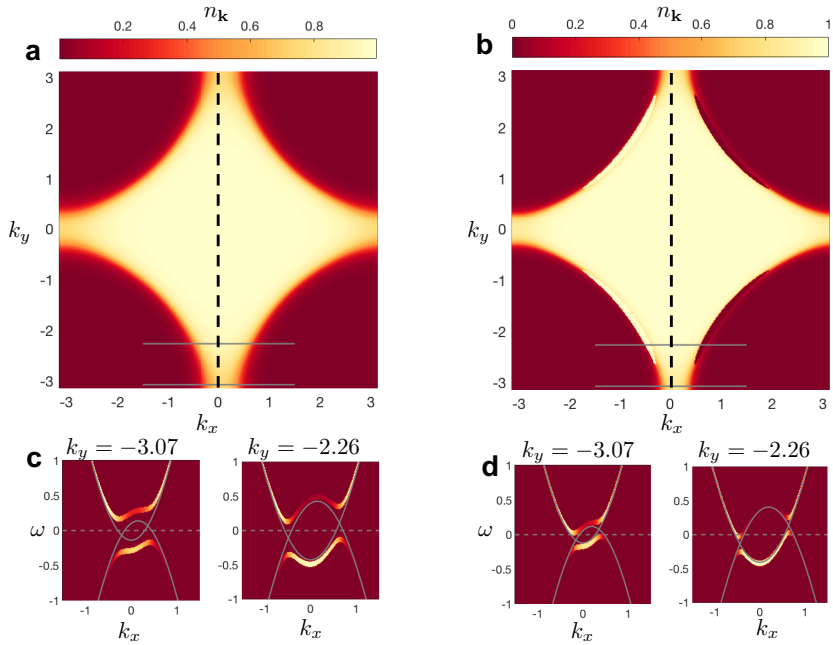


**Figure 6.2:** Electronic occupation and spectral-weight for superconducting state with finite current ($T = 0$, $n = 0.8$). Panels **a**,**b** (**c**,**d**) correspond to a condensate momentum shift $q_s = 0.15 (q_s = 0.195)$ in positive $x$ direction. In **a** the electronic occupation, $n_{\mathbf{k}}$, is shifted, yielding a finite current and **b** shows the corresponding shift in spectral function. In **c**, **d** the shift is higher and the bands touch the FS (see Figure 6.3**b**). This leads to quasiparticle excitations where particles are transfered to the trailing edge of the electronic occupation distribution in **c**. The gray lines in **b** and **d** shows the bare dispersions $\xi(\mathbf{k})$ and $-\xi(\mathbf{k}-\mathbf{q})$.

This MF Hamiltonian can be written as

$$H_{\mathrm{MF}} = \sum_i \mu_i A_i \tag{6.9}$$

where $A_i$ are a set of normal and anomalous quadratic (fermion) operators, and $\mu_i$ are variational parameters [110]. $A_i$ can be picked in whatever way is most suitable for the problem at hand. The procedure is then to pick the variational parameters in order to minimize the free energy of the full Hamiltonian

$$F_{\mathrm{MF}} = \langle H \rangle_{\mathrm{MF}} - T S_{\mathrm{MF}} \tag{6.10}$$

where $\langle ... \rangle_{\mathrm{MF}}$ indicates averages with regard to the density matrix of the MF Hamiltonian. This method relies on a theorem (see for instance [110]) that states that expectation values taken with regard to any density matrix $\rho$ will overestimate the exact free energy, $F_{\mathrm{exact}} \leq F_\rho$. Thus, we pick $\rho = \rho_{\mathrm{MF}}$, which is always possible to solve. To minimize (6.10) the variational parameters should satisfy

$$\mu_i = \frac{\partial \langle H \rangle_{\mathrm{MF}}}{\partial \langle A_i \rangle_{\mathrm{MF}}}. \tag{6.11}$$

For the mean-field treatment of the BCS Hamiltonian, this leads to the self-consistent gap equation, where $\Delta$ is a variational parameter. Importantly, stationarity implies that the full set of quadratic operators $A_i$, generated by a complete Wick decomposition of $\langle H \rangle_{\mathrm{MF}}$, should be included in the MF Hamiltonian. For example, since the LO state implies the existence of a CDW, the mean-field solutions will acquire non-vanishing expectation values of terms like $\langle \hat{c}^\dagger_{\mathbf{k}+\mathbf{q}} \hat{c}_{\mathbf{k}} \rangle$, and a self-consistent solution must then include CDW terms in $H_{\mathrm{MF}}$.

We want to consider a fixed particle number. However, we minimize the grand canonical potential, $\Omega = F - \mu N$, with fixed chemical potential $\mu$, which yields a fluctuating particle number $N$. Nevertheless, in standard fashion, the variance of the particle number vanishes in the thermodynamic limit, and this approach becomes exact. Since we want to consider solutions with the same particle number it is vital that we use $F$ and not $\Omega$ when we compare MF Hamiltonians that may require different $\mu$ for the same particle number[3].

The construction of a shifted condensate to study a supercurrent can be seen as a generalized mean-field treatment. We let the above-mentioned $\mathbf{q}_s$ be some parametrization of mean-field Hamiltonians, which yields some current, we then minimize $F$ among those solutions.

## 6.3 Homogeneous superconductor without/with supercurrent

It is instructive to study the spectral function of a superconductor since its quasiparticles are split up into hole and electron like excitations. The spec-

[3] This was the error detected in [103] that led to an underestimation of the coupling strength needed to generate a stable PDW from an ordinary nearest-neighbor interaction.

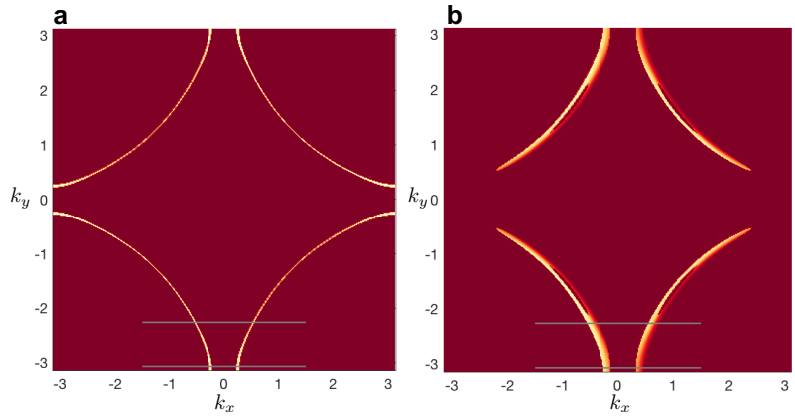


**Figure 6.3:** Spectral weight at the FS for the normal state (**a**) and superconducting state (**b**) with condensate momentum $q_s = 0.195$ (see also Figure 6.2**b**,**d**). The FS for the superconducting state with lower momentum is vanishing. (Note the similarities with the pseudogap in Figure 3.1bf c. These are indeed very "arc-like", however they are closed pockets, with low spectral weight on one side. The FF state is very similar to the current carrying state considered in this section.)

tral function is given by the imaginary part of the retarded Greens function $A(\mathbf{k},\omega) = -2\mathrm{Im}G^R(\mathbf{k},\omega)$ where $G^R = \bar{G}_{11}(\omega + i0^+)$. In Figure 6.1 we show some cuts of the spectral function for an (on-site s-wave) homogeneous superconductor $\Delta_{\mathbf{q}=0}$ alongside the occupation number $n_{\mathbf{k}} = \int \frac{\mathrm{d}\omega}{2\pi} \frac{A(\mathbf{k},\omega)}{e^{\beta\omega}+1}$ (per spin). We also included the normal state for reference.

In Figure 6.2 we show the same properties for a state with finite supercurrent $\Delta_{\mathbf{q}_s}$ using two shifts, $\mathbf{q}_s = 0.15\hat{x}$ and $\mathbf{q}_s = 0.195\hat{x}$ (in inverse lattice length). In Figure 6.2**a**, we see a shift of the occupation, indicating a current running in the positive $x$ direction, accompanied by a Doppler-shifted dispersion, shown in panel **c**. Note, however, that the spectral function does not cross the Fermi level. In contrast, for $q_s = 0.195$, shown in panel **b** and **d**, the spectral function does cross the Fermi level and quasiparticle states are occupied, clearly visible as unpaired electrons in **b**. (This corresponds to exceeding the Landau critical velocity, see Appendix D.) This does not destroy the condensate, but leads to a trailing edge of electrons in the occupation (**c**), constituting a back-propagating current. This effect can also be seen by studying the occupation near the Fermi surface, shown in Figure 6.3 for the

normal state (Figure 6.3**a**) and current-carrying superconducting state with $q_s = 0.195$ (Figure 6.3**b**), corresponding to Figure 6.2**b**,**d**.

## 6.4 The FF state and Bloch's theorem on the ground state current

From the above it is clear that formally there is no difference between a supercurrent - carrying condensate with momentum $\mathbf{q}$ and a single-component finite-momentum FF state. Both are describe by a mean-field Hamiltonian with the anomalous expectation value $\Delta_{\mathbf{q}} = \langle \hat{c}_{\downarrow,\mathbf{k}+\frac{\mathbf{q}}{2}} \hat{c}_{\uparrow,-\mathbf{k}+\frac{\mathbf{q}}{2}} \rangle$, thus from a symmetry perspective they are the same. Therefore Figure 6.2 and 6.3 also represents the spectral signatures of an FF state. The important difference is of course that the FF should be stable ground state, compared to the supercurrent carrying state which is only metastable. To conclude which state is the stable ground state we need to compare absolute energies of the states (6.5), since (6.7) only ensures locally stable $\Delta_{\mathbf{q}}$ solutions.

An obvious question then arises regarding the possibility of a FF ground state: does it carry current? Since it breaks both time-reversal and parity, it is in general expected that such a state should carry a current[4]. However, there is a theorem attributed to Bloch[5], stating that a ground state current cannot exist[6]. So in order for a stable FF state, we must make sure it does not infer a current. In the context of a Zeeman split population of spins, time-reversal symmetry is already broken, and the FF state is not current-carrying due to the unpaired quasiparticle current [33]. However, the FF-PDW spontaneously breaks time-reversal symmetry; thus, there are no trivially occurring unpaired electrons on the FS. From (6.1), the only remedy seems to be that in a crystalline system, $\mathbf{v}_{\mathbf{k}}$ is periodic and we anticipate to find a zero current solution for momentum on the order of the Brillouin zone boundary. While this could be an approach worth exploring further, it will require fine-

[4]This is in contrast to the LO state $\Delta_{\mathbf{q}} = \Delta_{-\mathbf{q}}$, which preserves parity and time-reversal, but breaks translational invariance.

[5]This theorem is sometimes confusingly called "Bloch's theorem" and should not be confused with Bloch's theorem on the particle wave-function in a periodic potential.

[6]The simplest way to understand this is to consider minimizing the energy with regard to the gauge potential, which requires $\frac{\partial H}{\partial \mathbf{A}} = 0$. This coincides with the definition of current, which then must be zero. Bloch's version of the theorem is apparently unpublished. The reader is instead referred to [115].

tuning. Furthermore, this would not yield a small momentum instability[7]. Because of this it came as a surprise when studying the Hamiltonian

$$\hat{H} = \sum_{\mathbf{k},\sigma} \varepsilon(\mathbf{k}) \hat{c}^{\dagger}_{\sigma,\mathbf{k}} \hat{c}_{\sigma,\mathbf{k}} + \frac{1}{N} \sum_{\mathbf{k},\mathbf{k}',\mathbf{q}} U(\mathbf{k},\mathbf{k}',\mathbf{q}) \hat{c}^{\dagger}_{\uparrow \mathbf{k}+\mathbf{q}/2} \hat{c}^{\dagger}_{\downarrow -\mathbf{k}+\mathbf{q}/2} \hat{c}_{\downarrow -\mathbf{k}'+\mathbf{q}/2} \hat{c}_{\uparrow \mathbf{k}'+\mathbf{q}/2} \tag{6.12}$$

in Paper A that the stable ground state turned out to be an FF state (d-wave) with a finite momentum $\mathbf{q} = \mathbf{Q}$. (Here, using (5.3) yields $U(\mathbf{k},\mathbf{k}',\mathbf{q}) = -g_0 T(\mathbf{q})[g_d(\mathbf{k}) g_d(\mathbf{k}') + g_s(\mathbf{k}) g_s(\mathbf{k}')]$, in the singlet channel, with the d-wave and extended s-wave structure factor $g_d(\mathbf{k}) = \cos(k_x) - \cos(k_y)$, $g_s(\mathbf{k}) = \cos(k_x) + \cos(k_y)$ respectively.) How come this state do not carry a current? The answer lies in that the interaction $T(\mathbf{q})$ couples to the gauge-field (or similarly does not commute with the density operator[8]) leading to a current operator of the form

$$\hat{\mathbf{J}} = \sum_{\mathbf{k},\sigma} \mathbf{v}_{\mathbf{k}} \hat{n}_{\mathbf{k},\sigma} + \frac{1}{N} \sum_{\mathbf{k},\mathbf{k}',\mathbf{q}} 2\left(\nabla_{\mathbf{q}} U(\mathbf{k},\mathbf{k}',\mathbf{q})\right) \hat{c}^{\dagger}_{\uparrow,\mathbf{k}+\frac{\mathbf{q}}{2}} \hat{c}^{\dagger}_{\downarrow,-\mathbf{k}+\frac{\mathbf{q}}{2}} \hat{c}_{\downarrow,-\mathbf{k}'+\frac{\mathbf{q}}{2}} \hat{c}_{\uparrow,\mathbf{k}'+\frac{\mathbf{q}}{2}} \,.$$

Here, in addition to the ordinary single particle term (6.1), we find an anomalous pair-hopping current that allows for the cancellation of current in the FF state (see Section III of Paper A). Note that this term is similar to a Josephson current, a current carried by pairs rather than electrons.

To study the supercurrent of an FF state then involves shifting the momentum away from the stable momentum $\mathbf{q} = \mathbf{Q} + \mathbf{q}_s$. However, studying the supercurrent of a two-component LO superconducting state $\Delta_{\mathbf{Q}} = \Delta_{-\mathbf{Q}}$ turned out to be trickier.

## 6.5 The LO state

In dealing with only one superconducting mode, we found the exact Gorkov Greens functions in (6.6). However when considering a mean-field Hamilto-

[7] Since the function $\mathbf{J}(\mathbf{q})$ generally is expected to be concave, with a maximum at the depairing current, one could imagine solutions $\mathbf{J}(\mathbf{q}) = 0$ for $\mathbf{q} > \mathbf{q}_{\mathrm{d}}$ where $\mathbf{J}(\mathbf{q}_{\mathrm{d}}) = \max_{\mathbf{q}} \mathbf{J}(\mathbf{q})$. However, these solutions will be unstable.

[8] A uniform current $\mathbf{J} = \mathbf{J}_{\mathbf{q}=0}$ can either be found from the continuity equation $\lim_{\mathbf{q}\to 0} \mathbf{q} \cdot \mathbf{J}_q = [H, \rho_{\mathbf{q}}]$ where $\rho_{\mathbf{q}} = \sum_{\mathbf{k},\sigma} c^{\dagger}_{\sigma,\mathbf{k}} c_{\sigma,\mathbf{k}+\mathbf{q}}$ or from $\mathbf{J} = \frac{\mathrm{d}H}{\mathrm{d}\mathbf{A}} |_{\mathbf{A}=0}$ where the gauge field $\mathbf{A}$ can be introduced through the Peierls substitution.

nian

$$\hat{H}_{\mathrm{MF}} = \sum_{\mathbf{k}} (\varepsilon(\mathbf{k}) - \mu)\hat{n}_{\mathbf{k}} + \sum_{\mathbf{q}=\mathbf{Q}_1,\mathbf{Q}_2} \left( \Delta^*_{\mathbf{q}}(\mathbf{k}) \hat{c}_{\downarrow,-\mathbf{k}+\frac{\mathbf{q}}{2}} \hat{c}_{\uparrow,\mathbf{k}+\frac{\mathbf{q}}{2}} + h.c. \right), \tag{6.13}$$

with two superconducting modes $\Delta_{\mathbf{Q}_1}, \Delta_{\mathbf{Q}_2}$ the system is no longer diagonalizable, unless we consider commensurate ordering vectors. Since we induce a supercurrent by shifting the momenta, we need to study general (incommensurate) periods. Thus, we need to truncate the matrix Hamiltonian. Also, the existence of two anomalous expectation values $\langle \hat{c}_{\downarrow,-\mathbf{k}+\frac{\mathbf{Q}_1}{2}} \hat{c}_{\uparrow,\mathbf{k}+\frac{\mathbf{Q}_1}{2}} \rangle$, $\langle \hat{c}_{\downarrow,-\mathbf{k}+\frac{\mathbf{Q}_2}{2}} \hat{c}_{\uparrow,\mathbf{k}+\frac{\mathbf{Q}_2}{2}} \rangle$ induce CDW fields, $\hat{\rho}_{\mathbf{Q}_{\mathrm{CDW}}} = \sum_{\mathbf{k},\sigma} \hat{c}^\dagger_{\sigma,\mathbf{k}} \hat{c}_{\sigma,\mathbf{k}+\mathbf{Q}_{\mathrm{CDW}}}$, where $\mathbf{Q}_{\mathrm{CDW}} = n(\mathbf{Q}_1 - \mathbf{Q}_2), n \in \mathbb{Z}$, as well as higher order superconducting modes, which should be included in (6.13).

In order to make approximations in a controllable way, we solved the Gorkov Greens functions, treating the $\Delta$ dependent part of (6.13) as a perturbation. In Paper A we used the notation $\mathscr{G}_{\mathbf{k},\mathbf{k}'}(\tau) = -\langle T\, \hat{c}_{\sigma,\mathbf{k}}(\tau) \hat{c}^\dagger_{\sigma,\mathbf{k}'}(0) \rangle$ for the single particle Greens function and $\mathscr{F}_{\mathbf{k},\mathbf{k}'}(\tau) = -\langle T\, \hat{c}_{\downarrow,-\mathbf{k}}(\tau) \hat{c}_{\uparrow,\mathbf{k}'}(0) \rangle$ for the anomalous one. This sets up a system of Dyson like equations including both off-diagonal $\mathscr{G}_{\mathbf{k},\mathbf{k}'}(\tau)$ and shifted $\mathscr{F}_{\mathbf{k},\mathbf{k}'}(\tau)$, consistent with CDW order and higher superconducting modes. Motivated by the small energy contribution from CDW order when using the pair-hopping interaction (see Appendix B Paper A) we neglected all off-diagonal $\mathscr{G}_{\mathbf{k},\mathbf{k}'}(\tau)$ as well as the explicit inclusion of CDW order in (6.13) (an approximation introduced in [103]).

### 6.5.1 Current induced phase-separation and mirror-symmetry breaking

To appreciate the difference between a two-component condensate and a single component condensate, we can imagine an LO state where the two components are traveling in the opposite direction, creating a standing wave pattern. One can drive current by either making one of the condensates have higher phase velocity or by making them unequal in magnitude. This gives rise to twice the amount of freedom when describing currents in the LO state, compared to the single-component superconductor.

In Paper A we considered a range of mean-field Hamiltonians given by (6.13) parametrized by $\mathbf{Q}_1 = \mathbf{Q}_0 + \mathbf{q}_1, \mathbf{Q}_2 = -\mathbf{Q}_0 + \mathbf{q}_2$, i.e. shifted from the LO-PDW ground state given by momenta $\mathbf{Q}_0$. This yields a degenerate mapping

$\mathbf{q}_1, \mathbf{q}_2 \rightarrow \mathbf{J}$, i.e., a mapping from a specific mean-field Hamiltonian to a state of a certain current. The procedure is in principle straightforward: we minimize the free energy over a subset of $\mathbf{q}_1, \mathbf{q}_2$, which corresponds to one specific current $\mathbf{J}$. In this work, we took a direct approach of simply solving for a large range of different $\mathbf{q}_1, \mathbf{q}_2$, and picking the state with the lowest energy corresponding to a certain current. This method gave Figure 6 in Paper A.

We found two new conceptual possibilities as a consequence of driving current in a superconductor with multiple orders. First, the current can induce a phase-separation between an LO current-carrying state and an FF current-carrying state (Section IV.A in Paper A). Second, a cusp can occur in the depairing current at $\theta = 0$, where $\theta$ is the angle from one crystal axis (see Section IV.B in Paper A). This cusp results from a crossing of two mirror-symmetric solutions, which are degenerate for currents running along said crystal axis. Furthermore, if the current is increased slightly, the system will spontaneously pick one of the branches, and a current will flow along one of the two transverse directions. This would imply that if the system were put on a cylindrical geometry (aligned with the crystal axis), a spontaneous current would flow along the circular direction.

# 7 Pair dynamics and the BCS-BEC crossover

Quite early after the discovery of BCS theory, it was understood that the BCS ground state provides a qualitatively correct ground state even for stronger coupling, but with the difference that the chemical potential, $\mu$, should be solved for self-consistently [96, 97] in order to account for the increasing number of fluctuating pairs. For strong enough coupling the FS will vanish, $\mu < 0$, and $T_c$ will be determined by the condensation of a Bose-Einstein condensate (BEC) [116, 99, 100]. The 2D case has been explored in the context of cuprate superconductivity using a functional integral technique [99, 101, 117], which is the method used here. Advances in optical lattices, where interaction can be tuned by utilizing the Feshbach resonance, has spurred additional theoretical investigations of the BSC-BEC crossover in recent years [118, 119].

In Section 5.5, we expressed the GL theory in terms of integrals over Greens function, explicitly assuming that we expand around an instability. The Thouless criterion gives the criterion for an instability

$$\min_{\mathbf{p}} -L^{-1}(\mathbf{p},0) = 0 \tag{7.1}$$

here including the possibility of a minimum at finite momentum $\mathbf{p}$. Usually, tuning the system to the transition point only requires changing $T$. Typically, one does need to consider that the condition on the chemical potential $\mu$ alters as the transition is approached. The chemical potential is determined by the condition of constant particle number

$$n = \frac{1}{\beta V}\frac{\partial \ln Z}{\partial \mu} = n_{\mathrm{F}} + n_{\mathrm{B}}\,, \tag{7.2}$$

where

$$n_{\mathrm{F}} = \frac{1}{\beta V}\frac{\partial \ln Z_0}{\partial \mu} = 2\int_{\mathbf{k}} \frac{1}{e^{\beta\xi(\mathbf{k})}+1}\,, \quad n_{\mathrm{B}} = \frac{1}{\beta V}\frac{\partial \ln Z_{\mathrm{GL}}}{\partial \mu}\,. \tag{7.3}$$

In Paper B we took $n_{\mathrm{B}}$ into account by considering the Gaussian fluctuations from the expansion of the pair propagators $L(\mathbf{p}, i\Omega)$ in (5.31) for zero and finite-momentum components respectively. To determine $n_{\mathrm{B}}$, we need to understand the analytic structure of $L$, which we will discuss in Section 7.2.

## 7.1 Superconducting instability in the BCS and BEC limit

To better understand the BCS-BEC crossover, we will consider the instability condition (7.1) in these two limits. The BCS limit corresponds to $\mu > 0$, while the BEC limit corresponds to $\mu < 0$. Focusing on zero momentum pairing and performing the Matsubara sum of (5.31) we find

$$L^{-1}(0,0) = d \int_{\frac{-\mu\beta}{2}}^{\frac{\varepsilon_\Lambda \beta}{2} - \frac{\mu\beta}{2}} \mathrm{d}x \frac{\tanh(x)}{2x} - \frac{1}{g} = 0 \tag{7.4}$$

where we introduced $g = g_0(1-4\alpha)$ and $d = \frac{m}{2\pi}$ as the 2D density of states. This integral is logarithmically divergent, and we introduced a cut-off $\varepsilon_\Lambda$ as the greatest energy scale. One way to interpret the need for this cut-off is to look at the corresponding scattering problem, which shows the same divergence. It turns out that we can re-express the bare coupling constant $g$ in the scattering length. In 2D there exists a bound state for arbitrarily small interactions and we can infer [120]

$$\frac{1}{dg} = \frac{1}{2} \ln\left(\frac{2\varepsilon_\Lambda}{E_b}\right) \tag{7.5}$$

where $E_b$ is the binding energy. We can use this result to express the *deep* BEC limit $\mu\beta \to -\infty$ of (7.4) as

$$\text{BEC:} \quad L^{-1}(0,0) \to -\frac{d}{2} \ln\left(\frac{2|\mu|}{E_b}\right). \tag{7.6}$$

Thus, the instability sets in for

$$\mu = -\frac{E_b}{2} \tag{7.7}$$

meaning that the binding energy of the pair has to be overcome to create fermionic excitations. This is consistent with interpreting the normal state of the BEC limit as being made up of pre-formed bosonic pairs. Further, the condition (7.7) is not temperature-dependent. Instead, the transition

temperature will be determined by the condition (7.2), which describe Bose-Einstein condensation of the pre-formed pairs.

Turning to the *deep* BCS limit, $\mu\beta \to \infty$, we instead find

$$\text{BCS:} \quad L^{-1}(0,0) \to -d\ln(T/T_{\text{MF}}) \tag{7.8}$$

with[1]

$$T_{\text{MF}} = \frac{2e^{\gamma}}{\pi}\sqrt{\xi_\Lambda|\mu|}e^{-\frac{1}{dg}}, \tag{7.9}$$

where $\xi_\Lambda = \varepsilon_\Lambda - \mu$ and $\gamma \approx 0.577$ the Euler Mascheroni constant ($\varepsilon_\Lambda > |\mu|$).

## 7.2 Pair occupation and dynamics

The (imaginary time) pair propagator $L$ is given by

$$L^{-1}(\mathbf{p}, i\Omega) = \int_{\mathbf{k}} \frac{\tanh(\beta\xi_+(\mathbf{k})/2) + \tanh(\beta\xi_-(\mathbf{k})/2)}{2(\xi_+(\mathbf{k}) + \xi_-(\mathbf{k}) - i\Omega)} - \frac{1}{g_0 T(\mathbf{p})} \tag{7.10}$$

where we introduced $\xi_\pm(\mathbf{k}) = \xi(\mathbf{k} \pm \frac{\mathbf{p}}{2})$. We have already considered the momentum dependent part $L(\mathbf{p}, i\Omega)$ in Section 5.6 and seen that it can develop local minima for finite momentum. Here we are interested in calculating the bosonic occupation number $n_{\text{B}}$. The spectral function is given by $-\text{Im}(L^R(\mathbf{p},\omega))$, where we find the retarded propagator $L^R$ by evaluating $L(\mathbf{p}, z)$ just above the real axis $L^R(\mathbf{p},\omega) = L(\mathbf{p}, \omega + i0^+)$. The typical spectral density for $\mu > 0$ and $\mu < 0$ respectively, are shown in Figure 7.1. Assuming a stable finite momentum $\mathbf{Q}$ mode, $L(\mathbf{p}, z)$ in general has a pole at $\mathbf{p} = \pm\mathbf{Q}, i\Omega = 0$, corresponding to the lowest energy bound state. For momenta away from $\mathbf{Q}$, the pole moves to finite $\Omega$. There is also a continuum of excitations given by a branch-cut for $i\Omega > -2\mu + \frac{(\mathbf{Q}+\delta\mathbf{p})^2}{4m}$. In the weak-coupling BCS limit ($\mu > 0$), this structure overlaps with the pole, which is damped out and loses its particle character. However, for strong coupling, $\mu < 0$, the branch cut and pole are separated (for small enough momenta).

[1] Ordinarily, in the BCS limit, the interaction is limited around the FS by the Debye frequency, $\omega_D$, which is typically smaller than $\mu$. In this case it would have been $\omega_D$ that occurred in the limits of (7.4) implying that we should replace $\sqrt{\xi_\Lambda|\mu|} \to \omega_D$ in (7.9). However, turning on the interaction, $\mu$ will inevitably become small, and the cut-off must be kept. Therefore, we use $\varepsilon_\Lambda$ as the greatest energy scale.

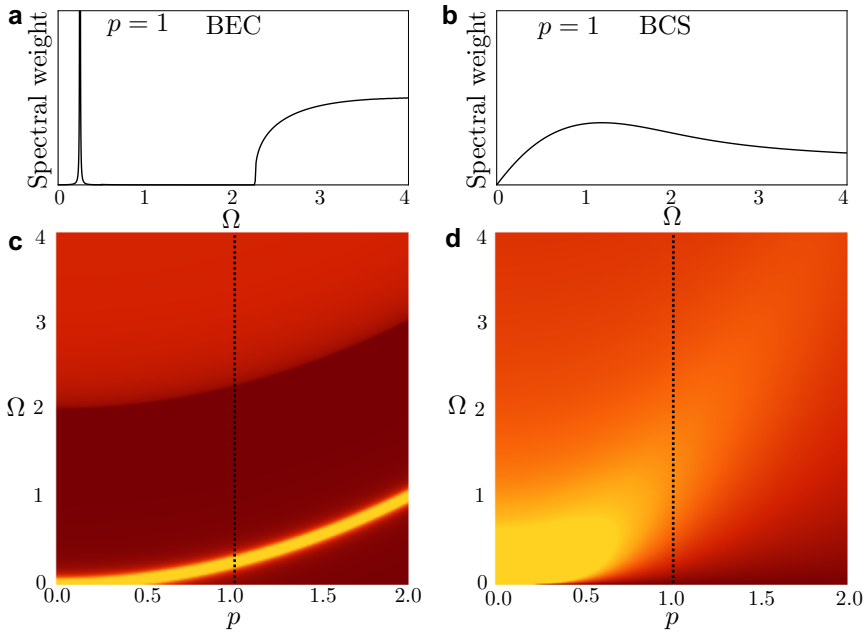


**Figure 7.1:** **c**, **d** Spectral density (in arbitrary units, lighter color corresponding to higher values) as a function of frequency and momenta for the (zero-momenta) BEC ($\mu=-1$) and BCS ($\mu=1$)limit respectively. **a** (**b**) shows the spectral weight along the dotted line in **c** (**d**), $\delta\mathbf{p}=1$. (Energies are measured in units of $(ml^2)^{-1}$ and momentum in $l^{-1}$, where $l$ is some inverse length.)

In the deep BEC limit, where $\mu=-E_b/2$, the onset of the excitation continuum can be identified with the breaking of pairs. As the binding energy increases, the branch cut becomes more separated from the pole, given by $\mathbf{p}=\pm\mathbf{Q}+\delta\mathbf{p}$, $i\Omega=\frac{\delta\mathbf{p}^2}{4m}$, and the low energy physics is well described by only keeping the freely propagating bound state. Considering $\alpha=0$,$\mathbf{Q}=0$, the pair propagator can be expressed as

$$L^{-1}(\mathbf{p},i\Omega)\approx\kappa i\Omega-(r+\frac{a_0}{2}p^2), \tag{7.11}$$

where $\kappa\in\mathbb{R}$. Using (7.3) we evaluate the bosonic occupation number

$n_{\rm B} = -\mathrm{Tr}\frac{\partial}{\partial\mu}\ln(-L^{-1})$ as

$$n_{\rm B} = 2\int_{\mathbf{q}} \frac{1}{\exp\left(\frac{q^2}{2m_{\rm p}}\right)-1}\,. \tag{7.12}$$

Here we used that $-\frac{1}{\kappa}\frac{\partial r}{\partial\mu} = 2$ (in the strong coupling limit) and introduced $m_{\rm p} = \frac{\kappa}{a_0}$ as the bosonic pair mass, reflecting the curvature at the saddle point. (A more rigors derivation of (7.12) is presented in Appendix E.) The evolution of $m_{\rm p}$ is shown in Figure 7.2**b** where it approaches the limiting value $2m$ in the strong coupling limit.

In evaluating (7.12), we do, however, run into an expected problem; there is no long-range order superconductivity in 2D. This is apparent since the integral in (7.12) diverges in 2D. However, we know there should be a transition in the Kosterlitz-Thouless (KT) sense, where the low energy state is one with quasi long-range order and a finite superfluid density. The physics of the KT-transition is lost by resorting to the Gaussian approximation. Instead, we choose to emulate the KT transition by regularizing the divergent integral by allowing the bosons to move out in the third dimension, the $z-$direction. A way to do this is by substituting $\frac{q_i^2}{2m_{{\rm p},i}} \to \frac{q^2}{2m_{\rm p}} + \frac{q_z^2}{2m_{{\rm p},z}}$, $\int \frac{\mathrm{d}^2q}{(2\pi)^2} \to \frac{2\pi}{\sqrt{\langle q_z^2\rangle}}\int\frac{\mathrm{d}^3q}{(2\pi)^3}$, where $\langle q_z^2\rangle = 2m_{{\rm p},z}T$ is the thermal expectation value of the momenta in the $z-$direction [101, 117]. With this substitution we find

$$n_{\rm B} \xrightarrow[\text{reg.}]{\text{3D}} \frac{\zeta(3/2)}{\sqrt{\pi}}Tm_{\rm p}\,. \tag{7.13}$$

Even though this expression was derived in the strong coupling limit, we use it for all coupling strengths since it yields a vanishing contribution to the particle number in the weak-coupling limit, consistent with the exact form. This is due to the vanishing of the effective mass in the weak-coupling limit (see Figure 7.2**b**), meaning that the pre-formed pairs become unimportant. However, at intermediate coupling when $\mu \sim 0$ and $n_{\rm B} \sim n_F$, there should be a substantial contribution from scattering states [121] which is not accounted for correctly in this approach. Nevertheless, since the bound state exists for all interactions in 2D (in contrast to the 3D case), there are reasons to believe that (7.13) might still give the qualitatively correct result [101].

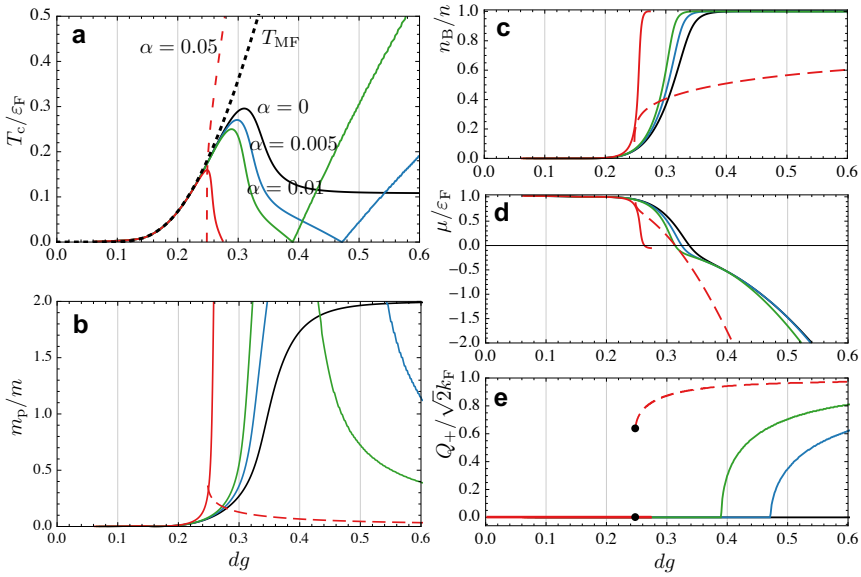


**Figure 7.2:** Evolution of the transition temperature ,$T$, (**a**) effective mass, $m_{\rm p}$, (**b**) bosonic occupation, $n_{\rm B}$, (**c**) and chemical potential, $\mu$, (**d**) across the BCS-BEC crossover for zero and finite pair-hopping $\alpha = 0, 0.005, 0.01, 0.05$. Panel **e** shows the evolution of the stable momenta ($Q_+ = (Q_x + Q_y)/2$). The onset of stable momenta (evolving from zero) occurs where the pair mass diverge (**b**) and $T_c$ suppressed to zero (**a**). For $\alpha = 0.05$ the stable solutions occur at finite momenta, $Q_x > 0$, (dashed red and marked with a black dot in **e**) and there is a coexistence region with the $Q_x = 0$ solution (solid red). The mean-field transition temperatures is plotted in dotted black in **a** for $\alpha = 0$ and should be compared with the qualitative phase diagram in Figure 4.1. This plot is also shown in Figure 7.3. (Plotted for $\varepsilon_\Lambda = 80\varepsilon_F$.)

## 7.3 The BCS-BEC crossover

We can now study the BCS to BEC crossover by simultaneously solving (7.4) and (7.2) for different interaction strengths. This is shown in Figure 7.2 where we plot $\mu, n_{\rm B}, m_{\rm p}$ and $T_c$ (for $\alpha = 0$). For weak interaction we recover the BCS results with $n = n_F, n_{\rm B} = 0, \mu = \varepsilon_F$ and vanishingly small pair mass $m_{\rm p}$. When increasing the interaction strength, pre-formed pairs become more important, corresponding to a higher $m_{\rm p}$. This leads to the occupation of bosonic modes $n_{\rm B}$, which in turn renormalizes $\mu$ to lower values. Increasing

the coupling further, the chemical potential becomes negative, $\mu < 0$ and the fermionic freedoms freeze out. At this point $n = n_{\rm B}$, and the effective pair mass saturates at $m_{\rm p} = 2m$.

Alongside the transition temperature, we plotted the mean-field transition temperature, $T_{\rm MF}$, given by (7.9). Often $T_{\rm MF}$ is interpreted as the temperature where local correlations develop, i.e., pre-formed pairs. These pairs condense first below $T_c$, where the superconducting state forms. In the BCS limit, we see that pair-formation and condensation occur simultaneously, but in the BEC, these are well separated, leading to an emergent Bose-liquid. Conceptually we can depict it as in Figure 4.1.

We should also comment on a principle difference between the 2D and 3D case for the crossover. The Cooper instability tells us that we need a finite density of states in order for a bound state to occur at an arbitrarily weak coupling. In 3D this implies the need of a FS in order to have a bound state at an arbitrary weak coupling, but a single pair of electrons do not need to form a bound state. However, in 2D, where the density of states is constant, there is always a bound state [98]. Put differently, the scattering length in 2D is always positive ($a_{2D} > 0$), while in 3D it is negative ($a_{3D} < 0$) for small interaction and a bound state ($a_{3D} > 0$) is formed only for higher interaction strengths. Therefore there exists a *unitary* point [122] in 3D, where the bound state forms $|a_{3D}| = 0$, whereas in 2D no such point exists.

### 7.3.1 Time-dependent Ginzburg-Landau functional for the BCS and BEC limit

After considering the dynamical effects, we can include time-dependence in the GL functional and consider the time-dependent Ginzburg-Landau (TDGL) functional for the limiting cases BCS and BEC. These forms highlight a few key differences between both limits. Expanding $L^{-1}(\mathbf{p}, \omega + i0^+)$ in frequency and momenta in the BCS limit we find

$$L^R(\mathbf{p}, \omega) = \frac{1}{d} \frac{1}{(\tau_0 - i\tau_0')i\omega - (\epsilon + \xi_0^2 \mathbf{p}^2)} \tag{7.14}$$

where

$$\xi_0 = \sqrt{\frac{7\zeta(3)}{32\pi^2}} \frac{v_F}{T_c}, \quad \tau_0 = \frac{\pi}{8T_c}, \quad \tau_0' = \frac{1}{4\varepsilon_F}, \quad d = \frac{m}{2\pi}, \quad \epsilon = \ln(T/T_c), \tag{7.15}$$

here $\xi_0, \tau_0$ are the BCS coherence length and time (see also [123]). Transforming back to real time and space and including the fourth order term we find the BCS TDGL-functional $S = \int_{\mathbf{x},t} \mathscr{L}_{\rm BCS}$

$$\mathscr{L}_{\rm BCS} = d\left[\epsilon|\Delta|^2 + \tau_0\Delta^*\partial_t\Delta - i\tau_0'\Delta^*\partial_t\Delta + \xi_0^2|\nabla\Delta|^2 + \frac{3\xi_0^2}{v_F^2}|\Delta|^4\right]. \tag{7.16}$$

This is an expansion in $\omega\tau_0, \omega\tau_0'$ and $\xi_0|\mathbf{p}|$, thus it is applicable for frequencies $\omega \ll \min(T_c, |\mu|)$ and spatial modulation $|\mathbf{p}| \ll T_c/v_F$.

In the BEC limit

$$\mathscr{L}_{\rm BEC} = \frac{d}{4|\mu|}\left[2|\mu|\ln\left(\frac{2|\mu|}{E_b}\right)|\Delta|^2 - i\Delta^*\partial_t\Delta + \frac{1}{2m_{\rm p}}|\nabla\Delta|^2 + \frac{1}{4|\mu|}|\Delta|^4\right] \tag{7.17}$$
$$\mu < 0, \quad m_{\rm p} = 2m,$$

which is a valid expansion if $\omega \ll E_b$ and $|\mathbf{p}| \ll \sqrt{mE_b}$. This expansion becomes increasingly better when $E_b \to \infty$, i.e. when the coupling strength increases.

The BCS limit and BEC limit describe fundamentally different physics. The BCS limit describes a damped mode since the loosely bound pairs break up into electrons, yielding dissipation. In the BEC limit the pairs are instead tightly bound, yielding the coherent propagating mode.

**Coupling to gauge field**

For most parts we do not consider the electromagnetic interactions in this work. Instead, we consider the limit of an extreme type II superconductor with the penetration depth taken to infinity $\lambda \to \infty$. In this limit all electromagnetic screening can be neglected and the charged and uncharged superfluid becomes indistinguishable. However, for completeness we note that the electromagnetic interaction can be added by including the electrostatic and vector potential $\mathbf{A}$ and $\phi$ through the minimal coupling $-i\nabla \to -i\nabla - \frac{2e}{\hbar}\mathbf{A}$ and $i\partial_t \to i\partial_t - \frac{2e}{\hbar}\phi$ where $\mathbf{B} = \nabla\times\mathbf{A}$ and $\mathbf{E} = -\partial_t\mathbf{A} - \nabla\phi$. We also need to include the electromagnetic field energy $\frac{1}{2\mu_0}\left(B^2 - \left(\frac{E}{c}\right)^2\right)$.

## 7.4 Finite-momentum BCS to BEC crossover

In Paper B, we studied the influence a finite pair-hopping $\alpha$ has on the BCS-BEC scenario. By using the same methods as described above, we solved for the coefficients, and $T, \mu, Q$, as a function of the interaction strength, $dg$, and the pair-hopping strength, $\alpha$. These results are shown alongside the $\alpha = 0$ situation in Figure 7.2 and 7.3 (Figure 1 and 3 in Paper B). This included considering the expansion of $L(\mathbf{p}, i\Omega)$ around a finite-momentum mode

$$-L^{-1}(\mathbf{Q}+\mathbf{q}, i\Omega) = r_{\mathbf{Q}} + a''_{i,\mathbf{Q}} q_i i\Omega + \frac{a_{i,\mathbf{Q}}}{2} q_i^2 , \tag{7.18}$$

instead of (7.11) when evaluating $n_{\mathrm{B}}$ (for details, see Appendix of Paper B). For this work, the term $a''_{i,\mathbf{Q}}$ can be neglected. The occurrence of this term should, however, be interesting to study in the context of electromagnetic response, since it couples electric and magnetic fields.

As described in Section 5.6 the instability towards finite-momentum state can be understood through a sixth-order polynomial in pairing momenta (5.38), where a finite-momentum state develops as a metastable solution, or the momenta develops from zero, corresponding to a Lifshits point. A nice way of summarizing the result of the BCS-BEC calculation is to identify $a \sim \text{constant} - dg$ and $c \sim \alpha_{\mathrm{SL}} - \alpha$, i.e., tuning the interaction corresponds to changing $a$, while changing the pair-hopping, $\alpha$, alters $c$. This is shown in Figure 7.3.

### 7.4.1 Diverging pair mass

When approaching the Lifshitz point, $a = 0$, the second derivative of the dispersion vanishes, which is equivalent to a diverging mass (see (5.38)). This inflection of the dispersion causes fluctuation to proliferate and drives the critical temperature to zero, $T_c = 0$, which is evident from (7.13). This is the significant finding in Paper B, and the corresponding phase diagram Figure 7.3 clearly shows the suppression of $T_c$ near the Lifshitz point. The divergence of mass is shown in Figure 7.2**b**, which also shows that the Lifshitz transition occurs on the strong coupling side (Figure 7.2**d**) with $\mu < 0$. In contrast, the transition to the metastable solution with finite momentum, in general, occurs on weak-coupling side (e.g. $\alpha = 0.05$)[2].

[2] Even if the finite-momentum solutions lose their support by becoming a saddle-point the mass only diverges in one direction implying a finite $T_c$. See Appendix of Paper B.

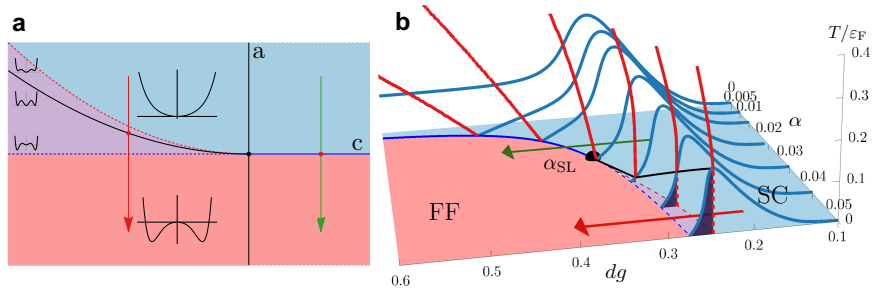


**Figure 7.3:** Finite momentum BCS-BEC crossover. **a** A simplified phase diagram based on (5.38) (for $b > 0$) which is "topological" equivalent to the full phase diagram in **b**. **b** $\alpha_{SL}$ marks the super-Lifshitz point ($a = c = 0$) where the zero and finite-momentum instability coincides. For $\alpha < \alpha_{SL}$ ($c > 0$) the transition will be through a Lifshitz-point (blue line). For $\alpha > \alpha_{SL}$ the Lifshitz-point (dashed blue) is preceded by a finite-momentum transition ($c < 0$). Note that there always exists a transition for any finite $\alpha$.

The vanishing of bosonic pair mass, together with the suppression of $T_c$, makes it possible to find an analytical expression for the location of the Lifshitz point. This line is plotted in blue (dashed blue for solutions hidden under a finite-momentum transition) in Figure 7.3. Interestingly it turns out that for all $\alpha > 0$, there exists a Lifshitz point at high enough coupling strength $dg$ (see (9) in Paper B). This establishes the possibility of a small momentum instability in a strong coupling system. It also has the more technical implication that the BCS-BEC crossover is not a crossover for $\alpha > 0$ since it necessarily contains a transition from zero to finite-momentum superconductivity[3].

[3]For a homogeneous s-wave superconductor, there is no phase-transition when moving between weak and strong coupling. For non-zero angular momenta, however, there seems to exist a transition between ungapped and fully gapped FSs [97, 124]. For spin-unbalanced Fermi gases, there is a region in the BCS limit which allows for the FFLO phase, and there is a transition to a homogeneous gas in BEC limit [125].

## 7.5 Discussion

We have seen how a finite-momentum instability should be signaled by suppression of $T_c$. That is, we approach a Lifshitz point where the mass is enhanced, leading to proliferating fluctuations (see (7.13)). The relevance of the Lifshitz point in cuprates is not immediately evident. One problem is that the Lifshitz point is an inherently strongly coupled point, i.e., the system is a BEC at the transition. Cuprates, even though they are highly correlated, do not seem to be a pure BEC since they do have a FS.

On the other hand, the bicritical line (for $\alpha > \alpha_{\mathrm{SL}}$, see Figure 7.3) might be more interesting since it can occur on the weakly coupled side. Nevertheless, the Lifshitz point might still be of relevance. A long-standing problem in cuprate superconductivity is the low $T_c$ for underdoped samples. From our results, it is natural to speculate that the suppression of $T_c$ might result from the proximity in parameter space to a Lifshitz point, even if the system does not develop a finite-momentum condensate.

For $\alpha > \alpha_{\mathrm{SL}}$, we predict a dome-like phase diagram as a function of interaction where, on one side, SC exists with sub-dominant PDW and, on the other side, we have PDW with sub-dominant SC order (see Figure 7.3). There is evidence for both of these regimes in cuprates. PDW order near vortex cores in BSCCO suggesting that suppression of SC enhances PDW order [126, 16, 21], which would be consistent with sub-dominant PDW order. At 1/8 doping in LBCO, evidence points to a 2D superconducting state, attributed to interlayer frustrated PDW [11, 14], which only at very low temperatures yields a 3D Meissner state with homogeneous SC, consistent with subdominant SC order.

# 8 Anisotropic paraconductivity

Wu et al. [23] reported a surprisingly large transverse resistivity in transport measurements on $La_{2-x}Sr_xCuO_4$ (LSCO), which was highly peaked just above $T_c$. The purpose of Paper C is to show how these measurements are consistent with the development of a highly anisotropic paraconductivity and to discuss the influence of a magnetic field. A direct discussion of the results and considerations of Paper C is left for Chapter 9. In this chapter, we will instead discuss the theory of paraconductivity, or fluctuating superconductivity. Of special interest is to derive the generalized expression for Aslamasov-Larkin expression of paraconductivity to the situation of anisotropic dynamics of the Cooper pairs $m_{\mathrm{p},x} \neq m_{\mathrm{p},y}$.

## 8.1 Phenomenology of paraconductivity

Above $T_c$, we expect some residual effect on conductivity from the superconducting state. A current is carried by excitations of the system, and as the temperature is lowered towards $T_c$, the Cooper pairs will constitute progressively lower-lying excited states. Thus, in addition to the normal conductivity channel, a Cooper pair channel will open up. This contribution is referred to as paraconductivity.

The paraconductivity is determined by the life-time of the pairs, the time before they break up into electrons. We calculated this in Section 7.3.1 from microscopic theory and found $\tau_{\mathrm{GL}} = \tau_0/\epsilon \propto \frac{\hbar}{k_B(T-T_c)}$. In light of the common Drude-expression for conductivity, $\sigma_D = \frac{nq^2\tau}{m}$, we understand that the diverging life-time will account for a progressively higher conductivity when approaching $T_c$. Indeed, in two dimensions the Aslamasov-Larkin contribution to paraconductivity [127] takes the form[1]

$$\sigma_{\mathrm{p}} = \frac{e^2}{16\hbar}\frac{T_{\mathrm{c}}}{T-T_{\mathrm{c}}}. \tag{8.2}$$

[1] The universal form of the Aslamasov-Larkin is special to 2D. In 3D it is dependent on the correlation length [128],

$$\sigma_{\mathrm{p}}^{\mathrm{3D}} = \frac{e^2}{32\xi}\sqrt{\frac{T_c}{T-T_c}} \tag{8.1}$$

(for the isotropic case).

The paraconductivity has been observed in cuprates [129, 130, 131]. In the pseudogap part of the cuprate phase diagram, where fluctuations abound over $T_c$, there are indications of nematic order, which breaks the $D_{4h}$ symmetry of the crystal. Thus, the paraconductivity is an ideal property to study anisotropic behavior in the Cooper-pair dynamics and investigating the relationship between nematicity and superconductivity.

## 8.2 Contributions to conductivity

The general relation between a current and an external gauge potential is given by

$$J_i(\mathbf{q}, \nu) = -Q^R_{ij}(\mathbf{q}, \nu) A_j(\mathbf{q}, \nu), \tag{8.3}$$

where $Q^R$ is the retarded (real frequency) London response kernel. The conductivity can be written as[2]

$$\sigma_{ij}(\mathbf{q}, \nu) = \frac{1}{-i\nu} Q^R_{ij}(\mathbf{q}, \nu). \tag{8.4}$$

The kernel $Q$ contains contributions from both normal conductivity and fluctuating conductivity. From linear response theory the Kubo formula gives an expression for $Q$ (see for instance [132])

$$Q^R_{ij}(\mathbf{q}, \nu) = \frac{ne^2}{m}\delta_{ij} - \Pi^R_{ij}(\mathbf{q}, \nu), \tag{8.5}$$

where $n$ is the particle density and $\Pi^R_{ij}(\mathbf{q}, \nu)$ is the retarded current-current correlator. We can find contributions to $Q$ by taking second momentum-derivatives of the free-energy [128]. This can be understood from noting that momentum derivatives on the greens functions introduces velocity vertex $\frac{\mathrm{d}}{\mathrm{d}\mathbf{q}} G(\mathbf{q}) = G(\mathbf{q})\mathbf{v}(\mathbf{q})G(\mathbf{q})$, generating current-current correlators.

To zeroth order in fluctuations, $F_0 = -T \ln Z_0$ (see (5.23)), and including impurity scattering, we find the normal (Drude) conductivity. Including second-order terms in $\Delta$ from the superconducting action, $F_{\mathrm{GL}} = -T \ln Z_{\mathrm{GL}}$ (see (5.23)), we find[3] the three terms shown in Figure 8.1**a**,**b** and **c**.

[2] Assuming a gauge without an electrostatic potential, $\mathbf{E} = -\partial_t \mathbf{A}$.

[3] Here we must remember that the pair propagator is dressed and that internal electron-propagators must be differentiated as well.

The first term, in Figure 8.1**a**, is the Aslamasov-Larkin (AL) expression which accounts for the contribution to conductivity from fluctuating Cooper pairs due to their direct coupling to the electromagnetic field through a velocity vertex $-\frac{\mathrm{d}L^{-1}}{\mathrm{d}\mathbf{q}}$. This vertex is mediated by electrons, which can been seen from considering the momentum derivative on the one-loop contribution to the pair propagator $L$, illustrated in Figure 8.1**d** and **e**.

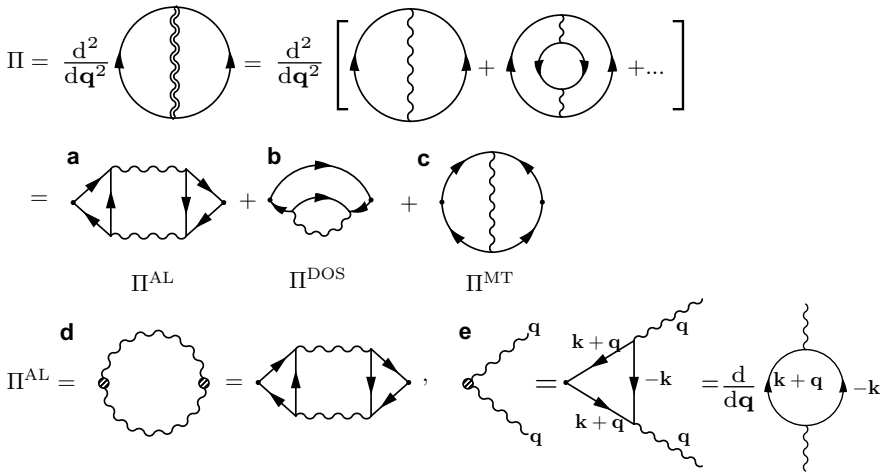


**Figure 8.1:** One-loop contribution to fluctuating conductivity. Solid lines correspond to electron propagators and wavy lines to pair propagators. The second derivative on the free energy gives the full contribution to fluctuating conductivity, which yields the AL (**a**), the DOS (**b**), and MT (**c**) contribution. **d** The AL contribution (considered in text) where the velocity vertex (shaded dot) is mediated by electrons. **d** The velocity vertex can be formed by considering a derivative on the electron-loop contribution to the pair propagator.

In addition to the AL contribution, we find the so-called density of state contribution (DOS) and the Maki-Thompson (MT) contribution, shown in Figure 8.1**b** and **c**, respectively. The DOS contribution is the intuitively most clear one; it accounts for the reduction of conductivity from the single-particle contribution. Paired-up electrons carrying charge cannot simultaneously conduct as a single-particle excitation. Thus, this contribution will be $\sigma_{\mathrm{DOS}} = -\frac{2n_{\mathrm{B}}e^2\tau}{m}$, where $n_{\mathrm{B}}$ is the number of fluctuating Cooper pairs. This contribution turns out to be less singular in $\epsilon = \frac{T-T_c}{T_c}$ than the AL contribution [128] ($\ln(\epsilon^{-1})$, rather than $1/\epsilon$) and is therefore often neglected.

The MT diagram, first considered by Maki [133], has caused some confusion in the literature since it was found that its contribution in 2D diverges. Thompson [134] resolved this problem by pointing out that the presence of a finite phase-breaking time introduces an IR cut-off in the diagram. The sensitivity to phase-breaking can be understood from its analogy to weak-localization, where instead of coherent scattering from impurities, the MT contribution comes from a coherent (Andreev) scattering of the same fluctuating Cooper pair. In HTC compounds, pair-breaking is quite high and gets suppressed by the d-wave character [135]. For cuprates, it is therefore almost always enough to only consider the AL contribution to the fluctuating conductivity when comparing to experiments [128, 129].

## 8.3 Anisotropic paraconductivity in magnetic field

In this section, we will walk through the derivation of the Aslamasov-Larkin contribution to conductivity[4]. The reason for this more detailed exposé is two-fold. First of all, we want to consider the generalized case with an anisotropic pair mass

$$\frac{1}{2m_{\mathrm{p}}}|(-i\hbar\nabla - e^*\mathbf{A})\Delta(\mathbf{x})|^2 \to \frac{1}{2m_{\mathrm{p},i}}|(-i\hbar\nabla_i - e^*A_i)\Delta(\mathbf{x})|^2\,, \tag{8.6}$$

which is used in Paper C. To the author's knowledge, no previous derivation of the case could be found in the literature. Second, the derivation contains some information about the underlying microscopic state, which is essential when exploring possible deviations from BCS predictions.

We calculate the AL contribution to the retarded current-current correlator in (8.5) by analytically continuing the imaginary-frequency expression

$$\Pi_{ij}(\mathbf{q}, i\nu_m) = \frac{1}{V\beta}\langle J_i(\mathbf{q}, i\nu_m)J_j(-\mathbf{q}, -i\nu_m)\rangle \tag{8.7}$$

where $i\nu_m = i2\pi m/\beta$ (we will use $i\nu$ for short) is a bosonic Matsubara frequency. The current $J_i$, refers to the unperturbed state

$$J_i(\mathbf{r}, t) = \frac{e^*}{2m_{p,i}}(\psi^\dagger(\mathbf{r}, t)\hat{\pi}_i\psi(\mathbf{r}, t) + (\hat{\pi}_i\psi(\mathbf{r}, t))^\dagger\psi(\mathbf{r}, t)) \tag{8.8}$$

[4]The derivation follows the development in [128].

with the kinematic momenta $\hat{\pi} = \hat{p}_i - e^* A_i$, where $A_i$ is the equilibrium gauge potential.

We are interested in the direct current (DC) and will consider the $\mathbf{q} \to 0$, $\nu \to 0$ limit. We set $\mathbf{q} = 0$ and drop the momentum label. The DC current must be finite in a non-superconducting state. This means that the total contribution to $Q$ (8.4) must vanish for $\nu \to 0$. Thus, we can write the AL contribution to the DC conductivity as

$$\sigma_{ij} = \lim_{\nu \to 0} \frac{1}{i\nu} \Big( \Pi^R_{ij}(\nu) - \Pi^R_{ij}(0) \Big). \tag{8.9}$$

Moreover, we are interested in the case with an equilibrium magnetic field pointing out of the $xy$-plane (using the gauge $\mathbf{A} = (0, Bx, 0)$). The basis functions to this system take the form of quantized cyclotron orbits, so-called Landau orbits. These functions are discussed in Appendix F. The $\mathbf{q} = 0$ current in the Landau-basis is given by the expression

$$J_i(i\nu) = \frac{e^*}{m_{\mathrm{p},i}} \frac{1}{\beta} \sum_{i\omega, \mathbf{k}_\perp} \sum_{n'n} \langle n | \hat{\pi}_i | n' \rangle c^\dagger_{n, \mathbf{k}_\perp}(i\omega + i\nu) c_{n', \mathbf{k}_\perp}(i\omega) \tag{8.10}$$

where $|n\rangle = c^\dagger_{n, \mathbf{k}_\perp} |0\rangle$ is the normalized basis state for the $n$th Landau level and $\mathbf{k}_\perp = (k_y, k_z)$. The current-current correlator takes the form (the corresponding diagram is shown in Figure 8.1**a**)

$$\Pi_{ij}(i\nu) = \frac{4e^2}{m_{\mathrm{p},i} m_{\mathrm{p},j}} \frac{1}{V\beta} \sum_{i\omega, \mathbf{k}_\perp} \sum_{n,n'} \pi_i^{nn'} \pi_j^{n'n} L_{n,k_z}(i\omega + i\nu) L_{n',k_z}(i\omega) \tag{8.11}$$

where we introduced the shorthand notation $\pi_i^{nn'} = \langle n | \hat{\pi}_i | n' \rangle$ and $L_{n,k_z}(i\omega_n)$ is the pair propagator $\hat{L}$ in the Landau basis. We can find the retarded propagator as in Section 7.3.1 and we write it as $\hat{L}^R(\omega) = (\gamma i\omega - \hat{H})^{-1}$, where $\gamma$ is in general complex and the *anisotropic* Hamiltonian is given by

$$\hat{H} = \eta\epsilon + \frac{\hat{\pi}_i^2}{2m_{\mathrm{p,i}}}, \tag{8.12}$$

where the constant $\eta$ carries unit energy[5]. This operator is diagonal in the Landau basis and we find[6] $L^R_{n,k_z}(\omega) = (\gamma i\omega - \varepsilon_n(k_z))^{-1}$ with $\varepsilon_n(k_z) =$

[5] Following the derivation in Section 7.3.1 $\eta = \frac{1}{da^2}$, i.e. the inverse density of states per unit-cell. However, this constant drops out of the calculation.

[6] We introduce a third $z$ direction as a regularization of the two-dimensional calculation. The two-dimensional limit will be taken in the end of the calculation.

$\eta\epsilon + \frac{k_z^2}{2m_{\mathrm{p,z}}} + \omega_c(n+1/2)$. These energies are independent of $k_y$, with $N_{\mathrm{Lan.}} = \frac{L_x L_y e|B|}{\pi}$ degenerate states (see Appendix F).

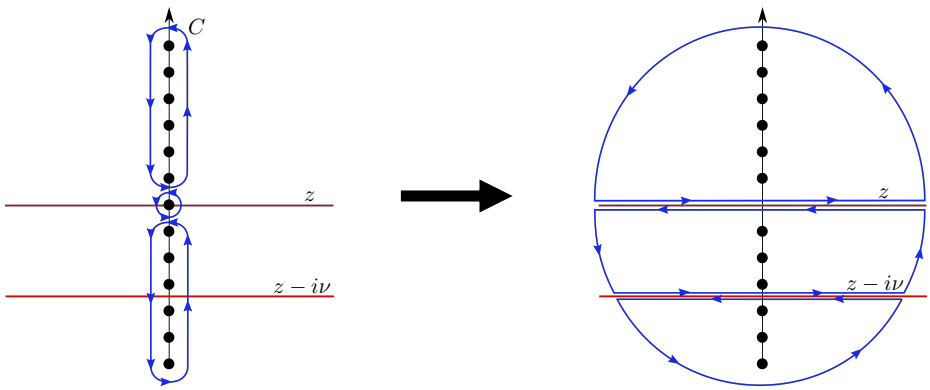


**Figure 8.2:** Deformation of the contour $C$ used to calculate the Matsubara sum in (8.13). Poles of $f_B(z)$ is marked with a black dot and non-analytic regions of $L_n(z+i\nu)L_{n'}(z)$ is marked in red. Note that the $i\omega = 0$ term in the sum of (8.13) cancel the pole occurring on the real axis of $f_B(z)$. We marked this by removing the pole at $z = 0$.

The Matsubara sum in (8.11) can be evaluated by the following integral (dropping the $k_z$ index)

$$\begin{aligned} I_{nn'}(i\nu) &= \frac{1}{2\pi i}\oint_C \mathrm{d}z\, f_B(z) L_n(z+i\nu) L_{n'}(z) \\ &= \frac{1}{\beta}\sum_{i\omega} L_n(i\omega + i\nu) L_{n'}(i\omega) \end{aligned} \tag{8.13}$$

where the contour $C$ (depicted in Figure 8.2) encloses all poles of $f_B(z) = \frac{1}{e^{\beta z}-1}$ along the imaginary axis. The propagator $L_n(z)$, at first defined for the Bosonic Matsubara frequencies, is non-analytic along the real line. We can analytically continue $L_n(z)$ to the upper and lower half plane, which will be the retarded and advanced propagator, $L_n^R(z), L_n^A(z)$, respectively. At the real axis these two can be related by complex conjugation $L_n^A(\omega) = (L_n^R(\omega))^*$. We therefore deform the contour according to Figure 8.2. Following Jordan's Lemma the circular part of the contour tends to zero as $|z| \to \infty$. Using the corresponding analytic function in each designated part of the complex

plane, the integral takes the form

$$\begin{aligned} I_{nn'}(i\nu) = &\frac{1}{2\pi i}\int_{-\infty}^{\infty} \mathrm{d}\omega f_B(\omega) L^R_n(\omega+i\nu)(L^R_{n'}(\omega)-L^A_{n'}(\omega)) \\ &+\frac{1}{2\pi i}\int_{-\infty}^{\infty} \mathrm{d}\omega f_B(\omega) L^A_{n'}(\omega-i\nu)(L^R_n(\omega)-L^A_n(\omega)). \end{aligned} \tag{8.14}$$

Here we shifted the variable with $i\nu$, using the periodicity of $f_B(z)$, in the last integral. It is convenient to symmetrize and anti-symmetrize the indices in the current-current correlator. As will be discussed in Section 9.1, the anti-symmetric component is related to the rotational invariant Hall response. Since the mass tensor is a symmetric object, the introduction of anisotropy does not alter the Hall response, and we leave out the treatment of this part and refer to other works [128]. Here we proceed with the symmetric component, using the notation $(ij) = (ij+ji)/2$. Analytically continuing to the upper half plane we find

$$\Pi^R_{(ij)}(\nu) = \frac{4e^2}{m_{\mathrm{p},i}m_{\mathrm{p},j}}\frac{1}{V}\sum_{\mathbf{k}_\perp}\sum_{n,n'} \pi_i^{nn'}\pi_j^{n'n} I^R_{(nn')}(\nu), \tag{8.15}$$

$$\begin{aligned} I^R_{(nn')}(\nu) = &\frac{1}{4\pi i}\int_{-\infty}^{\infty} \mathrm{d}\omega f_B(\omega)(L^R_n(\omega+\nu)+L^A_n(\omega-\nu))(L^R_{n'}(\omega)-L^A_{n'}(\omega)) \\ &+(n\longleftrightarrow n'), \end{aligned} \tag{8.16}$$

where the $ij$ index symmetrization has moved to the Landau index, $nn'$, in the Matsubara integral. Focusing on $ij = xx$ and using $L^R_n(\omega)-L^A_n(\omega) = 2i\mathrm{Im}(L^R_n(\omega))$ we can express (8.9) by expanding (8.16) for small $\nu$

$$\begin{aligned} &\sigma_{xx} = \\ &i\frac{8e^2}{m^2_{\mathrm{p},x}}\frac{1}{V}\sum_{\mathbf{k}_\perp}\sum_{nn'} \pi_x^{nn'}\pi_x^{n'n}\frac{1}{2\pi i}\int_{-\infty}^{\infty}\mathrm{d}\omega f_B(\omega)\frac{\mathrm{d}}{\mathrm{d}\omega}\left(\mathrm{Im}(L^R_{n'}(\omega))\mathrm{Im}(L^R_n(\omega))\right) \end{aligned} \tag{8.17}$$

where the $\nu = 0$ term has canceled. The integral can be simplified further by partial integration, moving the derivative to $f_B(\omega)$. So far no approximations

have been made. However, to proceed we note that the most important contributions are the one which are most singular in $\epsilon = \frac{T-T_c}{T_c}$, which comes from parts of the integral where $\omega \sim T - T_c$. Thus, near $T_c$, where $(T-T_c)/T$ is small, we expand $\frac{\mathrm{d}}{\mathrm{d}\omega} f_B(\omega)$ for small $\beta\omega$. Using $\mathrm{Im}(L_n^R(\omega)) = -\mathrm{Re}(\gamma)\omega L_n^R(\omega) L_n^A(\omega)$

$$\begin{aligned}\sigma_{xx} = i\frac{\mathrm{Re}(\gamma)^2}{\beta}\frac{8e^2}{m_{\mathrm{p},x}^2}\frac{1}{V}\sum_{\mathbf{k}_\perp}\sum_{nn'}\pi_x^{nn'}\pi_x^{n'n}\times \\ \frac{1}{2\pi i}\int_{-\infty}^{\infty}\mathrm{d}\omega L_n^R(\omega)L_{n'}^R(\omega)L_n^A(\omega)L_{n'}^A(\omega).\end{aligned} \tag{8.18}$$

To solve the integral we can close the contour in the upper half plan, where $L_n^A(z)$ has poles at $z_n = i\varepsilon_n/\gamma^*$

$$\sigma_{xx} = \frac{\mathrm{Re}(\gamma)|\gamma|^2}{\beta}\frac{4e^2}{m_{\mathrm{p},x}^2}\frac{1}{V}\sum_{\mathbf{k}_\perp}\sum_{nn'}\frac{\pi_x^{nn'}\pi_x^{n'n}(\varepsilon_n+\varepsilon_{n'})}{\varepsilon_n\varepsilon_{n'}|\gamma\varepsilon_n+\gamma^*\varepsilon_{n'}|^2} \tag{8.19}$$

following a symmetrization in the sum. Using the matrix elements of the Landau levels we find (see Appendix (F.4))

$$\sigma_{xx} = \frac{\mathrm{Re}(\gamma)|\gamma|^2}{\beta}\frac{4e^2\omega_c}{m_{\mathrm{p},x}}\frac{1}{V}\sum_{\mathbf{k}_\perp}\sum_{n=0}\frac{(n+1)(\varepsilon_{n+1}+\varepsilon_n)}{\varepsilon_n\varepsilon_{n+1}|\gamma\varepsilon_n+\gamma^*\varepsilon_{n+1}|^2}. \tag{8.20}$$

Since the energy is independent of $k_y$ the sum results in $N_{\mathrm{Lan.}}$. Regarding the $k_z$ sum we have not used any information about the dispersion in the $z$-direction yet. For cuprates it is natural to consider a layered structure, and appeal to a Lawrence-Doniach model [92]. Here the dispersion in the $z$-direction takes the form of $r(1-\cos(k_z s))$, where $r$ sets the coupling strength, and $s$ is the distance between each layer. Considering very weakly coupled layers $r \to 0$, corresponding to a 2D limit, no dependence on $k_z$ remains, and we replace $\frac{1}{L_z}\sum_{k_z} = \int_{-\pi/s}^{\pi/s}\frac{\mathrm{d}k_z}{2\pi} \to 1/s$

$$\sigma_{xx} = \frac{\mathrm{Re}(\gamma)|\gamma|^2}{\beta}\frac{2e^2\omega_c^2}{\pi s}\sqrt{\frac{m_{\mathrm{p},y}}{m_{\mathrm{p},x}}}\sum_{n=0}\frac{(n+1)(\varepsilon_{n+1}+\varepsilon_n)}{\varepsilon_n\varepsilon_{n+1}|\gamma\varepsilon_n+\gamma^*\varepsilon_{n+1}|^2}. \tag{8.21}$$

Usually, when performing the Landau-sum, one assumes that the dynamics is completely relaxational, and $\gamma$ is taken to be real. This can be motivated from

the BCS values $\gamma = \gamma' + i\gamma'' = \eta\left(\frac{\pi}{8k_B T_c} - i\frac{1}{4\epsilon_F}\right)$, thus $|\gamma''/\gamma'| = 2T_c/\pi T_F$, which is very small for any conventional superconductor. However, in the interest of discussing a non-BCS like scenario, with the possibility of anomalous relaxation dynamics, we will expand in $\upsilon = \gamma''/\gamma'$. Evaluating the sum to second order in $\upsilon$ (see Appendix F.1) and reinserting factors of $\hbar$, we find

$$\begin{aligned}\sigma_{xx} =& \frac{e^2}{2\hbar}\frac{1}{s\epsilon}\sqrt{\frac{m_{\mathrm{p},y}}{m_{\mathrm{p},x}}}\left(F_1\left(\frac{\epsilon}{2b}\right) - \upsilon^2 F_2\left(\frac{\epsilon}{2b}\right)\right)\frac{\gamma'(1+\upsilon^2)}{\gamma_{\mathrm{BCS}}} + \mathcal{O}(\upsilon^4)\\ F_1(x) =& x^2\left(\psi\left(x+\frac{1}{2}\right) - \psi(x) - \frac{1}{2x}\right)\\ F_2(x) =& F_1(x) - \frac{2x\psi'(x) + x^2\psi''(x))}{8}\end{aligned} \tag{8.22}$$

and $\sigma_{yy} = \sigma_{xx}\frac{m_{\mathrm{p},x}}{m_{\mathrm{p},y}}$. Here $b = \frac{\hbar\omega_c}{2\eta} = B/B_{c2}$ with $B_{c2} = \frac{\hbar}{2e\xi_{0,x}\xi_{0,y}}$, $\xi_{0,(x,y)} = \frac{\hbar^2}{2m_{\mathrm{p},(x,y)}\eta}$ is the upper critical field, $\psi(z)$ is the Digamma function(F.7), and we introduced $\gamma_{\mathrm{BCS}} = \frac{\eta\pi}{8k_B T_c}$. To unravel the result we note that the last factor, $\gamma'(1+\upsilon^2)/\gamma_{\mathrm{BCS}} \to 1$ for $\gamma \to \gamma_{\mathrm{BCS}}$, i.e. in the BCS limit. In the zero field limit $b \to 0 \Rightarrow x \to \infty$ we have $F_1(x) \to 1/8$ and $F_2(x) \to 0$. Further $F_1(x) \to x/2$ for $x \to 0$. Thus, in the zero-field ($h = 0$) BCS limit

$$\begin{aligned}\sigma_{xx} &= \frac{e^2}{16\hbar s}\frac{1}{\epsilon}\sqrt{\frac{m_{\mathrm{p},y}}{m_{\mathrm{p},x}}}\\ \sigma_{yy} &= \frac{e^2}{16\hbar s}\frac{1}{\epsilon}\sqrt{\frac{m_{\mathrm{p},x}}{m_{\mathrm{p},y}}}.\end{aligned} \tag{8.23}$$

The high-field limit expression takes the form

$$\sigma_{xx} \to \frac{e^2}{4\hbar s}\frac{1}{b}\sqrt{\frac{m_{\mathrm{p},y}}{m_{\mathrm{p},x}}}, \quad b \gg \epsilon\,. \tag{8.24}$$

In the isotropic case $m_{\mathrm{p},x} = m_{\mathrm{p},y}$ (8.23) coincides with the already stated Aslamasov-Larkin expression (8.2). The inclusion of anisotropy, which is key to the work in Paper C, takes a very simple form, only dependent on the quotient of masses.

### 8.3.1 Magnetoresistivity

The inclusion of a magnetic field has two distinct effects on the conductivity. First and foremost it induces a shift in $T_c$. This can be seen from the removal

of the zero-field divergence at $\epsilon = 0$ since $\frac{1}{x}F_1(x)$ and $\frac{1}{x}F_2(x)$ in (8.22) are finite for $x = 0$. Instead the divergence occur at $x = -1/2$, yielding an exponential suppression of $T_c$ from the zero field value to

$$T_c(B) = T_c(B=0)e^{-B/B_{c2}}. \tag{8.25}$$

Physically, this is all very sound and expected from the general competition of superconductivity and magnetic field. However, it is quite fascinating to see this effect enter at this level of analysis. In writing the GL functional, the divergence of superconducting susceptibility is included explicitly, with no additional information on the underlying origin of $T_c$. Still, a correction is added to this seemingly robust model, where one singularity is removed and another is added.

The second effect is that of magnetoresistivity. In the presence of a magnetic field, the resistivity is generally expected to increase. This can be seen as an effect of the tendency for circulating currents, which effectively localizes the particles. Including the first non-vanishing contribution to magnetoresistivity from $\gamma''$, corresponding to the $F_2(x)$ term, leads to additional suppression of conductivity (even though the overall conductivity increases due to $\gamma''$). This is consistent with the physical picture of $\gamma''$ describing a coherent propagation. The pairs tend to get stuck in the Landau orbits.

### 8.3.2 2D limits

We treated the sum over $k_z$ in the limit of uncoupled layers; this led to the expression in (8.21), which is essentially 2D but normalized with the layer thickness $s$. Note that this limit is also approached for a bulk sample of a layered material, meaning that the layers carry the current individually. Another 2D limit is given by considering increasingly thinner films, $L_z \to 0$, which is not necessarily layered internally. As the sample becomes progressively thinner, the energies associated with higher modes ($k_z = \pi n/L_z$) increase and become well separated. Thus, only the $n = 0$ mode contribute in this limit and we replace $\frac{1}{L_z}\sum_{k_z} \to \frac{1}{L_z}$, i.e. $s$ in (8.21) is replaced with $L_z$. Physically the situation is clear; we either consider one layer, or a stack of layers in parallel, with the latter leading to higher conductivity.

The validity of these two limits depends on the coherence length in the $z$-direction $\xi_z$, which sets the smallest length scale over which the wavefunction varies. The 2D layered limit holds if $\xi_z \ll s$, which implies uncorre-

lated layers. Close to $T_c$, where $\xi_z$ diverges, this condition is violated, and a crossover to a 3D expression is anticipated (see [129]). However, for a finite sample, the bulk 2D limit, $\xi_z \gg L_z$, is eventually encountered sufficiently close to the transition. Thus, for thin samples made up of a small number of layers, the 3D limit is likely not observed. In Paper C, we considered thin, 20 layers ($L_z = 20s$) of LSCO and we used the layered expression (8.23) (with $s = 13.2$ Å) and found no significant deviation, even though a crossover from $s \to L_z$ is anticipated close enough to the transition.

# 9 LSCO — The nematic fluctuating superconductor

Paper C is based on transports experiments on $La_{2-x}Sr_xCuO_4$ (LSCO) done by the Božović group at Brookhaven National Laboratory, following a previous study by Wu et al. [23]. The experiments are set up as a sunflower configuration of Hall bars with different orientation to the crystallographic axes (see Figure 9.1**a**). The bars were manufactured out of the same thin film of LSCO and display a transverse resistance that depends on the orientation, in a way nominally consistent with the in-plane response of an orthorhombic crystal (see (9.2) below). However, a tetragonal substrate constrains the crystal, and the anisotropy is instead attributed to the development of electronic nematic order.

The transverse resistivity is highly peaked just above $T_c$, indicating that the nematicity is connected to superconductivity (see Figure 9.1). In Paper C, we show that the signal in the transverse response can be accounted for by the onset of *anisotropic* paraconductivity, consistent with the form presented in (8.23). In order to quantitatively account for the measured response, the paraconductivity must be highly anisotropic, in contrast to the normal conductivity, which remains substantially isotropic. Also, Paper C includes transport measurements done in the presence of a magnetic field, showing suppression of the transverse resistivity, consistent which a superconducting origin.

Paper C contains a quite detailed discussion about how anisotropy can be extracted from fitting a model to experimental data. The same model was used to show consistent behavior with measurements in magnetic fields. In this chapter, we discuss a more tractable and simplified model that qualitatively accounts for the effects. Furthermore, we include a discussion of the nematic state seen in LSCO. In particular, one bewildering observation in this study is that the nematic director of the electronic order seems to be unpinned and unrelated to the crystal axis, varying both with doping and temperature (see Figure 9.1) [23]. In Paper C, this was attributed to two Ising nematic fields, $xy$ and $x^2-y^2$. In general, this leads to a normal and superconducting conductivity component with a director not aligned with the crystal axis nor each other. The two nematic fields can also account for the twist of the total conductivity director as a function of temperature. The

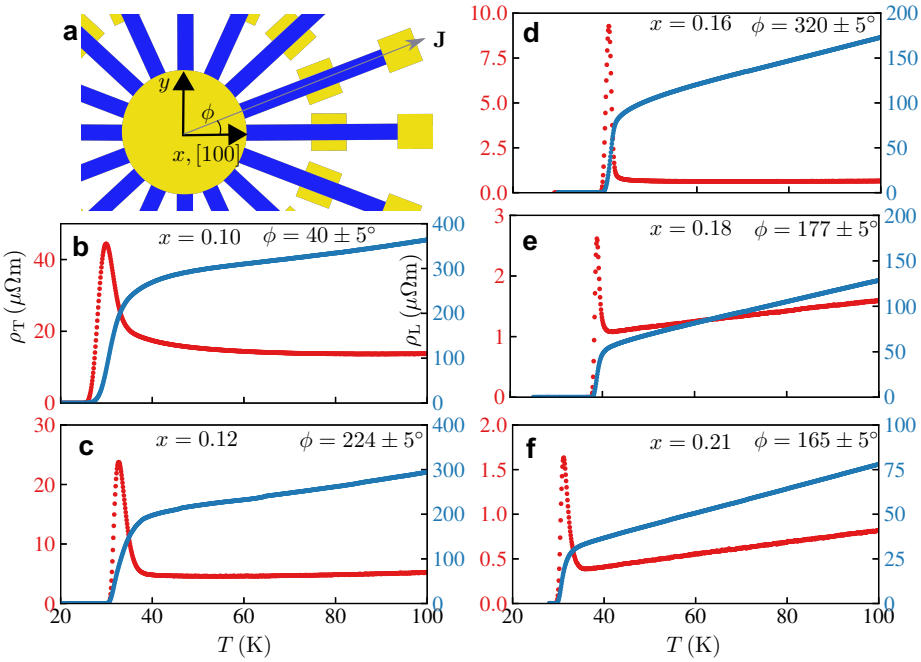


**Figure 9.1:** **a** Experimental setup of Wu et. al [23] and Paper C. Etched out "Hall bars" of LSCO (blue) with gold contacts (yellow). **b–f** Longitudinal (blue dots) and transverse resistance (red dots) for various dopings, recreated from [23]. Each sample is measured along the angle $\phi$ to the crystal axes (**a**).

system is tuned from being dominated by the superconductor near $T_c$, to that of the normal state at higher temperatures. Here we will comment on this proposal and discuss the origin of nematicity leading up (and including some) of the work of Paper D.

## 9.1 Conductivity in 2D

A general in-plane conductivity takes the form of a $2\times 2$ tensor, which can be decomposed according to its transformation under rotation,

$$\bar{\sigma} = \sigma_0 \bar{I} + i\sigma_H \bar{\tau}_2 + \bar{\sigma}^S = \begin{bmatrix} \sigma_0 + \sigma_1^S & \sigma_H + \sigma_2^S \\ -\sigma_H + \sigma_2^S & \sigma_0 - \sigma_1^S \end{bmatrix} \tag{9.1}$$

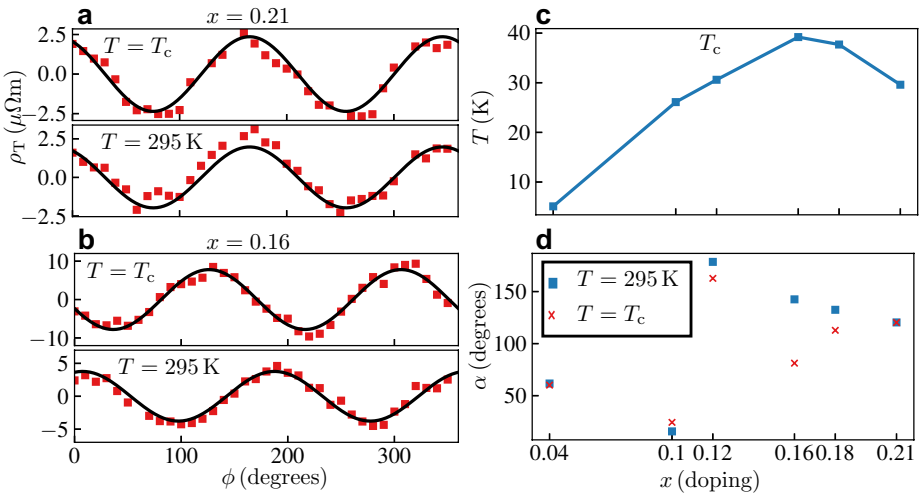


**Figure 9.2:** **a**,(**b**) Fit of measured transverse resistivity on $x = 0.21$ ($x = 0.16$) sample as a function of angle, (9.2), for $T = 295\,\mathrm{K}$ and just above $T_c$. **c** Critical temperature extracted from Figure 9.1. **d** The nematic director, $\alpha$, at $T = 295\,\mathrm{K}$ $T = T_c$, fitted from the angular fit in **a**, **b**.

where the trace $\sigma_0 = \frac{\sigma_{xx}+\sigma_{yy}}{2}$ and the Hall part $\sigma_H = \frac{\sigma_{xy}-\sigma_{yx}}{2}$ are left invariant under rotation, while $\bar{\sigma}^S = \sigma_1^S \bar{\tau}_3 + \sigma_2^S \bar{\tau}_1$, $\sigma_1^S = \frac{\sigma_{xx}-\sigma_{yy}}{2}, \sigma_2^S = \frac{\sigma_{xy}+\sigma_{yx}}{2}$ transforms as a traceless symmetric tensor. Here $\bar{\tau}_i, i = 1,2,3$ and $\bar{I}$ are the Pauli matrices and the identity matrix respectively. Driving a current $\mathbf{J}$ will in general induce a voltage drop both in the longitudinal, and transverse direction. Defining the longitudinal and transverse resistivity as $\rho_\mathrm{L} = \mathbf{E}\cdot\mathbf{J}/|\mathbf{J}|^2$, $\rho_\mathrm{T} = \hat{z}\cdot\mathbf{E}\times\mathbf{J}/|\mathbf{J}|^2$, we find

$$\begin{aligned} \rho_\mathrm{L}(\phi) &= \frac{\sigma_0 + \sqrt{|\det(\bar{\sigma}^S)|}\cos(2(\phi-\alpha))}{(\sigma_H)^2 + \sigma_0^2 + \det(\bar{\sigma}^S)}, \\ \rho_\mathrm{T}(\phi) &= \frac{\sigma_H + \sqrt{|\det(\bar{\sigma}^S)|}\sin(2(\phi-\alpha))}{(\sigma_H)^2 + \sigma_0^2 + \det(\bar{\sigma}^S)}, \end{aligned} \tag{9.2}$$

where $\phi$ is the angle between the current and $x$-axis, and $\alpha = \frac{1}{2}\arctan\left(\sigma_2^S/\sigma_1^S\right)$ is the angle of the principal axis, for which $\bar{\sigma}^S$ is diagonal. The longitudinal component is finite (for all non-superconducting systems) since it contains the rotational invariant trace $\sigma_0$. The transverse resistivity can occur for two

reasons. One, a finite antisymmetric component $\sigma_H$ due to the presence of a magnetic field, which is the famous Hall effect. Two, the appearance of a traceless symmetric component $\bar{\sigma}^S$, which is only finite in a system with $x-y$ anisotropy. Thus, a clear signature of an $x-y$ asymmetry is the development of a transverse resistivity. Even in the presence of a magnetic field, the effect is distinguishable from a finite $\sigma_H$ since this is rotationally invariant and tunable with a magnetic field, while $\bar{\sigma}^S$ is not[1].

## 9.2 Nematic order

In Figure 9.2 the transverse resistivity data of Wu et. al [23] is shown. These measurements are consistent with a conductivity described by (9.2) (in absence of a magnetic field, $\sigma_H = 0$), with $\rho_T(\phi) \propto \sin(2(\phi-\alpha))$. The angle is measured with respect to one of the crystallographic axes. In an orthorhombic crystal, the principal axes should lie along the diagonals $\alpha = \pm 0, \pm\pi/4, \pm\pi/2$. Here, however, $\alpha$ is changing with temperature and doping, seemingly unrelated to the crystal frame (see Figure 9.1).

Let us consider the symmetry of a *nematic* order associated with (9.2). Nematic order is in general described by a traceless symmetric tensor [49]. From (9.1) we identify *conductivity-nematic* order $\overline{N}$ with $\bar{\sigma}^S$

$$\overline{N} = \begin{bmatrix} N_{11} & N_{12} \\ N_{12} & -N_{11} \end{bmatrix} = \begin{bmatrix} \sigma_1^S & \sigma_2^S \\ \sigma_2^S & -\sigma_1^S \end{bmatrix}. \tag{9.3}$$

Under continuous rotational symmetry, O(2), the nematic tensor $\overline{N}$ transforms according to

$$\overline{N} \to R(\phi)\overline{N}R^T(\phi), \quad R(\phi) = \begin{bmatrix} \cos(\phi) & -\sin(\phi) \\ \sin(\phi) & \cos(\phi) \end{bmatrix} \tag{9.4}$$

or in a "vector"-like notation as

$$\begin{bmatrix} N_{11} \\ N_{12} \end{bmatrix} \to \begin{bmatrix} \cos(2\phi) & -\sin(2\phi) \\ \sin(2\phi) & \cos(2\phi) \end{bmatrix} \begin{bmatrix} N_{11} \\ N_{12} \end{bmatrix}. \tag{9.5}$$

[1] A rotationally dependent component will also be induced in the longitudinal resistivity, but since $\sigma_0$ is likely dominating, the effect will be small.

Thus $\overline{N}$ is a 2D irreducible representation[2] and we are left with a residual rotational freedom of the director (a headless arrow along one principal axis), i.e. $\alpha = \frac{1}{2}\arctan(N_{12}/N_{11})$ can take any value. This is called an XY nematic order [49].

If we on the other hand consider a tetragonal symmetry $C_4$ (or $D_{4h}$ for the highest tetragonal symmetry) the rotational symmetry is constrained to 90° rotations. With $\phi = 90°$ (9.5) reduces to

$$\begin{bmatrix} N_{11} \\ N_{12} \end{bmatrix} \rightarrow \begin{bmatrix} -1 & 0 \\ 0 & -1 \end{bmatrix} \begin{bmatrix} N_{11} \\ N_{12} \end{bmatrix} \tag{9.6}$$

implying that $\overline{N}$ reduces to two 1D representations. Due to their transformation under the rest of the point-group symmetries $N_{11}$ and $N_{12}$ can be identified with an $x^2 - y^2$ ($B_{1g}$) and an $xy$ ($B_{2g}$) nematic order respectively. These orders are in general referred to Ising nematic orders. The nematic director $\alpha = \frac{1}{2}\arctan(N_{12}/N_{11})$ is not associated with any rotational freedom, it just quantifies the relative strength of the two Ising nematic orders[3]. With only $x^2 - y^2$ ($xy$) nematic order the director will lie along either axis (diagonal).

The seemingly unpinned director of the nematic director, $\alpha$, in LSCO, can be interpreted in two ways. One is to say that $\alpha$ is pinned by a random symmetry breaking field, i.e., appealing to some emergent rotational symmetry and an XY nematic order. While this is likely not the case since the director is robust under thermal cycling[4], such an enhancement of symmetry turns out to be possible in principle; this is discussed in Paper D. The other interpretation is to appeal to the appearance of *two* Ising nematic order and that the evolution of $\alpha$ as a function of doping and temperature mirrors the evolution of these two nematic components. This view was taken in Paper C with the added flavor that the temperature dependence of $\sigma$ is explained by a two-fluid model consisting of a normal and a superconducting part, which couples independently to two *fixed* nematic fields.

[2] If $\overline{N}$ allows for complex values we can reduce it further into $N_{11} \pm iN_{12}$ transforming in the $m = \pm 2$ representation ($e^{im\phi}$) under rotation.

[3] In a tetragonal symmetry $\alpha$ is really a senseless characteristic of nematic order since $N_{11}$ and $N_{12}$ have arbitrary normalizations. It will depend on what quantity is measured (in this case, conductivity).

[4] Private correspondence with authors of [23].

## 9.3 A two-fluid model for anisotropic conductivity

To explain the peak in the transverse resistivity near $T_c$ we need to model the conductivity-nematic order. We consider a full conductivity tensor made up by a normal and a paraconducting part

$$\bar{\sigma} = \bar{\sigma}_{\mathrm{n}} + \bar{\sigma}_{\mathrm{p}}, \quad \bar{\sigma}_{\mathrm{n}} = ne^2\tau\bar{m}_{\mathrm{n}}^{-1}, \quad \bar{\sigma}_{\mathrm{p}} = \sigma_{\mathrm{p},0}\frac{T_{\mathrm{c}}}{T-T_{\mathrm{c}}}\sqrt{\det(\bar{m}_{\mathrm{p}})}\bar{m}_{\mathrm{p}}^{-1} \tag{9.7}$$

where $\bar{\sigma}_{\mathrm{n}}$ is the normal anisotropic Drude-resistivity with relaxation time $\tau$, and $\bar{\sigma}_{\mathrm{p}}$ the anisotropic paraconductivity (8.23) with $\sigma_{\mathrm{p},0} = \frac{e^2}{16\hbar s}$. Instead of directly identifying the conductivity tensor $\bar{\sigma}$ with the development of nematic order we consider the inverse effective masses

$$\bar{m}_{\mathrm{p}}^{-1} = m_{\mathrm{p},0}^{-1} + \bar{S}, \quad \bar{m}_{\mathrm{n}}^{-1} = m_{\mathrm{n},0}^{-1} + \bar{S}' \tag{9.8}$$

where the traceless symmetric part $\bar{S}$ and $\bar{S}'$ couples to two Ising nematic orders in distinct ways[5]

$$\begin{aligned} S_{11} &= \gamma_{SC-1}N_{x^2-y^2}, \quad S_{12} = \gamma_{SC-2}N_{xy}, \\ S'_{11} &= \gamma_{N-1}N_{x^2-y^2}, \quad S'_{12} = \gamma_{N-2}N_{xy}. \end{aligned} \tag{9.10}$$

We can identify the conductivity-nematic order (9.3) as

$$\begin{aligned} N_{11} = \sigma_1^S &= ne^2\tau S'_{11} + S_{11}\frac{\sigma_{\mathrm{p},0}}{\sqrt{m_{\mathrm{p},0}^{-2} - S_{11}^2 - S_{12}^2}}\frac{T_{\mathrm{c}}}{T-T_{\mathrm{c}}} \propto N_{x^2-y^2} \\ N_{12} = \sigma_2^S &= ne^2\tau S'_{12} + S_{12}\frac{\sigma_{\mathrm{p},0}}{\sqrt{m_{\mathrm{p},0}^{-2} - S_{11}^2 - S_{12}^2}}\frac{T_{\mathrm{c}}}{T-T_{\mathrm{c}}} \propto N_{xy}. \end{aligned} \tag{9.11}$$

Due to the divergence of paraconductivity the conductivity-nematicity is naturally enhanced near $T = T_c$. The main finding in Paper C is that this simple temperature dependence is enough to explain the peak in measured transverse resistivity, leaving the Ising-nematic orders $N_{1g}, N_{2g}$ temperature-independent. Furthermore, this accounts for the twist of the conductivity-nematic director $\alpha = \frac{1}{2}\arctan(N_{12}/N_{11})$ as function of temperature.

[5] We define

$$\bar{S} = \begin{bmatrix} S_{11} & S_{12} \\ S_{12} & -S_{11} \end{bmatrix}. \tag{9.9}$$

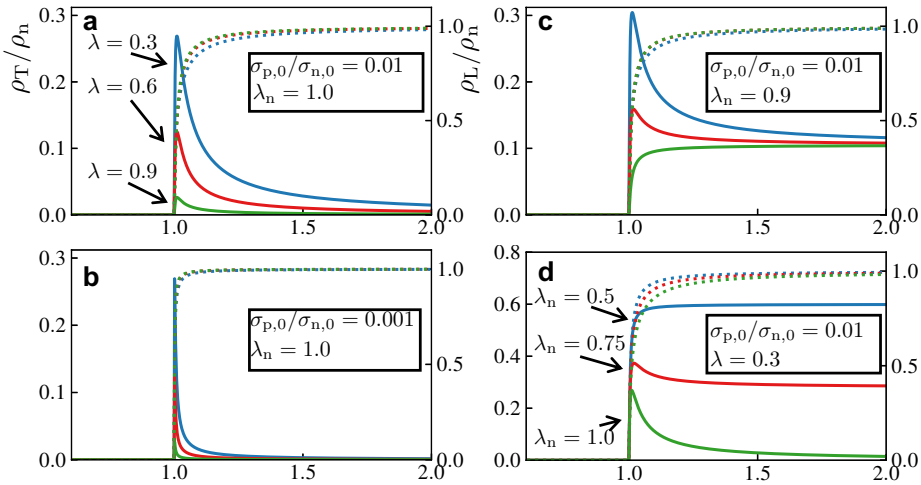


**Figure 9.3:** The transverse (solid) and longitudinal (dashed) resistivity (see (9.2)) from a fluctuating anisotropic superconductor assuming a constant (temperature-independent) normal resistivity component. In panel **a** and **b** three different superconducting mass anisotropies $\lambda$ are shown for two different realizations of $\sigma_{p,0}/\sigma_n$, without normal mass anisotropy, $\lambda_n = 1$. In panel **c**, with a normal mass anisotropy $\lambda_n = 0.9$. In panel **d** different realization for $\lambda_n$ for fixed $\sigma_{p,0}/\sigma_n$ and $\lambda$ is shown.

Just above $T_c$, $\overline{N}$ is dominated by the paraconductivity and $\alpha(T_c) = \frac{1}{2}\arctan(S_{12}/S_{11})$, while for higher temperatures $\overline{N}$ is given by the normal component and $\alpha(T=\infty) = \frac{1}{2}\arctan\left(S'_{12}/S'_{11}\right)$. In Paper C we simply align $\bar{S}$ and $\bar{S}'$ with the measured $\alpha$ at $T_c$ and $T = 295\,\mathrm{K}$, assuming that the coupling factors $\gamma_{SC-1,2}, \gamma_{N-1,2}$ account for the difference in orientation.

Due to different dependence on the mass tensor of the normal and paraconductivity component in (9.7) there is a residual dependence on the trace of the mass tensor for paraconductivity term in (9.11). This yields an additional divergence as a function of mass. We will argue that this is the key reason for such a high anisotropy in the paraconductivity channel, while the normal conductivity remains more or less isotropic.

## 9.4 Simplified model for resistivity in LSCO

To give a simplified model, we here consider the situation where the principal axes of $\bar{S}$ and $\bar{S}'$ coincide. Aligning with the principal frame, referred to as $x'y'$, we find a diagonal conductivity

$$\bar{\sigma} = \bar{\sigma}_{\mathrm{n}} + \bar{\sigma}_{\mathrm{p}} = \begin{bmatrix} \sigma_{\mathrm{n},x'} + \sigma_{\mathrm{p},x'} & 0 \\ 0 & \sigma_{\mathrm{n},y'} + \sigma_{\mathrm{p},y'} \end{bmatrix}, \tag{9.12}$$

with

$$\begin{aligned} &\sigma_{\mathrm{p},x'} = \sigma_{\mathrm{p},0} \frac{T_{\mathrm{c}}}{T - T_{\mathrm{c}}} \lambda, \quad \sigma_{\mathrm{p},y'} = \sigma_{\mathrm{p},0} \frac{T_{\mathrm{c}}}{T - T_{\mathrm{c}}} \lambda^{-1}, \\ &\sigma_{\mathrm{n},x'} = \lambda_{\mathrm{n}} \sigma_{\mathrm{n}}, \quad \sigma_{\mathrm{n},y'} = \lambda_{\mathrm{n}}^{-1} \sigma_{\mathrm{n}}. \end{aligned} \tag{9.13}$$

Here we introduced

$$\lambda = \sqrt{\frac{m_{\mathrm{p},y'}}{m_{\mathrm{p},x'}}} = \sqrt{\frac{m_{\mathrm{p},0}^{-1} + \sqrt{S_{11}^2 + S_{12}^2}}{m_{\mathrm{p},0}^{-1} - \sqrt{S_{11}^2 + S_{12}^2}}} \tag{9.14}$$

and $\lambda_{\mathrm{n}} = \sqrt{m_{\mathrm{n},y'}/m_{\mathrm{n},x'}}$ analogously. In the BCS limit $\sigma_{\mathrm{p},0} = \frac{e^2}{16\hbar s}$ , however in fitting to data, we can treat $\sigma_{\mathrm{p},0}$ as a free parameter and explore how well it agrees with the theoretical value. The longitudinal and transverse response along $\phi = 0$ takes the form (9.2)

$$\rho_{\mathrm{T}} = \frac{\sigma_{y'} - \sigma_{x'}}{2\sigma_{x'}\sigma_{y'}}, \quad \rho_{\mathrm{L}} = \frac{\sigma_{y'} + \sigma_{x'}}{2\sigma_{x'}\sigma_{y'}}, \tag{9.15}$$

which is shown in Figure 9.3 for a few realizations assuming $\sigma_{\mathrm{p},0} \ll \sigma_{\mathrm{n},0}$(the experimentally relevant regime) and $\sigma_y > \sigma_x$ (such that $\lambda, \lambda_{\mathrm{n}} \leq 1$). Also, we assumed a $T$-independent conductance of the normal component $\sigma_{\mathrm{n}}(T) = \sigma_{\mathrm{n},0}$.

The contribution to the longitudinal resistivity from the paraconductivity is small except very close to $T_{\mathrm{c}}$, where it gives a rapid drop in resistivity. Furthermore, $\rho_{\mathrm{L}}$ is very insensitive to the both mass anisotropies $\lambda, \lambda_{\mathrm{n}}$. For the transverse resistivity, which directly measures the nematicity, the situation is very different. With a finite superconducting anisotropy, $\lambda < 1$, the response is peaked near $T_{\mathrm{c}}$, reflecting the dominating paraconductivity as the singularity is approached. A normal component anisotropy, $\lambda_{\mathrm{n}} < 1$ enhances the

| $p$ | $\lambda$ | $\sigma_{\mathrm{p},0}\left(\frac{e^2}{16\hbar s}\right)$ |
|---|---|---|
| 0.10 | 0.24 | 4.46 |
| 0.12 | 0.57 | 2.97 |
| 0.16 | 0.69 | 3.18 |
| 0.18 | 0.80 | 4.21 |
| 0.21 | 0.81 | 14.99 |

**Table 9.1:** In the upper panel values from fitting to the peak is shown for dopings $p = 0.10, 0.12, 0.16, 0.18, 0.21$. As a measure of normal component resistivity $\rho_n = 283, 200, 111, 60, 31\,\mu\Omega$cm was used. (Here $\rho_n = 1/\sigma_{\mathrm{n},0}$ is the extrapolated longitudinal response at $T_\mathrm{c}$ using a fit from $2T_\mathrm{c}$ to 295 K and $s =$ 13.2 Å.)

high-temperature tail of the transverse response but suppresses the peak. In fact, the existence of a peak requires $\lambda < \lambda_\mathrm{n}^2$, thus the mere existence of a peak in the transverse data of Figure 9.1 indicates a high superconducting anisotropy compared to the normal component[6].

### 9.4.1 Extracting parameters

The model is in good qualitative agreement with the experimental measured resitivities in Figure 9.1. As a rough estimate we can extract the superconducting anisotropy, $\lambda$, and paraconductivity strength, $\sigma_{\mathrm{p},0}$, by fitting to the peak in the transverse response, which is given by $\rho_{T,\mathrm{peak}} = \frac{1}{2\sigma_{\mathrm{n},0}}(1-\lambda)/(1+\lambda)$ located at $T_\mathrm{peak} = T_\mathrm{c}\left(1+\sigma_{\mathrm{p},0}/\sigma_{\mathrm{n},0}\right)$ assuming $\lambda_\mathrm{n} = 1$, i.e. no normal component anisotropy[7]. The results are presented in Table 9.1.

In Paper C, we used a more sophisticated fitting procedure accounting for a temperature-dependent anisotropic normal conductivity, spread in $T_c$, as well as different principal frames of the paraconductivity and normal conductivity; which makes it possible to account for the variation of $\alpha$ with temperature. However, the anisotropic measures obtain in Table 9.1 are consistent with the ones obtained in Paper C. The major difference is that

[6] For $\lambda > 1$ the requirement for a peak reads $\lambda_\mathrm{n}^2 < \lambda$.

[7] Normal conductivity anisotropy mainly affects the tail of the transverse response. As an estimate of $T_\mathrm{c}$ we use the temperature where the resistance dropped to 1% of the value at the peak.

$\sigma_{\mathrm{p},0}$ better agrees with the BCS value, using the fits in Paper C[8].

## 9.5 Effect in magnetic field

Paper C includes a study of the effect in a magnetic field. Due to the competition with superconductivity, we anticipate a suppression of the peak in the presence of a magnetic field. Also, if the variation of $\alpha$ arises due to a difference in the principal axis of $\bar{\sigma}_n$ and $\bar{\sigma}_p$ we expect the twist to disappear. Indeed these effects were observed in strong support of our model. Paper C includes a model of this behavior.

As discussed in Section 9.1, a magnetic field induces a Hall resistivity, both from the normal Drude conductivity and paraconductivity. This yields a rotational invariant part of the transverse response, which is easy to extract from data. Moreover, the Hall term contributes to the overall determinant of the conductivity, contributing to the magnetoresistivity. However, this term was estimated to be small, and the Hall conductance was excluded from the model altogether. More important was to include is the suppression of $T_c$ as described in Section 8.3.1.

However, the most pronounced effect when studying the resistive transition of a type II superconductor in the presence of a magnetic field is a broadening, or fanning out, of the transition, due to vortex-motion. Instead of embarking on a more complicated model, we used a qualitative result by Tinkham [136] stating that the broadening of the transition is given by $\Delta T \propto B^{2/3}$. This relation was found to be in good agreement with measurements. Thus to model the vortex motion, we added this additional broadening of $T_c$ as a Gaussian distribution of samples with different $T_c$.

## 9.6 Discussion

After concluding that substantial anisotropic superconducting fluctuations can explain the resistivity measurements in LSCO, one pertinent question is why such a dramatic electronic nematicity has not been previously observed?

[8] In fact, due to sensitivity in fitting $\sigma_{\mathrm{p},0} = \frac{e^2}{16\hbar s}$ was used in Paper C with consistent results. Thus no significant deviation from the BCS expression could be detected.

### 9.6.1 Macroscopic alignment of nematicity

Nematicity is inherently sensitive to disorder. In the presence of quenched disorder, no long-range nematic order can exist in 2D, and we anticipate domains[9]. Indeed, such domains of electronic nematicity have previously been observed in cuprate compounds [70]. The macroscopic manifestation of nematicity in LSCO, independent of interpretation, implies that the domains must be aligned.

Transport measurements on macroscopic samples have many non-ideal features, ranging from impurities to contact effects, which might scatter currents, leading to unexpected results. Some local probe of nematicity should probably be of aid to sort out the details of what is happening. Nevertheless, we believe that the study made in [23] as well as that in Paper C shows convincing evidence for this enigmatic nematic order being an intrinsic property of the system. For instance, impurities and contact effects are not a likely source of transverse resistivity since the different Hall bars in the sunflower configured sample shows the same macroscopic alignment of the nematic director. Instead, this suggests that there is some macroscopic symmetry-breaking field aligning the Hall bars, strong enough to overcome impurity effects, which would otherwise show up as a difference between samples. Thus, we ascribe this previous lack of observation of nematicity to the exceptional nature of the mesoscale thin-film LSCO structures.

Our interpretation is that the symmetry-breaking field arises from the substrate. Supporting this interpretation is the alignment of the nematic director with the crystal axis for an orthorhombic substrate [23]. Here the transverse signal remains in the same order of magnitude as for the tetragonal sample, suggesting that the symmetry-breaking field present is of similar strength as the one imposed by strain in the orthorhombic sample. One scenario would be that the tetragonal substrates resolve the four-fold degeneracy of the $N_{x^2-y^2}, N_{xy}$ nematic state, while not strong enough to cause the actual ordering.

[9] XY nematic order cannot exist for $d < 4$ and Ising nematic for $d \leq 2$ in the presence of a random symmetry breaking field [49].

### 9.6.2 Origin of nematicity

The asserted Ising nematic fields $N_{x^2-y^2}, N_{xy}$ should in principle couple to all physical properties, like an anisotropic penetration depth, depairing current, vortex dynamics, gap structure, etc. First of all, we note an apparent discrepancy already occurring in the observations made above. The superconducting conductivity fluctuations become highly anisotropic, while the normal state remains essentially isotropic. One possible reason lies in the structure of (9.11), as well as (9.14). The contribution to the nematic signal in conductivity can become divergent if the isotropic pair mass fulfills $m_{\mathrm{p},0}^{-2} = S_{11}^2 + S_{12}^2$, which means that the superconductor becomes highly susceptible to anisotropic distortions. Typically we expect $m_{\mathrm{p},0}^{-2} > S_{11}^2 + S_{12}^2$, however, we have seen how the effective pair mass of a superconductor can become divergent, $m_{\mathrm{p},0} \to \infty$, when approaching a Lifshitz-point due to a PDW instability. In fact, which is the main topic of Paper D, and discussed in Chapter 11, PDW can give rise to the nematic order itself through a vestigial ordering $N = (|\Delta_{\mathbf{Q}_x}|^2 + |\Delta_{-\mathbf{Q}_x}|^2) - (|\Delta_{\mathbf{Q}_y}|^2 + |\Delta_{-\mathbf{Q}_y}|^2)$. Thus a PDW instability can provide both the sensitivity to nematicity and nematicity itself. The former would distinguish this proposal of PDW as the source for nematicity from, e.g., a vestigial CDW nematic order.

We should also stress the nature of the nematic superconductivity we study here. We refer to anisotropy in the pair mass. Thus, it is really that the superconductor's dynamical response becomes anisotropic. This implies that the constituent electrons do not necessarily share this property. For instance, it is not related to a Pomeranchuk instability of the FS, and the FS can remain essentially rotational invariant. Since we are studying a single-component superconductor, this is the only way to relate nematicity to it[10]. In contrast, for triplet superconductors, the order parameter itself can develop nematic order (see, e.g., [102]).

[10] An induced s-wave superconducting order would, however, yield a nematic gap $\Delta_s \Delta_d$.

# 10 Fluctuations and vestigial orders

We have seen how an effective (time-dependent) Ginzburg-Landau free energy functional can be obtained as an effective theory of the superconducting condensate. We found the pair propagator, $L$, accounting for the dynamics of the pairs, which we used to understand the fluctuating conductivity, the paraconductivity.

BCS theory is often considered the "solution" to the problem of conventional superconductivity since it provides a microscopic origin and explains the emergence of the gaped single-particle spectrum [128]. Nevertheless, many properties of traditional superconductors are captured by the Ginzburg-Landau (GL) theory. Historically the (phenomenological) GL theory preceded the BCS theory but was put on firmer footing when it was derived from the microscopic BCS theory by Gorkov [137]. BCS theory is essentially a mean-field theory, only taking into account a static condensate and not its fluctuations, while GL theories are useful in describing fluctuations.

While the singe-particle spectra of a superconductor is a defining feature, the fluctuations are more universal, as is emphasized by the generic form of the GL theory, which is simply an expansion in order parameters with the microscopic physics hidden in the coefficients. Many different microscopic theories have similar-looking effective theories, depending only on the symmetry and dimensionality. Indeed, many phenomena observed in nature, like phase transitions, turn out to be universal. From a practical standpoint, this gives us the possibility of writing down models from mere symmetry principles, without any knowledge about the microscopic details, and study the possible phenomena this theory can generate.

One universal piece of physics induced by fluctuations is that of vestigial ordering [76]. Often we consider systems with orders and phases that break many symmetries simultaneously. A common feature of such systems is that the transition may split up, with additional (vestigial) phases in which only a subset of symmetries are broken. This effect can be understood as a result of proliferating fluctuations that partially disorder the broken symmetry phase. This chapter will serve as an introduction to these fluctuation concepts[1].

[1] Inspiration to this chapter is taken from Chaikin et. al [110] and lecture notes by Schmalian [138].

## 10.1 Breakdown of mean-field theory

Mean-field theory is valid when fluctuations around the mean-field value are less than the mean-field value $\langle(\psi-\psi_0)^2\rangle \ll \psi_0^2$ which leads to the *Ginzburg criterion*

$$\left(\frac{|T-T_c|}{T_c}\right)^{(4-d)/2} \gg \frac{k_B}{8\Delta c_V \xi_0^d} \tag{10.1}$$

for fluctuations to be unimportant (here $\Delta c_V$ is the change in specific heat at the transition, and $\xi_0$ the coherence length) [139]. The dimension $d = 4$ defines what is called the upper critical dimension $d_u$. For $d > 4$, the left-hand side diverges as $T_c$ is approached. Thus the inequality is fulfilled, and mean-field theory will hold. For $d < 4$ the Ginzburg criterion will be violated for temperatures within the so-called Ginzburg region $|T - T_c| < T_c\left(\frac{k_B}{8\Delta c_V \xi_0^d}\right)^{2/(4-d)}$. There is also a lower critical dimension $d_l$, under which no order can be present. The lower critical dimension will, for continuously broken symmetries, be determined by the Mermin-Wagner theorem, which tells us that no order can exist in dimensions below 2, i.e., $d_l = 2$.

In the case of conventional clean bulk superconductors, the Ginzburg region is very narrow ($\sim 10^{-12}$ K) and virtually inaccessible to experiments [128]. This is the fundamental reason for the success of the BCS treatment for conventional superconductivity. As discussed in Section 4.1.1 fluctuations are much more important in cuprates and we have studied the fluctuating contribution to conductivity in Chapters 8 and 9. In this chapter, we concentrate on the influence of fluctuations on the ordering transition.

## 10.2 The self-consistent field approximation

In this section we will explore the basic methods of treating fluctuations of a GL functional used in Paper D. We will start by considering a single-component superconductor which is invariant under point-group symmetries

$$\begin{aligned} Z &= \int \mathscr{D}\Delta\, e^{-S(\Delta)} \\ S(\Delta) &= \int_{\mathbf{x}} r|\Delta(\mathbf{x})|^2 + \kappa|\nabla\Delta(\mathbf{x})|^2 + \frac{u}{2}|\Delta(\mathbf{x})|^4 . \end{aligned} \tag{10.2}$$

Here $S = \beta F$ is the action[2] and $r = a(T - T_{\rm MF})$, with $T_{\rm MF}$ the predicted mean-field transition temperature. We will concentrate on the normal state where $r > 0$ and therefore assert $\langle \Delta(\mathbf{x}) \rangle = 0$. As the critical temperature is approaches $r \to 0$, we expect fluctuations $\langle |\Delta(\mathbf{x})|^2 \rangle$ to increase. In this case the interaction term becomes important and we will employ the HS transformation to decouple this term,

$$\frac{u}{2}|\Delta(\mathbf{x})|^4 \to -\frac{\psi(\mathbf{x})^2}{2u} + \psi(\mathbf{x})|\Delta(\mathbf{x})|^2 , \tag{10.3}$$

yielding

$$\begin{aligned} Z &= \int \mathscr{D}\Delta \mathscr{D}\psi \, e^{-S_{\rm eff}(\Delta,\psi)} \\ S_{\rm eff} &= \int_{\mathbf{x}} (r + \psi(\mathbf{x}))|\Delta(\mathbf{x})|^2 + \kappa |\nabla \Delta(\mathbf{x})|^2 - \frac{\psi(\mathbf{x})^2}{2u} , \end{aligned} \tag{10.4}$$

where we introduced $\psi(\mathbf{x})$ as a real field (with white-noise correlations), to mediate the interaction between the $\Delta$ fields[3]. We proceed by substituting $\psi(\mathbf{x})$ for its mean-field value, given by the saddle-point equation $\frac{\delta S(\psi)}{\delta \psi} = 0$. Since (10.4) is quadratic in $\Delta$ we integrate over all field-configuration yielding an action only in terms of $\psi$. Going over to momentum space, setting $\psi(\mathbf{q}) = \psi \delta(\mathbf{q})$ (preparing for finding the homogeneous mean-field solution), and using the identity $\ln \mathrm{Det}(A) = \mathrm{Tr} \ln(A)$ we find

$$Z(\psi) = \frac{1}{\mathrm{Det}(r + \psi + \kappa q^2)} e^{\int_{\mathbf{x}} \frac{\psi^2}{2u}} = \int \mathscr{D}\psi \, e^{\int_{\mathbf{q}} \frac{\psi^2}{2u} - V \ln(r + \psi + \kappa q^2)} \tag{10.5}$$

where $V$ is the system volume, and the full partition function is given by $Z = \int \mathscr{D}\psi Z(\psi)$. The saddle -point approximation to $Z$, or equally, optimizing the free energy $F(\psi) = -\ln(Z(\psi))/\beta$, yields

$$\psi = u \int_{\mathbf{q}} \frac{1}{r + \psi + \kappa q^2} . \tag{10.6}$$

[2] A factor of $\beta$ is included in the coefficients of (10.2).

[3] $\psi$ is taken along an imaginary contour since we assume $u > 0$, for a stable action (see Appendix B).

This is a self-consistent equation for $\psi$, whose solutions we will discuss in the next section. Before that, we will comment on the meaning of $\psi$, acquiring an expectation value. By identifying $Z(\psi)$ in (10.4) we see that a stationary point in the action with regard to $\psi$ implies

$$0 = \frac{\delta S}{\delta \psi(\mathbf{x})} = \langle |\Delta(\mathbf{x})|^2 \rangle - \psi(\mathbf{x})/u \,. \tag{10.7}$$

Thus, an expectation value for $\psi(\mathbf{x})$ implies fluctuations of the field $\langle |\Delta(\mathbf{x})|^2 \rangle$. By accounting for a $\psi$ on a mean-field level is the same thing as replacing $\frac{u}{2}|\Delta(\mathbf{x})|^4 \to u\langle |\Delta(\mathbf{x})| \rangle |\Delta(\mathbf{x})|^2$, i.e accounting for interaction between the field and its average value.

### 10.2.1 Lower and upper critical dimension

The transition to the ordered state is given by the point where the static susceptibility $\chi(\mathbf{q}=0)$ diverges. From (10.4) we read of the susceptibility as $\chi(\mathbf{q}=0) = r'^{-1}$, where $r' = r + \psi$ is the renormalized inverse bare susceptibility. From (10.6) we write

$$r' = r + u \int_{\mathbf{q}} \frac{1}{r' + \kappa q^2} \,. \tag{10.8}$$

The transition to the ordered state occurs for $r = r_c$, which fulfills $r' = 0$. For $d > 2$ we find

$$r_c = -u K_d \int_0^\infty \mathrm{d}q \frac{q^{d-1}}{\kappa q^2} = -u K_d \frac{\Lambda^{d-2}}{\kappa(d-2)} \tag{10.9}$$

where $K_d = \Omega_d/(2\pi)^d$ and $\Omega_d$ is the solid angle in $d$ dimensions and $\Lambda$ a momentum cut-off[4]. The new critical temperature $T_c$, renormalized by fluctuations, can be expressed as $r - r_c = a(T - T_c)$. For $d \leq 2$ the integral in (10.8) is divergent for small momenta (a so-called infrared (IR) divergence) as $r' \to 0$. Thus the onset of transition is never reached and $T_c = 0$ for $d = 2$. This determines the lower critical dimension $d_l = 2$.

[4] Typically taken as the inverse coherence length $\xi_0^{-1} = (\kappa/a\,T_c)^{-1/2}$.

To explore the upper critical dimension we will consider the critical behaviour of the susceptibilities. The mean-field uniform static susceptibility is given by

$$\chi_{\mathrm{MF}}(q=0)=\frac{1}{r}\propto(T-T_{\mathrm{MF}})^{-1} \tag{10.10}$$

(here we can defined the so-called critical exponent $\gamma=1$). To find the form of the renormalized susceptibility, given by $\chi(\mathbf{q}=0)=(r')^{-1}$, we must solve for the temperature dependence of $r'$. Using $r-r_c=a(T-T_c)$ we write (10.8) as

$$\begin{aligned} r' &= r-r_c+u\int_{\mathbf{q}}\frac{1}{r'+\kappa q^2}-\frac{1}{\kappa q^2}\Rightarrow \\ r' &= \frac{r-r_c}{1+\frac{uK_d}{\kappa}\int_0^{\Lambda}\mathrm{d}q\,\frac{q^{d-3}}{r'+\kappa q^2}}. \end{aligned} \tag{10.11}$$

Here the integral in the denominator is convergent for $r'\to 0$ if $d>4$ and just as in the mean-field case we find

$$\chi(\mathbf{q}=0)=\frac{1}{r'}\propto(r-r_c)^{-1}\propto(T-T_c)^{-1},\quad d>4. \tag{10.12}$$

However, for $d<4$ the integral in (10.11) is IR divergent. Absorbing the divergence we can write

$$r'=\frac{r-r_c}{1+\frac{uK_d}{\kappa^{d/2}}r'^{(d-4)/2}I_d(\Lambda\sqrt{\kappa/r'})},\quad I_d(y)=\int_0^y\mathrm{d}x\,\frac{x^{d-3}}{1+x^2} \tag{10.13}$$

where $I_d(y)$ is convergent for $y\to\infty$ (and $d<4$). If $r-r_c\gg 1$ the one in the denominator dominates and we again find the mean-field behaviour (consistent with the Ginzburg region). For $r'\to 0$, however, the second term in the denominator diverges and we find

$$\chi(\mathbf{q}=0)\propto(T-T_c)^{-2/(d-2)},\quad d<4. \tag{10.14}$$

Indeed we have found what was stated above. Above $d>4$ we find mean-field behaviour, however with renormalized transition temperature $T_{\mathrm{MF}}\to$

$T_c$ and pre-factors of the susceptibilities. For $d < 4$, we found a general correction to the mean-field behavior close to the transition (with an altered critical exponent). We also found the lower critical dimension to be $d_l = 2$, under which no ordering takes place.

### 10.2.2 Comments

Approximating $\psi$ by its saddle-point value in (10.4) implies accounting for an average background *self consistently* (as can be seen from (10.6)) and this is sometimes called the self-consistent field approximation [110]. This approximation can be formalized by the so-called large N expansion where one introduces $N$ replicas of the same field, proceeded by expanding in factors of $1/N$. The first term in such expansion will be the saddle-point approximation, thus for $N \to \infty$, the self-consistent field approximation becomes exact. Even though this expansion is only a formality, it gives some insights into what kind of approximations are made, and how they can be corrected. For one, we concluded that $d_l = 2$ was the lower critical field. However, from the Mermin-Wagner theorem, we know that this should only be true for continuously broken symmetries. For the discrete symmetry Ising-model, the lower critical field is known to be $d = 1$, but formally the above procedure can be applied to the 2D Ising model as well. The breakdown of the estimate for the lower critical field for the Ising model can be understood as a consequence of the Ising model belonging to the $N = 1$, case, poorly captured by the $N \to \infty$ limit.

## 10.3 Vestigial ordering

We have seen how fluctuations can drastically alter the mean-field behavior below the upper critical dimension. We will now continue to see how the mean-field behavior of an order parameter that breaks more than one symmetry gets altered by fluctuations. As an example, let us consider the action

$$\begin{aligned} S(\vec{\Delta}) = S_{\text{Dyn.}}(\vec{\Delta}) + \int_{\mathbf{x}} & r(|\Delta_X(\mathbf{x})|^2 + |\Delta_Y(\mathbf{x})|^2) + \frac{u}{2}(|\Delta_X(\mathbf{x})|^2 + |\Delta_Y(\mathbf{x})|^2)^2 \\ & - \frac{g}{2}(|\Delta_X(\mathbf{x})|^2 - |\Delta_Y(\mathbf{x})|^2)^2 \end{aligned} \tag{10.15}$$

where we introduced two order parameters $\vec{\Delta} = (\Delta_X(\mathbf{x}), \Delta_Y(\mathbf{x}))$ that transforms as the coordinates $(x, y)$ under tetragonal symmetry. The action is constructed to be invariant under these symmetry transformations[5] where we left out the dynamical piece for the time being. (Stability of the action requires $u > g$.) The superconducting order sets in for $r < 0$ with $\langle\vec{\Delta}\rangle \neq 0$. For $g < 0$ we will have a tetragonal symmetric ground state with $\vec{\Delta} = \left(\frac{|r|}{2u}, \frac{|r|}{2u}\right)$. For $g > 0$ the mean-field ground state will instead be

$$\vec{\Delta} = \left(\frac{|r|}{u-g}, 0\right) \text{ or } \left(0, \frac{|r|}{u-g}\right), \tag{10.16}$$

breaking the tetragonal symmetry, differentiating between $x$ and $y$. This is an example of a *nematic* state, where rotational symmetry is broken, but translational symmetry is maintained.

According to the mean-field calculation, both nematic order and superconductivity sets in simultaneously. However, we have seen that including fluctuations changes the structure of the transition. In particular, we concluded that even if $\langle\Delta\rangle = 0$ we will in general have finite fluctuations $\langle|\Delta|^2\rangle > 0$. This opens up the possibility of measuring an expectation value of nematic order in the form of $\langle|\Delta_X|^2 - |\Delta_Y|^2\rangle \neq 0$, even though $\langle\vec{\Delta}\rangle = 0$. This indicates a state where fluctuations of an order parameter, not yet condensed, breaks the rotational symmetry of the system.

### 10.3.1 Decoupling the action

We proceed as in (10.4) by rewriting the interaction using the HS transformation. We decouple the two interaction terms in (10.15) using two independent fields $\psi, N$. The former for the isotropic component $|\Delta_X|^2 + |\Delta_Y|^2$ and the latter for the nematic component $|\Delta_X|^2 - |\Delta_Y|^2$. The partition function takes

[5] A possible realization of this order parameter could be a triplet superconductor with d-vector $\hat{z}(\Delta_X \sin(k_x) + \Delta_Y \sin(k_x))$.

the form

$$\begin{aligned} Z &= \int \mathscr{D}\vec{\Delta}\mathscr{D}\psi\mathscr{D}N\, e^{-S_{\text{eff}}(\Delta,\psi,N)}, \\ S_{\text{eff}}(\Delta,\psi,N) &= \int_{\mathbf{q}} (r+\psi+N+\kappa_+(\mathbf{q}))|\Delta_X(\mathbf{q})|^2 + (r+\psi-N+\kappa_-(\mathbf{q}))|\Delta_Y(\mathbf{q})|^2 \\ &\quad + \int_{\mathbf{x}} \frac{N^2}{2g} - \frac{\psi^2}{2u} \end{aligned} \tag{10.17}$$

where we included the uniform part $N(\mathbf{q}) = N\delta(\mathbf{q}), \psi(\mathbf{q}) = \psi\delta(\mathbf{q})$. We introduced $\kappa_\pm(\mathbf{q}) = (\kappa_1 \pm \kappa_2)q_x^2 + (\kappa_1 \mp \kappa_2)q_y^2 + \kappa_z q_z^2, \kappa_1 \mp \kappa_2 > 0$ (neglecting the last term in 2D), from the dynamical part of the action

$$\begin{aligned} S_{\text{Dyn.}}(\vec{\Delta}) = \int_{\mathbf{x}} & \kappa_1(|\nabla_x\Delta_X(\mathbf{x})|^2 + |\nabla_x\Delta_Y(\mathbf{x})|^2 + |\nabla_y\Delta_X(\mathbf{x})|^2 + |\nabla_y\Delta_Y(\mathbf{x})|^2) \\ & + \kappa_2(|\nabla_x\Delta_X(\mathbf{x})|^2 - |\nabla_x\Delta_Y(\mathbf{x})|^2 - |\nabla_y\Delta_X(\mathbf{x})|^2 + |\nabla_y\Delta_Y(\mathbf{x})|^2) \\ & + \kappa_z(|\nabla_z\Delta_X(\mathbf{x})|^2 + |\nabla_z\Delta_Y(\mathbf{x})|^2). \end{aligned} \tag{10.18}$$

Again, assuming an unordered superconducting state $\langle\vec{\Delta}\rangle = 0$, we proceed by integrating out the superconducting order parameters in the now quadric action (10.17), yielding

$$S_{\text{eff}}(\psi,N) = \int_{\mathbf{x}} \frac{N^2}{2g} - \frac{\psi^2}{2u} + V\int_{\mathbf{q}} \ln(r+\psi+N+\kappa q^2)(r+\psi-N+\kappa q^2) \tag{10.19}$$

where we assumed $\kappa = \kappa_+ = \kappa_-$ for simplicity. Proceeding to the mean-field equations $\frac{\delta S_{\text{eff}}}{\delta\psi} = 0, \frac{\delta S_{\text{eff}}}{\delta N} = 0$

$$N = 2g\int_{\mathbf{q}} \frac{N}{(r'+\kappa q^2)^2 - N^2}, \quad r' = r + 2u\int_{\mathbf{q}} \frac{r'+\kappa q^2}{(r'+\kappa q^2)^2 - N^2} \tag{10.20}$$

with $r' = r + \psi$ as before[6]. The first equation always admits $N = 0$ solutions. However, a non-trivial solution is possible when

$$\chi_N^{-1} = 1 - 2g \int_{\mathbf{q}} \frac{1}{(r' + \kappa q^2)^2} = 1 - 2g K_d \int_0^\Lambda \frac{q^{d-1}\,\mathrm{d}q}{(r' + \kappa q^2)^2} = 0 \tag{10.21}$$

where we introduced $\chi_N$ as the susceptibility for nematic order. For $d > 4$, the integral is finite for all values of $r'$, meaning that as $r'$ is decreased, there is no guarantee this condition will hold. However, for $d < 4$ the integral becomes divergent for $r' = 0$. Extracting the singular behavior, we write

$$\chi_N^{-1} = 1 - \frac{2g K_d}{\kappa^{d/2} (r')^{(4-d)/2}} J_d(\Lambda \sqrt{\kappa / r'}), \quad J_d(y) = \int_0^y \frac{x^{d-1}}{(1+x^2)^2}\,\mathrm{d}x\,, \tag{10.22}$$

where $J(y)$ is convergent for $y \to \infty$. Thus, as $r' \to 0$, the nematic susceptibility is bound to diverge for some finite $r' > 0$ (when $g > 0$).

### 10.3.2 Vestigial order and dimensions

What we just discovered is quite remarkable. Remembering that the superconducting order $\langle \vec{\Delta} \rangle \neq 0$ sets in for $r' = 0$, we see that the nematic order necessarily develops before the onset of superconductivity for $d < 4$. Furthermore, in 2D, for which superconducting long-range order can never develop, and $r' > 0$, we can still find nematic order.

Note that this is consistent with the Mermin-Wagner theorem. For 2D, no long-range broken continuous symmetry can exist. However, the vestigial nematic order discussed here is of Ising type, i.e., the ground state has a $Z_2$ degeneracy. In 2D, long-range discrete symmetry breaking is at finite temperature, which is indeed what we have found.

We see how fluctuations drastically change the phase diagram by the generic occurrence of vestigial order. Note that this phenomenology explains why various orders might seem parasitically joined. The possibility of vestigial orders describes how various orders, arising from the same underlying fields, are dependent on each other. This phenomenology is not naturally

[6] The second equation reduces to (10.8) in the limit $N \to 0$. The extra factor of 2 is accounted for by the definition of $\psi$ as the fluctuation of two fields.

recreated from a mean-field calculation since it would require fine-tuning of transition temperatures and competing order terms.

### 10.3.3 Susceptibilities in the nematic phase

From (10.17) we find the susceptibilities for $\Delta_X$ and $\Delta_Y$ as

$$\chi_X(q) = \frac{1}{r' + N + \kappa q^2}, \quad \chi_Y(q) = \frac{1}{r' - N + \kappa q^2} \tag{10.23}$$

with the corresponding correlations lengths given by $\xi_{X,Y} = \sqrt{\frac{\kappa}{r' \pm N}}$. Before entering the nematic phase, $N = 0$, the correlation length will be equal $\xi_X = \xi_Y = \xi = \sqrt{\frac{\kappa}{r'}}$. However, in the nematic phase, $N > 0$, the correlation lengths will differ, and one will diverge before the other, with superconducting ordering setting in at $r' - N = 0$. In this sense, a preemptive transition in the form of the vestigial nematic phase increases the ordering temperature.

The calculation outlined above only holds in the normal state of the superconductor. At $r' - N = 0$ the susceptibility will diverge for ordering of $\Delta_X$ ($N > 0$). When this happens, we have to expand (10.15) around the expectation value of $\Delta_X$ (see for instance [140]). In Paper D, we are interested in the unordered state of a PDW. Specifically, we will consider calculations for the 2D case only.

# 11 Vestigial PDW phases and the anisotropic superconductor

The various possible vestigial orders in a system are made up of bilinears of some primary order parameter and can be classified by the irreducible representations of the symmetry group[1]. Just as outlined in the previous chapter, the interaction terms can be decomposed into these bilinears, which then will be used to decouple the action using the HS transformation. In Paper D, we consider an effective theory for a PDW state and its possible vestigial orders in order to explore the scenario of PDW as the "mother state" of cuprates. Of particular interest is the exploration of vestigial LC orders, which are naturally generated by a PDW primary order. The other topic of Paper D is to explore how the vestigial ordering of a PDW state might affect a coexisting homogeneous superconducting order. In particular, we show how the traceless symmetric inverse pair mass tensor $\bar{S}$ in (9.8) can arise from the coupling between a homogeneous superconducting order and PDW order, that develops vestigial nematic orders.

In Section 5.4 and 5.5 we discussed how an effective theory for a PDW state, $\Delta_{\mathbf{q}}$, with $\mathbf{q} = \pm\mathbf{Q}$ could be obtained from microscopic considerations. In Paper D we consider a more complete set of PDW fields in a tetragonal symmetry, $D_{4h}$. Motivated by the phenomenological finite-momentum instability found in Paper B we used the ordering momenta $\mathbf{q} \in \{0, \pm\mathbf{Q}_x, \pm\mathbf{Q}_y, \pm\mathbf{Q}_+, \pm\mathbf{Q}_-\}$, describing the possible local minima of the dispersion (5.38). Here $\mathbf{Q}_{x,y}$ are aligned with the $x$, $y$ axis and $\mathbf{Q}_\pm$ are aligned with the diagonals. As a simplification we will only consider $\mathbf{q} = \mathbf{Q}_{x,y}$ here[2]. The inclusion of homogeneous superconducting order is left for Section 11.4.

[1] This chapter assumes some knowledge of point-group symmetries and group theory (see, for instance, [141]). For an excellent web-tool for character and multiplication tables, see [142].

[2] Since $\mathbf{Q}_{x,y}$ and $\mathbf{Q}_\pm$ do not transform into each other under tetragonal symmetry the corresponding orders do not mix in second order terms, motivating the division into sector A and B, discussed in Paper D.

## 11.1 Symmetry decomposition

The order parameter we will be considering is $\Gamma = [\Delta_{\mathbf{Q}_x}, \Delta_{-\mathbf{Q}_x}, \Delta_{\mathbf{Q}_y}, \Delta_{-\mathbf{Q}_y}]$. In addition to the point group symmetry, the action will be invariant under $U(1)$ symmetry, translational symmetry and time-reversal symmetry. Under these symmetries the order parameters transform as $\Delta_{\mathbf{Q}} \xrightarrow{U(1)} \Delta_{\mathbf{Q}} e^{i\theta}$, $\Delta_{\mathbf{Q}} \xrightarrow{\mathrm{T}} \Delta_{\mathbf{Q}} e^{i\mathbf{T}\cdot\mathbf{Q}}$, and $\Delta_{\mathbf{Q}} \xrightarrow{\mathscr{T}} \Delta^*_{-\mathbf{Q}}$. The full tetragonal point-group symmetry is given by $D_{4h}$. We will only use ordering vectors that lie within the $x-y$ plane, thus we consider the subgroup $C_{4v}$ which is generated by $\{C_4, \sigma_v\}$, where $C_4$ is a four-fold rotation about the $z$-axis, and $\sigma_v$ reflection in the $xz(yz)$ plane. Under these generators the order parameter transforms as

$$\begin{aligned}\{\Delta_{\mathbf{Q}_x}, \Delta_{-\mathbf{Q}_x}, \Delta_{\mathbf{Q}_y}, \Delta_{-\mathbf{Q}_y}\} &\xrightarrow{C_4} \{\Delta_{\mathbf{Q}_y}, \Delta_{-\mathbf{Q}_y}, \Delta_{-\mathbf{Q}_x}, \Delta_{\mathbf{Q}_x}\} \\ &\xrightarrow{\sigma_v} \{\Delta_{\mathbf{Q}_x}, \Delta_{-\mathbf{Q}_x}, \Delta_{-\mathbf{Q}_y}, \Delta_{\mathbf{Q}_y}\}\end{aligned}. \tag{11.1}$$

The full symmetry group is given by $U(1) \otimes T \otimes \mathscr{T} \otimes D_{4\mathrm{h}}$, we are however mostly interested in phases that break the point-group symmetries, and not $U(1)$ or $T$. We, therefore, consider the following set of bilinears

$$\Gamma^{(2)} = [|\Delta_{\mathbf{Q}_x}|^2, |\Delta_{-\mathbf{Q}_x}|^2, |\Delta_{\mathbf{Q}_y}|^2, |\Delta_{-\mathbf{Q}_y}|^2] \tag{11.2}$$

which transforms in the trivial representation for $U(1)$ and $T$. A systematic way of finding the irreducible representations of $\Gamma^{(2)}$ is to calculate the characters[3] $\chi_{\Gamma^{(2)}} = (4,0,0,0,2,2,0,0)$ and compare to the character table of $C_{4v}$ (see Table 11.1). We then project[4] the characters on each irreducible representation $(\chi_{\Gamma^{(2)}}, \chi_{A_{1g}}) = 1$, $(\chi_{\Gamma^{(2)}}, \chi_{A_{2g}}) = 0$, $(\chi_{\Gamma^{(2)}}, \chi_{B_{1g}}) = 1$, $(\chi_{\Gamma^{(2)}}, \chi_{B_{2g}}) = 0$ and $(\chi_{\Gamma^{(2)}}, \chi_{E_u}) = 1$, which yields $\Gamma^{(2)} = A_{1g} \oplus B_{1g} \oplus E_u$.

[3] The character can be found as the trace of the matrix that realizes the symmetry operation.

[4] Utilizing the grand-orthogonality theorem in group theory [141]

$$(\chi_i, \chi_j) = \frac{1}{|G|} \sum_{g \in G} \chi_i(g) \chi_j(g) = \delta_{ij} \tag{11.3}$$

where $i, j$ labels the irreducible representations of the group.

| | E | $2C_4$ | $C_2$ | $2\sigma_v$ | $2\sigma_d$ |
|---|---|---|---|---|---|
| $A_{1g}$ | 1 | 1 | 1 | 1 | 1 |
| $A_{2g}$ | 1 | 1 | 1 | -1 | -1 |
| $B_{1g}$ | 1 | -1 | 1 | 1 | -1 |
| $B_{2g}$ | 1 | -1 | 1 | -1 | 1 |
| $E_u$ | 2 | 0 | -2 | 0 | 0 |

**Table 11.1:** Character table for the irreducible representations of $C_{4v}$ (the relevant subgroup of $D_{4h}$ for (11.2)). The irreducible representations are listed to the left and their character of each and every symmetry operation. The size of the group $|G| = 8$.

Explicitly, the decomposition takes the form

$$\begin{aligned} A_{1g}: &\quad \psi_\Delta = |\Delta_{\mathbf{Q}_x}|^2 + |\Delta_{-\mathbf{Q}_x}|^2 + |\Delta_{\mathbf{Q}_y}|^2 + |\Delta_{-\mathbf{Q}_y}|^2 \\ B_{1g}: &\quad N_\Delta = |\Delta_{\mathbf{Q}_x}|^2 + |\Delta_{-\mathbf{Q}_x}|^2 - |\Delta_{\mathbf{Q}_y}|^2 - |\Delta_{-\mathbf{Q}_y}|^2 \\ E_u: &\quad \vec{l}_\Delta = \begin{bmatrix} |\Delta_{\mathbf{Q}_x}|^2 - |\Delta_{-\mathbf{Q}_x}|^2 \\ |\Delta_{\mathbf{Q}_y}|^2 - |\Delta_{-\mathbf{Q}_y}|^2 \end{bmatrix}. \end{aligned} \tag{11.4}$$

All these bilinears can acquire a finite expectation value while the underlying order parameters remain unordered, $\langle \Delta_{\mathbf{Q}} \rangle = 0$, indicating vestigial ordering.

Note that $\psi_\Delta, N_\Delta, \vec{l}_\Delta$ are not the actual quantities we identify with the vestigial order parameters. First after promoting these to independent fluctuating fields, using the HS transformation, we will call them order parameters. (The subscript $\Delta$ indicates the direct dependence on the PDW fields.) Furthermore, it should also be noted that a finite expectation value of $\psi_\Delta$ does not indicate order, but only fluctuations.

## 11.2 Action

The most general action can be found by writing down all terms that are invariant under the full symmetry group. Starting with the stationary part of the action we see that second order terms in $\Delta$ can only be formed by $\psi_\Delta$, which transforms in the trivial representation. To fourth order in fields we can construct terms by products of $\Gamma^{(2)}$, i.e. $\Gamma^{(2)} \otimes \Gamma^{(2)} = (A_{1g} \oplus B_{1g} \oplus E_u) \otimes (A_{1g} \oplus B_{1g} \oplus E_u) = 3A_{1g} \oplus A_{2g} \oplus 3B_{1g} \oplus B_{2g} \oplus 4E_u$. (Products of two irreducible representation can be constructed by multiplying their character for each

group element and then decompose it as before[5]). We find three possible fourth order terms that transforms in the trivial $A_{1g}$ representation. Two of them are the products $\psi_\Delta^2, N_\Delta^2$ ($A_{1g}\otimes A_{1g}=A_{1g}, B_{1g}\otimes B_{1g}=A_{1g}$) and the third comes from the product of two $\vec{l}_\Delta$ ($E_u\otimes E_u = A_{1g}\oplus A_{2g}\oplus B_{1g}\oplus B_{2g}$). Thus, to fourth order in fields

$$S_{\text{Stat.}}(\Delta)=\int_{\mathbf{x}} r\psi_\Delta(\mathbf{x})+\frac{u_0}{2}\psi_\Delta(\mathbf{x})^2+\frac{u_1}{2}N_\Delta(\mathbf{x})^2+\frac{u_2}{2}\vec{l}_\Delta(\mathbf{x})^2. \tag{11.5}$$

To find all possible terms including derivatives we consider forming products between $\vec{D}=(D_x,D_y)=-i\nabla-e^*\mathbf{A}$, transforming as $E_u$, and the bilinears $\Gamma^{(2)}=A_{1g}\oplus B_{1g}\oplus E_u$. To first order in derivatives we can only form invariants by multiplying $\vec{D}\otimes\vec{l}_\Delta = A_{1g}\oplus\ldots$ where we find

$$\Delta^*_{\mathbf{Q}_x}(D_x\Delta_{\mathbf{Q}_x})-\Delta^*_{-\mathbf{Q}_x}(D_x\Delta_{-\mathbf{Q}_x})+\Delta^*_{\mathbf{Q}_y}(D_y\Delta_{\mathbf{Q}_y})-\Delta^*_{-\mathbf{Q}_y}(D_y\Delta_{-\mathbf{Q}_y})+c.c. \tag{11.6}$$

However, the existence of such a term implies that the action is not minimized with regard to the momentum of the PDW fields. Thus, by the assumption of stability, this term is left out. To second order in derivatives $\vec{D}\otimes\vec{D}=A_{1g}\oplus A_{2g}\oplus B_{1g}\oplus B_{2g}$, multiplying these objects with $\Gamma^{(2)}$ we find two symmetry invariant terms

$$\begin{aligned}S_{\text{Dyn.}}(\Delta)=\int_{\mathbf{x}} &\sum_{\mathbf{q}=\pm\mathbf{Q}_x,\pm\mathbf{Q}_y}\kappa_1\Big((D_x\Delta_{\mathbf{q}})^*(D_x\Delta_{\mathbf{q}})+(D_y\Delta_{\mathbf{q}})^*(D_y\Delta_{\mathbf{q}})\Big)\\ &+\sum_{\mathbf{q}=\pm\mathbf{Q}_x}\kappa_2\Big((D_x\Delta_{\mathbf{q}})^*(D_x\Delta_{\mathbf{q}})-(D_y\Delta_{\mathbf{q}})^*(D_y\Delta_{\mathbf{q}})\Big)\\ &-\sum_{\mathbf{q}=\pm\mathbf{Q}_y}\kappa_2\Big((D_x\Delta_{\mathbf{q}})^*(D_x\Delta_{\mathbf{q}})-(D_y\Delta_{\mathbf{q}})^*(D_y\Delta_{\mathbf{q}})\Big).\end{aligned} \tag{11.7}$$

Finally, we decouple the fourth-order terms in (11.5) using the HS transformation by introducing the auxiliary fields $\psi, N$ and $\vec{l}$

$$\begin{aligned}S_{\text{Stat.}}(\Delta,\psi,N,\vec{l})=\int_{\mathbf{x}} &r\psi_\Delta(\mathbf{x})+\psi(\mathbf{x})\psi_\Delta(\mathbf{x})+N(\mathbf{x})N_\Delta(\mathbf{x})+\vec{l}(\mathbf{x})\cdot\vec{l}_\Delta(\mathbf{x})\\ &-\frac{\psi(\mathbf{x})^2}{2u_0}-\frac{N(\mathbf{x})^2}{2u_1}-\frac{\vec{l}(\mathbf{x})^2}{2u_2}.\end{aligned} \tag{11.8}$$

[5]This is a property of the trace of a Kronecker product $\text{Tr}(A\otimes B)=\text{Tr}(A)\text{Tr}(B)$.

The total action $S_{\text{Stat.}}(\Delta, \psi, N, \vec{l}) + S_{\text{Dyn.}}(\Delta)$ is quadratic in $\Delta$ which can be integrated out analogously to what we did before; yielding an effective action $S_{\text{eff}}(\psi, N, \vec{l})$, only dependent on the vestigial orders.

## 11.3 High and low temperature vestigial phase from PDW

Whether or not a preemptive transition in reality occurs can seem a bit clouded from the final action $S_{\text{eff}}(\psi, N, \vec{l})$. However, since fluctuations generally act to disorder, not order, we anticipate that a certain vestigial phase only occurs if there is a stable mean-field state breaking the corresponding symmetry.

Consider the PDW action in (11.5). Stability of the action requires $u_0 > 0$, while mean-field order occur for $r < 0$. With $u_1, u_2 > 0$ the development of $B_{1g}$ and $E_u$ order cost energy, thus the mean-field ground state will be tetragonally symmetric[6]. For $u_1 < 0$ developing nematic order will be advantageous. Similarly for $u_2 < 0$, developing $\vec{l}$ order is energetically favorable. Furthermore, $E_u$ order implies a subleading nematic order $l_x^2 - l_y^2, l_x l_y$. This means that we, in general, should anticipate a finite nematic order, $N \neq 0$, for $u_2 < 0$, $u_1 > 0$ as well[7]. Put together, we anticipate to find a nematic vestigial phase (with $\Delta = 0$) for $u_1 < 0$, and a vestigial LC phase for $u_2 < 0$. Indeed this turns out to be the case.

However, as discussed in Paper D, within the region $u_2 < 0, u_1 > 0$ a special exception to this "rule" occurs. With a mean-field state given by $[\Delta_{\mathbf{Q}_x}, \Delta_{-\mathbf{Q}_x}, \Delta_{\mathbf{Q}_y}, \Delta_{-\mathbf{Q}_y}] = [\Delta, 0, \Delta, 0]$, i.e., a state with LC and subleading $B_{2g}$ nematic order $l_x l_y$, the vestigial phase turned out to be split into two different phases. One low-temperature vestigial phase, with $l_x = l_y$, consistent with the mean-field ground state, but also one high-temperature vestigial phase with $l_x \neq 0, l_y = 0$, breaking another symmetry of the point-group. To reconcile this result with the mean-field calculation, we note that the first excited mean-field state is of the form $[\Delta_{\mathbf{Q}_x}, \Delta_{-\mathbf{Q}_x}, \Delta_{\mathbf{Q}_y}, \Delta_{-\mathbf{Q}_y}] = [\Delta, 0, \Delta', \Delta']$, having LC and subleading $B_{1g}$ nematic order. Thus, the interpretation is that fluctuations induce a transition between the would-be mean-field ground

[6] $\Delta_{\mathbf{Q}_x} = \Delta_{\mathbf{Q}_y} = \Delta_{-\mathbf{Q}_x} = \Delta_{-\mathbf{Q}_y}$.

[7] In Paper D we refer to $N \sim |\Delta_{\mathbf{Q}_x}|^2 + \Delta_{-\mathbf{Q}_x}|^2 - |\Delta_{\mathbf{Q}_y}|^2 - \Delta_{-\mathbf{Q}_y}|^2$ as a primary $B_{1g}$ nematic order to distinguish it from the subleading $(B_{1g}, B_{2g})$ nematic orders $l_x^2 - l_y^2, l_x l_y$. Note that there is no support for a primary $B_{2g}$ nematic order outline here.

state, and the first excited state.

### 11.3.1 Emergent rotational symmetry

The occurrence of a high and low-temperature vestigial phase, both with LC order, but with different subleading nematic orders, $l_x = 0, l_y \neq 0; l_x = l_y$, implies an enhanced symmetry at the transition, $C_4 \to C_8$. It turns out that for a specific set of parameters, this symmetry is enhanced even further, to rotational symmetry, $C_8 \to C_\infty$. At this point, the LC order becomes rotational symmetric, $\vec{l} = |\vec{l}|(\cos(\phi), \sin(\phi))$, with arbitrary $\phi$. Thus, the subleading nematic orders define an XY nematic order

$$\begin{bmatrix} \frac{l_x^2 - l_y^2}{2} & l_x l_y \\ l_x l_y & \frac{l_y^2 - l_x^2}{2} \end{bmatrix}, \tag{11.9}$$

instead of two Ising nematic orders. While this is indeed a result of fine-tuning we see that in vicinity of this transition, $B_{1g}$ and $B_{2g}$ nematic orders would be near degenerate and easily influenced by an external field.

## 11.4 Coupling to a homogeneous superconductivity — the nematic superconductor

The other major theme of Paper D was to investigate the influence of the PDW action on a homogeneous superconducting field. Since a homogeneous superconducting field, $\Delta_0$ transforms in the trivial representation under point-group symmetries, it does not couple to any static PDW field term in any other way besides a pure "competition" term, $|\Delta_0|^2|\Delta_{\mathbf{Q}}|^2$. However, allowing for derivatives $\vec{D}$, transforming as $E_u$, acting on $\Delta_0$, we can form terms transforming as $B_{1g}$ and $B_{2g}$ to second order in $\vec{D}$ and $\Delta_0$. These terms will couple to the PDW bilinears $N_{x^2-y^2} \sim (|\Delta_{\mathbf{Q}_x}|^2 + |\Delta_{-\mathbf{Q}_x}|^2 - |\Delta_{\mathbf{Q}_y}|^2 - |\Delta_{-\mathbf{Q}_y}|^2)$ and $N_{xy} \sim (|\Delta_{\mathbf{Q}_+}|^2 + |\Delta_{-\mathbf{Q}_+}|^2 - |\Delta_{\mathbf{Q}_-}|^2 - |\Delta_{-\mathbf{Q}_-}|^2)$. Thus assuming the development of vestigial nematic order we can write an effective superconducting

action as

$$
\begin{aligned}
S_{SC}(\Delta_0) &= \int_{\mathbf{x}} r_0' |\Delta_0(\mathbf{x})|^2 + \left(\frac{1}{2\overline{m}_{\mathrm{p}}}\right)_{ij} (D_i\Delta_0(\mathbf{x}))(D_j\Delta_0(\mathbf{x}))^* \\
\frac{1}{\overline{m}_{\mathrm{p}}} &= \frac{\bar{I}}{\overline{m}} + \bar{S}, \quad \bar{S} = \begin{bmatrix} \frac{\gamma_1}{u_1} N_{x^2-y^2} & \frac{\gamma_1'}{u_1'} N_{xy} \\ \frac{\gamma_1'}{u_1'} N_{xy} & -\frac{\gamma_1}{u_1} N_{x^2-y^2} \end{bmatrix}
\end{aligned}
\tag{11.10}
$$

where we find $S$ on the same form as in (9.10)[8].

Terms to fourth order in fields and second order in derivatives are usually not included in GL theory since they are less significant compared to derivative terms arising to second order in fields. Here we assume that this is still true for PDW fields, but for the homogeneous superconducting field near the Lifshitz point, we know that the dispersion for second-order terms in $\Delta$ becomes flat. Thus, in this case, derivative terms occurring to fourth order in fields will become important.

[8] Here $\gamma$ is the coupling constant for the term $\gamma_1(|D_x\Delta_0|^2 - |D_y\Delta_0|^2)(|\Delta_{\mathbf{Q}_x}|^2 + |\Delta_{-\mathbf{Q}_x}|^2 - |\Delta_{\mathbf{Q}_y}|^2 - |\Delta_{-\mathbf{Q}_y}|^2)$. The prime $'$ refers to the $\pm$ coordinates..

# PART III
# CONCLUSION AND OUTLOOK

An underlying pair-density wave (PDW) instability in the cuprate system is an intriguing proposal with the possibility of unifying many features seen in the pseudogap. In this thesis, we discussed both the nature of the PDW instability and the observable consequences of a PDW state.

In Paper A, we identify the unnatural occurrence of a PDW state based on weak-coupling scenarios from ordinary density-density like interactions. While others have used methods taking stronger correlations into account [9, 107] we decided to study a more general type of interaction, including the so-called pair-hopping interaction. The pair-hopping interaction is likely to be relevant only as an effective emergent interaction, arising due to strong correlation[9]. However, this interaction emphasizes the uniqueness of having a stable PDW state. Since an FF-PDW state breaks time-reversal, in addition to violating U(1) symmetry, we expect a finite supercurrent. However, a true ground state can not have a finite current. Through the emergence of an anomalous Josephson-like current term, the pair-hopping interaction provides at least one possible explanation of how such a current can cancel.

In Paper B, we continued the investigation of the pair-hopping interaction but in a milder form, considering only a small tendency of pairs to jump. From this, we saw how a pair-hopping interaction naturally generates a superconducting dispersion with the possibility of developing minima at finite momentum. Indeed this form is expected as a (long-wavelength) effective (field) theory of a PDW instability, and the microscopic form of the pair-hoping interaction is irrelevant; we simply view it as one possibility of many microscopic realizations of the same effective theory. However, when using the BCS-BEC crossover framework, we found that a finite pair-hopping term *always* gives rise to finite momentum instability for strong enough interaction. Thus, even a small microscopic pair-hopping term could explain the occurrence of a PDW instability in a strong-coupling system.

[9] It should, however, be noted that a finite pair-hopping term should be generated even from a microscopic interaction [40].

In Paper C, we digressed from the possibility of a PDW, focusing on the homogeneous superconducting state instead. We showed that transport measurements on thin films of LSCO are consistent with a highly anisotropic fluctuating superconducting state. This observation is puzzling since a single-component d-wave superconducting order can not be decomposed into a nematic order. Instead, we asserted the development of nematic order in the dynamical response of the superconducting state, the effective mass.

While Paper C did not assume any origin of the nematic response in Paper D, we considered a scenario of a vestigial PDW phase. In contrast to the single-component SC order, a multi-component PDW has the possibility of setting up nematic phases. Other multi-component order could just as well be considered to generate a nematic phase, like CDW. However, as discussed, a PDW instability can explain the high susceptibility towards anisotropic fluctuations of the superconductor through a renormalization of the pair mass.

Furthermore, in Paper D, we explored the possibility of a ME PDW state, a state with LC order, as a contestant for the pseudogap state. We showed that the vestigial phase set up by a LC state has the possibility of developing an emergent rotational symmetric state. We discussed this as an origin for a soft nematic state, a state where the nematic director easily gets pinned along an arbitrary direction.

# 12 The PDW instability — a possible scenario for the cuprates

As a way to summarize the findings in this thesis, as well as connect it to the experimental status of the cuprates, we consider the phenomenological phase diagram in Figure 12.1, where the pseudogap state consists of a fluctuating PDW state. Inspired by the results of Paper B and D, we roughly identify the increase of doping with increased interaction (Figure 7.3).

At low doping and temperature, we have a mean-field PDW state, possibly disordered (by fluctuations or impurities). When the doping increases, the SC dome develops, in general, with the possibility of a coexistence phase. The PDW state yields several possible vestigial phases at higher temperatures, including loop-current (LC) and nematic order. At the intersection between

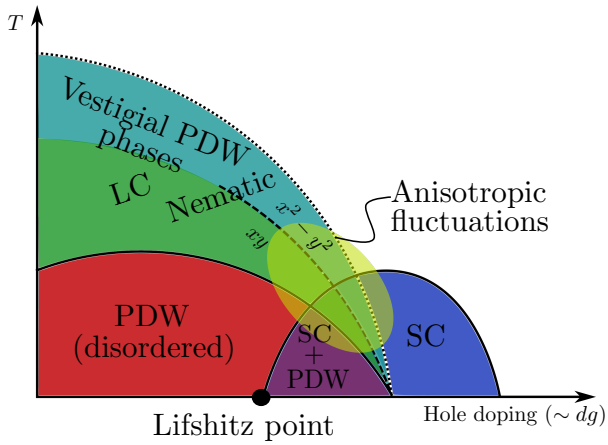


**Figure 12.1:** A suggestive phase diagram based on the PDW instability, discussed in this thesis. The pseudogap is imagined to consist of a fluctuating PDW state with possible vestigial orders, including loop-current (LC) and nematic order. Above the transition temperature on the underdoped side, we expect to find anisotropic fluctuations. Included here is also the scenario of Paper D where the PDW vestigial phase is split into a low-temperature $xy$ and high-temperature $x^2-y^2$ nematic phase. The intersection between the two phases, a soft nematic state is anticipated to occur, marked by a dashed line.

the nematic phase and the superconducting phase, we find anisotropic superconducting fluctuations. We also identify the possibility of a splitting of the vestigial phase into a low-temperature, $xy$ nematic, and a high-temperature $x^2-y^2$ nematic phase, separated by a first-order transition (indicated by a dashed line). According to the result in Paper D, this can give rise to an emergent rotational symmetry and a soft nematic state.

The phenomenological discussion of the PDW instability in Paper B gave rise to two distinct possibilities. One where the PDW develops from zero momentum through a Lifshitz point, with a diverging pair mass, and one where the momenta develop at a finite value. In Figure 12.1, we considered the latter case, with the Lifshitz point hidden under the transition. This situation seems to agree best with the "1/8 anomaly" in LBCO, where the PDW momenta are given by stripes $Q \approx 2\pi/8a$ [11]. In this case, the superconducting state at $x = 1/8$ should be identified with a PDW, possibly with subleading SC. However, the experimental findings of PDW in vortex halos in BSCCO are

of the opposite type, with leading SC and subleading PDW, since the PDW only occur after the SC component been suppressed by a magnetic field [16].

The study of anisotropic fluctuating nematicity in LSCO, presented in Paper C and interpreted in Paper D, also belongs to the assumption of a subleading PDW with leading SC. However, here we identified the need for a rather strong mass renormalization, suggesting proximity to the Lifshitz point. This also accounts for the decreasing $T_c$ on the underdoped side of the superconducting dome. Usually, this effect is attributed to the small number of carriers [93]. However, it is really the phase stiffness, $\rho_s = \frac{\hbar^2 n}{2m_\mathrm{p}}$ that matters, which can become small either from low number of carriers, $n$, or a large mass $m_\mathrm{p}$, or both.

There is also some experimental evidence for a soft nematic state in the cuprate system. In Paper C, we assumed the occurrence of two constant coexisting $xy$ and $x^2-y^2$ nematic orders. The evolution of the nematic director resulted from the temperature dependence of the paraconductivity and the normal component conductivity. However, one could imagine a twist of the nematic director itself due to a soft nematic state. Especially, we note that the rapid evolution of the nematic director as a function of temperature is confined near optimum doping. A soft nematic state is also expected to be sensitive to quenched disorder, which could explain the vanishing nematic domains in BSSCO [71], again near optimum doping. Thus, both the nematic order in LSCO and BSCCO might be explained by a soft nematic state, with the difference that the nematicity is pinned in LSCO while left to disorder in BSCCO.

# 13 Outlook

The picture in Figure 12.1 is a crudely painted one. In particular, one crucial feature of the cuprate system missing is the anti-ferromagnetic (AF) state. Also, the pair-hopping interaction does not take the lattice into account. A more complete scenario could be to consider a PDW instability, possibly generated by pair-hopping, pinned by stripes, which in turn arise from an AF instability. Superimposing the scenario of Figure 12.1 with that of an AF and stripe instability might yield a phase diagram more reminiscent of the cuprate phase diagram.

In Paper B, we found that the pair-hoping interaction leads to the existence of a new critical point, the super-Lifshitz point, where second and fourth-order derivative terms cancel simultaneously. Exploration of the critical behavior of this point could be worth pursuing in order to find fingerprints of the pair-hopping interaction.

Intermediate coupling strengths are seemingly the most relevant for the cuprate system. In this regime, fermionic and bosonic excitations are of equal importance, and our considerations of the weak and strong coupling limits receive corrections. In particular, it would be interesting to consider more exact approaches to treat the pair-hopping interaction, like exact diagonalization and density-matrix renormalization group. A more direct extension on the work done on vestigial orders in Paper D is to consider the fate of the fermionic excitations in these phases.

The high anisotropic fluctuations seen in LSCO remain, to some extent, a puzzling observation, and more experimental work is needed to unravel the workings of this material. Most important is to look for signs of anisotropy in other experimental probes. A direct extension to the transport measurements considered in Paper C is to look at the supercurrent as well as vortex dynamics.

“But, why?”
- Ryan Reynolds
*Harold and Kumar Go To White Castle*

# Bibliography

[1] P. W. Anderson, *More is different*, Science **177**, 393–396 (1972).

[2] J. G. Bednorz and K. A. Müller, *Possible high $T_c$ superconductivity in the Ba- La- Cu- O system*, Zeitschrift für Physik B Condensed Matter **64**, 189–193 (1986).

[3] E. Fradkin, S. A. Kivelson and J. M. Tranquada, *Colloquium: Theory of intertwined orders in high temperature superconductors*, Reviews of Modern Physics **87**, 457 (2015).

[4] J. Tranquada, H. Woo, T. Perring, H. Goka, G. Gu, G. Xu, M. Fujita and K. Yamada, *Quantum magnetic excitations from stripes in copper oxide superconductors*, Nature **429**, 534–538 (2004).

[5] A. Mesaros, K. Fujita, S. D. Edkins, M. H. Hamidian, H. Eisaki, S.-i. Uchida, J. S. Davis, M. J. Lawler and E.-A. Kim, *Commensurate 4a-period charge density modulations throughout the $Bi_2Sr_2CaCu_2O_{8+x}$ pseudogap regime*, Proceedings of the National Academy of Sciences **113**, 12661–12666 (2016).

[6] J. Tranquada, B. Sternlieb, J. Axe, Y. Nakamura and S. Uchida, *Evidence for stripe correlations of spins and holes in copper oxide superconductors*, Nature **375**, 561 (1995).

[7] E. H. da Silva Neto, P. Aynajian, A. Frano, R. Comin, E. Schierle, E. Weschke, A. Gyenis, J. Wen, J. Schneeloch, Z. Xu *et al.*, *Ubiquitous interplay between charge ordering and high-temperature superconductivity in cuprates*, Science **343**, 393–396 (2014).

[8] R. Comin, R. Sutarto, F. He, E. da Silva Neto, L. Chauviere, A. Frano, R. Liang, W. Hardy, D. Bonn, Y. Yoshida *et al.*, *Symmetry of charge order in cuprates*, Nature materials **14**, 796–800 (2015).

[9] A. Himeda, T. Kato and M. Ogata, *Stripe states with spatially oscillating d-wave superconductivity in the two-dimensional t- t'- J model*, Physical Review Letters **88**, 117001 (2002).

[10] E. Berg, E. Fradkin and S. A. Kivelson, *Theory of the striped superconductor*, Physical Review B **79**, 064515 (2009).

[11] E. Berg, E. Fradkin, E.-A. Kim, S. A. Kivelson, V. Oganesyan, J. M. Tranquada and S. Zhang, *Dynamical layer decoupling in a stripe-ordered high-$T_c$ superconductor*, Physical Review Letters **99**, 127003 (2007).

[12] P. A. Lee, *Amperean pairing and the pseudogap phase of cuprate superconductors*, Physical Review X **4**, 031017 (2014).

[13] A. Moodenbaugh, Y. Xu, M. Suenaga, T. Folkerts and R. Shelton, *Superconducting properties of $La_{2-x}Ba_xCuO_4$*, Physical Review B **38**, 4596 (1988).

[14] Q. Li, M. Hücker, G. Gu, A. Tsvelik and J. Tranquada, *Two-dimensional superconducting fluctuations in stripe-ordered $La_{1.875}Ba_{0.125}$ $CuO_4$*, Physical Review Letters **99**, 067001 (2007).

[15] M. Hamidian, S. Edkins, S. H. Joo, A. Kostin, H. Eisaki, S. Uchida, M. Lawler, E.-A. Kim, A. Mackenzie, K. Fujita *et al.*, *Detection of a cooper-pair density wave in $Bi_2Sr_2CaCu_2O_{8+x}$*, Nature **532**, 343–347 (2016).

[16] S. D. Edkins, A. Kostin, K. Fujita, A. P. Mackenzie, H. Eisaki, S. Uchida, S. Sachdev, M. J. Lawler, E.-A. Kim, J. S. Davis *et al.*, *Magnetic field–induced pair density wave state in the cuprate vortex halo*, Science **364**, 976–980 (2019).

[17] E. Berg, E. Fradkin and S. A. Kivelson, *Charge-4e superconductivity from pair-density-wave order in certain high-temperature superconductors*, Nature Physics **5**, 830–833 (2009).

[18] D. G. Barci and E. Fradkin, *Role of nematic fluctuations in the thermal melting of pair-density-wave phases in two-dimensional superconductors*, Physical Review B **83**, 100509 (2011).

[19] D. Agterberg and H. Tsunetsugu, *Dislocations and vortices in pair-density-wave superconductors*, Nature Physics **4**, 639–642 (2008).

[20] D. F. Agterberg, D. S. Melchert and M. K. Kashyap, *Emergent loop current order from pair density wave superconductivity*, Physical Review B **91**, 054502 (2015).

[21] Y. Wang, S. D. Edkins, M. H. Hamidian, J. S. Davis, E. Fradkin and S. A. Kivelson, *Pair density waves in superconducting vortex halos*, Physical Review B **97**, 174510 (2018).

[22] Z. Dai, Y.-H. Zhang, T. Senthil and P. Lee, *Pair density wave, charge density wave and vortex in high $t_c$ cuprates*, arXiv preprint arXiv:1802.03009 (2018).

[23] J. Wu, A. Bollinger, X. He and I. Božović, *Spontaneous breaking of rotational symmetry in copper oxide superconductors*, Nature **547**, 432 (2017).

[24] H. Kamerlingh Onnes, *The resistance of pure mercury at helium temperatures*, Commun. Phys. Lab. Univ. Leiden, b **120** (1911).

[25] W. Meissner and R. Ochsenfeld, *Ein neuer effekt bei eintritt der supraleitfähigkeit*, Naturwissenschaften **21**, 787–788 (1933).

[26] F. London, *A new conception of supraconductivity*, 1937.

[27] J. Bardeen, L. N. Cooper and J. R. Schrieffer, *Theory of superconductivity*, Physical Review **108**, 1175 (1957).

[28] A. Schilling, M. Cantoni, J. Guo and H. Ott, *Superconductivity above 130 K in the Hg–Ba–Ca–Cu–O system*, Nature **363**, 56–58 (1993).

[29] V. Ginzburg, *On the theory of superconductivity*, Zh. eksper. teor. Fiz. **20**, 1064–1082 (1950).

[30] L. N. Cooper, *Bound electron pairs in a degenerate fermi gas*, Physical Review **104**, 1189 (1956).

[31] P. Coleman, *Introduction to many-body physics*. Cambridge University Press, 2015.

[32] P.-G. De Gennes, *Superconductivity of metals and alloys*. CRC Press, 2018.

[33] P. Fulde and R. A. Ferrell, *Superconductivity in a strong spin-exchange field*, Physical Review **135**, A550 (1964).

[34] A. Larkin and I. Ovchinnikov, *Inhomogeneous state of superconductors(production of superconducting state in ferromagnet with fermi surfaces, examining green function)*, Soviet Physics-JETP **20**, 762–769 (1965).

[35] J. Bardeen and D. Pines, *Electron-phonon interaction in metals*, Physical Review **99**, 1140 (1955).

[36] J. Orenstein and A. Millis, *Advances in the physics of high-temperature superconductivity*, Science **288**, 468–474 (2000).

[37] P. W. Anderson, *The resonating valence bond state in la2cuo4 and superconductivity*, science **235**, 1196–1198 (1987).

[38] J. M. Tranquada, *Spins, stripes, and superconductivity in hole-doped cuprates*, in *AIP Conference Proceedings*, vol. 1550, pp. 114–187, AIP. 2013.

[39] E. Pellegrin, N. Nücker, J. Fink, S. Molodtsov, A. Gutiérrez, E. Navas, O. Strebel, Z. Hu, M. Domke, G. Kaindl *et al.*, *Orbital character of states at the fermi level in* $La_{2-x}Sr_xCuO_4$ *and* $R_{2-x}Ce_xCuO_4$ *(R= Nd, Sm)*, Physical Review B **47**, 3354 (1993).

[40] J. Hubbard, *Electron correlations in narrow energy bands*, Proc. R. Soc. Lond. A **276**, 238–257 (1963).

[41] P. W. Anderson, *New approach to the theory of superexchange interactions*, Physical Review **115**, 2 (1959).

[42] E. Fradkin, *Field theories of condensed matter physics*. Cambridge University Press, 2013.

[43] I. Božović, X. He, J. Wu and A. Bollinger, *Dependence of the critical temperature in overdoped copper oxides on superfluid density*, Nature **536**, 309 (2016).

[44] B. Keimer, S. A. Kivelson, M. R. Norman, S. Uchida and J. Zaanen, *From quantum matter to high-temperature superconductivity in copper oxides*, Nature **518**, 179 (2015).

[45] C. Varma, P. B. Littlewood, S. Schmitt-Rink, E. Abrahams and A. Ruckenstein, *Phenomenology of the normal state of Cu-O high-temperature superconductors*, Physical Review Letters **63**, 1996 (1989).

[46] J. Xia, E. Schemm, G. Deutscher, S. Kivelson, D. Bonn, W. Hardy, R. Liang, W. Siemons, G. Koster, M. Fejer *et al.*, *Polar Kerr-effect measurements of the high-temperature $YBa_2Cu_3O_{6+x}$ superconductor: evidence for broken symmetry near the pseudogap temperature*, Physical Review Letters **100**, 127002 (2008).

[47] L. Li, Y. Wang, S. Komiya, S. Ono, Y. Ando, G. Gu and N. Ong, *Diamagnetism and Cooper pairing above $T_c$ in cuprates*, Physical Review B **81**, 054510 (2010).

[48] A. Achkar, M. Zwiebler, C. McMahon, F. He, R. Sutarto, I. Djianto, Z. Hao, M. J. Gingras, M. Hücker, G. Gu *et al.*, *Nematicity in stripe-ordered cuprates probed via resonant x-ray scattering*, Science **351**, 576–578 (2016).

[49] E. Fradkin, S. A. Kivelson, M. J. Lawler, J. P. Eisenstein and A. P. Mackenzie, *Nematic fermi fluids in condensed matter physics*, Annu. Rev. Condens. Matter Phys. **1**, 153–178 (2010).

[50] M. Zelli, C. Kallin and A. J. Berlinsky, *Mixed state of a $\pi$-striped superconductor*, Physical Review B **84**, 174525 (2011).

[51] M. Norman and J. Davis, *Quantum oscillations in a biaxial pair density wave state*, arXiv preprint arXiv:1802.04333 (2018).

[52] S. A. Kivelson, E. Fradkin and V. J. Emery, *Electronic liquid-crystal phases of a doped mott insulator*, Nature **393**, 550 (1998).

[53] S. Uchida, T. Ido, H. Takagi, T. Arima, Y. Tokura and S. Tajima, *Optical spectra of $La_{2-x}Sr_xCuO_4$: Effect of carrier doping on the electronic structure of the $CuO_2$ plane*, Physical Review B **43**, 7942 (1991).

[54] J. Zaanen, G. Sawatzky and J. Allen, *Band gaps and electronic structure of transition-metal compounds*, Physical Review Letters **55**, 418 (1985).

[55] V. Emery, *Theory of high-$T_c$ superconductivity in oxides*, Physical Review Letters **58**, 2794 (1987).

[56] A. Bianconi, J. Budnick, A. Flank, A. Fontaine, P. Lagarde, A. Marcelli, H. Tolentino, B. Chamberland, C. Michel, B. Raveau *et al.*, *Evidence of $3d^9$-ligand hole states in the superconductor $La_{1.85}Sr_{0.15}CuO_4$ from $L_3$ X-ray absorption spectroscopy*, Physics Letters A **127**, 285–291 (1988).

[57] C. Chen, F. Sette, Y. Ma, M. Hybertsen, E. Stechel, W. Foulkes, M. Schulter, S. Cheong, A. Cooper, L. Rupp Jr *et al.*, *Electronic states in $La_{2-x}Sr_xCuO_{4+\delta}$ probed by soft-X-ray absorption*, Physical Review Letters **66**, 104 (1991).

[58] F. Zhang and T. Rice, *Effective hamiltonian for the superconducting cu oxides*, Physical Review B **37**, 3759 (1988).

[59] T. Yoshida, X. Zhou, T. Sasagawa, W. Yang, P. Bogdanov, A. Lanzara, Z. Hussain, T. Mizokawa, A. Fujimori, H. Eisaki *et al.*, *Metallic behavior of lightly doped $La_{2-x}Sr_xCuO_4$ with a fermi surface forming an arc*, Physical Review Letters **91**, 027001 (2003).

[60] C. Tsuei, J. R. Kirtley, C. Chi, L. S. Yu-Jahnes, A. Gupta, T. Shaw, J. Sun and M. Ketchen, *Pairing symmetry and flux quantization in a tricrystal superconducting ring of $YBa_2Cu_3O_{7-\delta}$*, Physical Review Letters **73**, 593 (1994).

[61] J. Zaanen and O. Gunnarsson, *Charged magnetic domain lines and the magnetism of high-$T_c$ oxides*, Physical Review B **40**, 7391 (1989).

[62] M. Vojta, *Lattice symmetry breaking in cuprate superconductors: stripes, nematics, and superconductivity*, Advances in Physics **58**, 699–820 (2009).

[63] S. A. Kivelson, I. P. Bindloss, E. Fradkin, V. Oganesyan, J. Tranquada, A. Kapitulnik and C. Howald, *How to detect fluctuating stripes in the high-temperature superconductors*, Reviews of Modern Physics **75**, 1201 (2003).

[64] M. Fujita, H. Goka, K. Yamada, J. Tranquada and L. Regnault, *Stripe order, depinning, and fluctuations in $La_{1.875}Ba_{0.125}CuO_4$ and $La_{1.875}Ba_{0.075}Sr_{0.050}CuO_4$*, Physical Review B **70**, 104517 (2004).

[65] M. Hücker, M. v. Zimmermann, G. Gu, Z. Xu, J. Wen, G. Xu, H. Kang, A. Zheludev and J. M. Tranquada, *Stripe order in superconducting* $La_{2-x}Ba_xCuO_4$ *(0. 095< x< 0. 155)*, Physical Review B **83**, 104506 (2011).

[66] J. Tranquada, G. Gu, M. Hücker, Q. Jie, H.-J. Kang, R. Klingeler, Q. Li, N. Tristan, J. Wen, G. Xu *et al.*, *Evidence for unusual superconducting correlations coexisting with stripe order in* $La_{1.875}Ba_{0.125}\ CuO_4$, Physical Review B **78**, 174529 (2008).

[67] N. D. Mermin and H. Wagner, *Absence of ferromagnetism or antiferromagnetism in one-or two-dimensional isotropic Heisenberg models*, Physical Review Letters **17**, 1133 (1966).

[68] J. M. Kosterlitz and D. J. Thouless, *Ordering, metastability and phase transitions in two-dimensional systems*, Journal of Physics C: Solid State Physics **6**, 1181 (1973).

[69] P. Minnhagen, *The two-dimensional coulomb gas, vortex unbinding, and superfluid-superconducting films*, Reviews of modern physics **59**, 1001 (1987).

[70] M. Lawler, K. Fujita, J. Lee, A. Schmidt, Y. Kohsaka, C. K. Kim, H. Eisaki, S. Uchida, J. Davis, J. Sethna *et al.*, *Intra-unit-cell electronic nematicity of the high-*$T_c$ *copper-oxide pseudogap states*, Nature **466**, 347 (2010).

[71] K. Fujita, C. K. Kim, I. Lee, J. Lee, M. Hamidian, I. Firmo, S. Mukhopadhyay, H. Eisaki, S. Uchida, M. Lawler *et al.*, *Simultaneous transitions in cuprate momentum-space topology and electronic symmetry breaking*, Science **344**, 612–616 (2014).

[72] S. Mukhopadhyay, R. Sharma, C. K. Kim, S. D. Edkins, M. H. Hamidian, H. Eisaki, S.-i. Uchida, E.-A. Kim, M. J. Lawler, A. P. Mackenzie *et al.*, *Evidence for a vestigial nematic state in the cuprate pseudogap phase*, Proceedings of the National Academy of Sciences 201821454 (2019).

[73] G. Ghiringhelli, M. Le Tacon, M. Minola, S. Blanco-Canosa, C. Mazzoli, N. Brookes, G. De Luca, A. Frano, D. Hawthorn, F. He *et al.*, *Long-range incommensurate charge fluctuations in (Y, Nd)* $Ba_2Cu_3O_{6+x}$, Science **337**, 821–825 (2012).

[74] J. Chang, E. Blackburn, A. Holmes, N. B. Christensen, J. Larsen, J. Mesot, R. Liang, D. Bonn, W. Hardy, A. Watenphul *et al.*, *Direct observation of competition between superconductivity and charge density wave order in $YBa_2Cu_3O_{6.67}$*, Nature Physics **8**, 871 (2012).

[75] S. Baruch and D. Orgad, *Spectral signatures of modulated d-wave superconducting phases*, Physical Review B **77**, 174502 (2008).

[76] R. M. Fernandes, P. P. Orth and J. Schmalian, *Intertwined vestigial order in quantum materials: nematicity and beyond*, Annual Review of Condensed Matter Physics **10**, 133–154 (2019).

[77] A. Shekhter and C. Varma, *Considerations on the symmetry of loop order in cuprates*, Physical Review B **80**, 214501 (2009).

[78] C. Varma, *Pseudogap phase and the quantum-critical point in copper-oxide metals*, Physical Review Letters **83**, 3538 (1999).

[79] C. Varma, *Proposal for an experiment to test a theory of high-temperature superconductors*, Physical Review B **61**, R3804 (2000).

[80] A. Kaminski, S. Rosenkranz, H. Fretwell, J. Campuzano, Z. Li, H. Raffy, W. Cullen, H. You, C. Olson, C. Varma *et al.*, *Spontaneous breaking of time-reversal symmetry in the pseudogap state of a high-$T_c$ superconductor*, Nature **416**, 610 (2002).

[81] B. Fauqué, Y. Sidis, V. Hinkov, S. Pailhes, C. Lin, X. Chaud and P. Bourges, *Magnetic order in the pseudogap phase of high-$T_c$ superconductors*, Physical Review Letters **96**, 197001 (2006).

[82] Y. Li, V. Balédent, N. Barišić, Y. Cho, B. Fauqué, Y. Sidis, G. Yu, X. Zhao, P. Bourges and M. Greven, *Unusual magnetic order in the pseudogap region of the superconductor $HgBa_2CuO_{4+\delta}$*, Nature **455**, 372 (2008).

[83] Y. Li, V. Balédent, N. Barišić, Y. Cho, Y. Sidis, G. Yu, X. Zhao, P. Bourges and M. Greven, *Magnetic order in the pseudogap phase of $HgBa_2CuO_{4+\delta}$ studied by spin-polarized neutron diffraction*, Physical Review B **84**, 224508 (2011).

[84] Y. Sidis and P. Bourges, *Evidence for intra-unit-cell magnetic order in the pseudo-gap state of high-$T_c$ cuprates*, in *Journal of Physics: Conference Series*, vol. 449, p. 012012, IOP Publishing. 2013.

[85] L. Mangin-Thro, Y. Sidis, P. Bourges, S. De Almeida-Didry, F. Giovannelli and I. Laffez-Monot, *Characterization of the intra-unit-cell magnetic order in $Bi_2Sr_2CaCu_2O_{8+\delta}$*, Physical Review B **89**, 094523 (2014).

[86] M. Simon and C. Varma, *Detection and implications of a time-reversal breaking state in underdoped cuprates*, Physical Review Letters **89**, 247003 (2002).

[87] C. Varma, *Theory of the pseudogap state of the cuprates*, Physical Review B **73**, 155113 (2006).

[88] J. Orenstein, *Optical nonreciprocity in magnetic structures related to high-$T_c$ superconductors*, Physical Review Letters **107**, 067002 (2011).

[89] V. M. Yakovenko, *Tilted loop currents in cuprate superconductors*, Physica B: Condensed Matter **460**, 159–164 (2015).

[90] P. A. Lee, N. Nagaosa and X.-G. Wen, *Doping a mott insulator: Physics of high-temperature superconductivity*, Reviews of modern physics **78**, 17 (2006).

[91] C. Kittel, P. McEuen and P. McEuen, *Introduction to solid state physics*, vol. 8. Wiley New York, 1996.

[92] M. Tinkham, *Introduction to superconductivity*. McGraw-Hill, New York, 1996.

[93] V. Emery and S. Kivelson, *Importance of phase fluctuations in superconductors with small superfluid density*, Nature **374**, 434 (1995).

[94] J. Schmalian, *Failed theories of superconductivity*, Modern Physics Letters B **24**, 2679–2691 (2010).

[95] M. Schafroth, S. Butler and J. Blatt, *Quasichemical equilibrium approach to superconductivity*, Helv. Phys. Acta **30**, 93–134 (1957).

[96] D. Eagles, *Possible pairing without superconductivity at low carrier concentrations in bulk and thin-film superconducting semiconductors*, Physical Review **186**, 456 (1969).

[97] A. J. Leggett, *Diatomic molecules and cooper pairs*, in *Modern trends in the theory of condensed matter*, pp. 13–27. Springer, 1980.

[98] M. Randeria, J.-M. Duan and L.-Y. Shieh, *Bound states, cooper pairing, and bose condensation in two dimensions*, Physical Review Letters **62**, 981 (1989).

[99] M. Drechsler and W. Zwerger, *Crossover from BCS-superconductivity to bose-condensation*, Annalen der Physik **504**, 15–23 (1992).

[100] C. S. De Melo, M. Randeria and J. R. Engelbrecht, *Crossover from BCS to Bose superconductivity: Transition temperature and time-dependent Ginzburg-Landau theory*, Physical Review Letters **71**, 3202 (1993).

[101] S. Stintzing and W. Zwerger, *Ginzburg-Landau theory of superconductors with short coherence length*, Physical Review B **56**, 9004 (1997).

[102] M. Hecker and J. Schmalian, *Vestigial nematic order and superconductivity in the doped topological insulator* $Cu_x Bi_2 Se_3$, npj Quantum Materials **3**, 26 (2018).

[103] F. Loder, A. P. Kampf and T. Kopp, *Superconducting state with a finite-momentum pairing mechanism in zero external magnetic field*, Physical Review B **81**, 020511 (2010).

[104] S. Robaszkiewicz and B. R. Bułka, *Superconductivity in the Hubbard model with pair hopping*, Physical Review B **59**, 6430 (1999).

[105] A. Ptok, M. M. Maśka and M. Mierzejewski, *The Fulde–Ferrell–Larkin–Ovchinnikov phase in the presence of pair hopping interaction*, Journal of Physics: Condensed Matter **21**, 295601 (2009).

[106] G. Japaridze, A. Kampf, M. Sekania, P. Kakashvili and P. Brune, *$\eta$-pairing superconductivity in the Hubbard chain with pair hopping*, Physical Review B **65**, 014518 (2001).

[107] P. Corboz, T. Rice and M. Troyer, *Competing states in the t-J model: Uniform d-wave state versus stripe state*, Physical Review Letters **113**, 046402 (2014).

[108] J. F. Dodaro, H.-C. Jiang and S. A. Kivelson, *Intertwined order in a frustrated four-leg t−J cylinder*, Phys. Rev. B **95**, 155116 (Apr, 2017).

[109] H. Kleinert, *Hubbard-Stratonovich transformation: Successes, failure, and cure*, arXiv preprint arXiv:1104.5161 (2011).

[110] P. M. Chaikin, T. C. Lubensky and T. A. Witten, *Principles of condensed matter physics*, vol. 1. Cambridge university press Cambridge, 1995.

[111] R. Hornreich, M. Luban and S. Shtrikman, *Critical behavior at the onset of k-space instability on the λ line*, Physical Review Letters **35**, 1678 (1975).

[112] E. B. Hansen, *Infinite conductivity of ordinary and gapless superconductors*, Physica **39**, 271–292 (1968).

[113] I. Khavkine, H.-Y. Kee and K. Maki, *Supercurrent in nodal superconductors*, Physical Review B **70**, 184521 (2004).

[114] H.-Y. Kee, Y. B. Kim and K. Maki, *Critical current of the spin-triplet superconducting phase in $Sr_2RuO_4$*, Physical Review B **70**, 052505 (2004).

[115] D. Bohm, *Note on a theorem of Bloch concerning possible causes of superconductivity*, Physical Review **75**, 502 (1949).

[116] P. Nozieres and S. Schmitt-Rink, *Bose condensation in an attractive fermion gas: From weak to strong coupling superconductivity*, Journal of Low Temperature Physics **59**, 195–211 (1985).

[117] J. Wallington and J. F. Annett, *BCS to bose crossover in anisotropic superconductors*, Physical Review B **61**, 1433 (2000).

[118] C. Regal, M. Greiner and D. S. Jin, *Observation of resonance condensation of fermionic atom pairs*, Physical Review Letters **92**, 040403 (2004).

[119] M. Zwierlein, C. Stan, C. Schunck, S. Raupach, A. Kerman and W. Ketterle, *Condensation of pairs of fermionic atoms near a Feshbach resonance*, Physical Review Letters **92**, 120403 (2004).

[120] M. Randeria, J.-M. Duan and L.-Y. Shieh, *Superconductivity in a two-dimensional fermi gas: Evolution from cooper pairing to bose condensation*, Phys. Rev. B **41**, 327–343 (Jan, 1990).

[121] R. Haussmann, *Properties of a F)ermi liquid at the superfluid transition in the crossover region between BCS superconductivity and Bose-Einstein condensation*, Physical Review B **49**, 12975 (1994).

[122] M. Randeria, W. Zwerger and M. Zwierlein, *The bcs–bec crossover and the unitary fermi gas*, in *The BCS-BEC Crossover and the Unitary Fermi Gas*, pp. 1–32. Springer, 2012.

[123] A. M. Schakel, *Time-dependent ginzburg-landau theory and duality*, in *Topological Defects and the Non-Equilibrium Dynamics of Symmetry Breaking Phase Transitions*, pp. 213–238. Springer, 2000.

[124] M. Randeria, J.-M. Duan and L.-Y. Shieh, *Superconductivity in a two-dimensional fermi gas: Evolution from cooper pairing to bose condensation*, Physical Review B **41**, 327 (1990).

[125] D. T. Son and M. Stephanov, *Phase diagram of a cold polarized fermi gas*, Physical Review A **74**, 013614 (2006).

[126] D. F. Agterberg and J. Garaud, *Checkerboard order in vortex cores from pair-density-wave superconductivity*, Physical Review B **91**, 104512 (2015).

[127] L. Aslamasov and A. Larkin, *The influence of fluctuation pairing of electrons on the conductivity of normal metal*, Physics Letters A **26**, 238–239 (1968).

[128] A. Larkin and A. Varlamov, *Theory of fluctuations in superconductors*. Clarendon Press, 2005.

[129] M. Cimberle, C. Ferdeghini, E. Giannini, D. Marre, M. Putti, A. Siri, F. Federici and A. Varlamov, *Crossover between Aslamazov-Larkin and*

*short-wavelength fluctuation regimes in high-temperature-superconductor conductivity experiments*, Physical Review B **55**, R14745 (1997).

[130] C. Carballeira, S. R. Currás, J. Vina, J. A. Veira, M. V. Ramallo and F. Vidal, *Paraconductivity at high reduced temperatures in $YBa_2Cu_3O_{7-\delta}$ superconductors*, Physical Review B **63**, 144515 (2001).

[131] S. R. Currás, G. Ferro, M. T. González, M. V. Ramallo, M. Ruibal, J. A. Veira, P. Wagner and F. Vidal, *In-plane paraconductivity in $La_{2-x}Sr_xCuO_4$ thin film superconductors at high reduced temperatures: Independence of the normal-state pseudogap*, Physical Review B **68**, 094501 (2003).

[132] H. Bruus and K. Flensberg, *Many-body quantum theory in condensed matter physics: an introduction*. Oxford university press, 2004.

[133] K. Maki, *Critical fluctuation of the order parameter in a superconductor. I*, Progress of Theoretical Physics **40**, 193–200 (1968).

[134] R. S. Thompson, *Microwave, flux flow, and fluctuation resistance of dirty type-II superconductors*, Physical Review B **1**, 327 (1970).

[135] S.-K. Yip, *Fluctuations in an impure unconventional superconductor*, Physical Review B **41**, 2612 (1990).

[136] M. Tinkham, *Resistive transition of high-temperature superconductors*, Physical Review Letters **61**, 1658 (1988).

[137] L. P. Gor'kov, *Microscopic derivation of the Ginzburg-Landau equations in the theory of superconductivity*, Sov. Phys. JETP **9**, 1364–1367 (1959).

[138] J. Schmalian, Lecture notes, nordita winter school 2018 in condensed matter physics. 2018.

[139] N. Goldenfeld, *Lectures on phase transitions and the renormalization group*. CRC Press, 2018.

[140] R. Fernandes, A. Chubukov, J. Knolle, I. Eremin and J. Schmalian, *Preemptive nematic order, pseudogap, and orbital order in the iron pnictides*, Physical Review B **85**, 024534 (2012).

[141] H. F. Jones, *Groups, representations and physics.* CRC Press, 1998.

[142] G. Katzer, *Character Tables for Point Groups used in Chemistry*. http://gernot-katzers-spice-pages.com/character_tables/index.html.

[143] L. Landau, *Theory of the superfluidity of helium II*, Physical Review **60**, 356 (1941).

[144] C. Bean and J. Livingston, *Surface barrier in type-II superconductors*, Physical Review Letters **12**, 14 (1964).

[145] L. Bulaevskii, M. Graf, C. Batista and V. Kogan, *Vortex-induced dissipation in narrow current-biased thin-film superconducting strips*, Physical Review B **83**, 144526 (2011).

[146] J. Pearl, *Current distribution in superconducting films carrying quantized fluxoids*, Applied Physics Letters **5**, 65 (1964).

[147] V. Gusynin, V. Loktev and I. Shovkovyi, *Toward a theory of superconductivity in two-dimensional systems with arbitrary carrier densities in an external magnetic field*, Journal of Experimental and Theoretical Physics **80**, 1111–1121 (1995).

# PART IV
# APPENDIX

## A Conventions

In this thesis we consider both the unit-less lattice operators $\hat{c}_i$ (with lattice-site $i$) and the field-operator $\hat{\psi}(\mathbf{r})$, where $\hat{\psi}^\dagger(\mathbf{r})|0\rangle = |\mathbf{r}\rangle$. These operators are related by $\hat{\psi}(\mathbf{r}_i) = \hat{c}_i/a^{d/2}$ where $a$ is the length of the unit-cell and $d$ the dimensionality. The momentum-space representation reads

$$\hat{c}_i = \frac{1}{\sqrt{N}} \sum_{\mathbf{k}} e^{i\mathbf{k}\mathbf{r}_i} \hat{c}_{\mathbf{k}}, \quad \hat{\psi}(\mathbf{r}) = \frac{1}{V} \sum_{\mathbf{k}} e^{i\mathbf{k}\mathbf{r}} \hat{\psi}_{\mathbf{k}} \tag{A.1}$$

where $V = Na^d$ is the system volume and $N$ the number of unit cells. This definition also implies $\hat{\psi}_{\mathbf{k}} = \sqrt{V}\hat{c}_{\mathbf{k}}$. Time-dependent operators is given by $\hat{c}(t) = e^{iHt}\hat{c}\,e^{-iHt}$. In imaginary time $t = -i\tau$ we use the Matsubara decomposition

$$\hat{\psi}(\tau) = \frac{1}{\beta} \sum_n e^{-i\omega_n \tau} \hat{\psi}_{i\omega_n} \tag{A.2}$$

with fermionic, $\omega_n = \frac{(2n+1)\pi}{\beta}$, and bosonic $\omega_n = \frac{2n\pi}{\beta}$ Matsubara frequencies respectively. We will move between the discrete sum by using

$$\frac{1}{V}\sum_{\mathbf{k}} = \int \frac{\mathrm{d}^d\mathbf{k}}{(2\pi)^d} = \int_{\mathbf{k}}, \quad \frac{1}{\beta}\sum_n = \int_{i\omega_n}. \tag{A.3}$$

It is also convenient to define the collective notation $k = (\mathbf{k}, i\omega_n)$. Correspondingly we infer $\delta_{k-k'} = \delta(\mathbf{k}-\mathbf{k}')\delta_{i\omega_n - i\omega_{n'}}$, $\delta_{i\omega_n - i\omega_{n'}} = \beta\delta_{n,n'}$ $\delta(\mathbf{k}-\mathbf{k}') = V\delta_{\mathbf{k},\mathbf{k}'}$.

### A.1 Functional determinants

Gaussian integrals over bosonic degrees of freedoms ($c_+$) takes the conventional form

$$\int \mathscr{D}c_+^* \mathscr{D}c_+ \, e^{-(c_+^* M c_+) - j^* c_+ - c_+ j} = \frac{e^{j^* M^{-1} j}}{\det M} \tag{A.4}$$

whereas an integral over fermionic degrees of freedoms ($c_-$) yields

$$\int \mathscr{D}c_-^*\mathscr{D}c_-\, e^{-(c_-^* M c_-)-j^* c_- - c_- j} = \det M\, e^{j^* M^{-1} j} \tag{A.5}$$

due to the anti-commuting property of the Grassman numbers $c_-$.

# B Hubbard-Stratonovich transformation

The Hubbard-Stratonovich transformation utilizes the identities (A.4). With $j$ being a second order in field (bosonic) term the left-hand side of (A.4) represents a decoupled action, which is second order in the field and readily diagonalizable in $c_+$.

Care must be taken when the sign of $M$ in (A.4) is negative, i.e. for repulsive interaction. In this case the integral is no longer convergent and we have to deform the contour for $c_+$ along the imaginary axis. That is, instead of utilizing the identity

$$e^{\frac{ax^2}{2}} = \sqrt{\frac{1}{2\pi a}} \int_{-\infty}^{\infty} e^{-\frac{y^2}{2a} - xy}\, \mathrm{d}y \tag{B.1}$$

we have to use

$$e^{-\frac{ax^2}{2}} = -i\sqrt{\frac{1}{2\pi a}} \int_{-i\infty}^{i\infty} e^{\frac{y^2}{2a} - xy}\, \mathrm{d}y\,. \tag{B.2}$$

Considering fluctuations in Chapter 10 (see footnote after (10.4)) we encountered a repulsive term. Optimizing the value of the action using the mean-field equation (10.7) implies a minimum of the action along the imaginary axis. However, for an analytic action, the mean-field solutions will be a maximum of the action with regard to real displacements of $\psi$.

# C Bogoliubov quasiparticles for a finite-momentum state

The mean-field Hamiltonian in (6.5) can be written

$$\begin{aligned}\hat{H}_{\mathrm{MF}} &= \sum_{\mathbf{k}\sigma} \xi(\mathbf{k}) \hat{c}^{\dagger}_{\mathbf{k}\sigma} \hat{c}_{\mathbf{k}\sigma} - \sum_{\mathbf{k}} \Delta_{\mathbf{q}} \hat{c}^{\dagger}_{\uparrow \mathbf{k}+\mathbf{q}/2} \hat{c}^{\dagger}_{\downarrow -\mathbf{k}+\mathbf{q}/2} + \\ &\sum_{\mathbf{k}} \Delta^{*}_{\mathbf{q}} \hat{c}_{\downarrow -\mathbf{k}+\mathbf{q}/2} \hat{c}_{\uparrow \mathbf{k}+\mathbf{q}/2} \\ &= \sum_{\mathbf{k}} E^{(-)}_{\mathbf{k}} \hat{\gamma}^{\dagger}_{\downarrow -\mathbf{k}} \hat{\gamma}_{\downarrow -\mathbf{k}} + E^{(+)}_{\mathbf{k}} \hat{\gamma}^{\dagger}_{\uparrow \mathbf{k}} \hat{\gamma}_{\uparrow \mathbf{k}} + \text{constant}.\end{aligned} \tag{C.1}$$

For notation see (6.8) and above. The fermionic operators $\gamma$ are the Bogoliubov quasiparticles for which

$$\begin{bmatrix} \hat{\gamma}^{\dagger}_{\downarrow -\mathbf{k}} \\ \hat{\gamma}_{\uparrow \mathbf{k}} \end{bmatrix} = \begin{bmatrix} v_{\mathbf{k}} & u_{\mathbf{k}} \\ u_{\mathbf{k}} & -v_{\mathbf{k}} \end{bmatrix} \begin{bmatrix} \hat{c}_{\uparrow \mathbf{k}+\mathbf{q}/2} \\ \hat{c}^{\dagger}_{\downarrow -\mathbf{k}+\mathbf{q}/2} \end{bmatrix}, \tag{C.2}$$

where

$$v_{\mathbf{k}} = \frac{1}{\sqrt{2}} \sqrt{1 - \frac{\epsilon_{+}(\mathbf{k})}{E_{\mathbf{k}}}}, \quad u_{\mathbf{k}} = \frac{1}{\sqrt{2}} \sqrt{1 + \frac{\epsilon_{+}(\mathbf{k})}{E_{\mathbf{k}}}}. \tag{C.3}$$

Note that for $\Delta \to 0, \mathbf{q} \to 0$

$$\hat{\gamma}^{\dagger}_{\uparrow \mathbf{k}} \to \begin{cases} \hat{c}^{\dagger}_{\uparrow \mathbf{k}} & \text{for } k > k_F \\ -\hat{c}_{\downarrow -\mathbf{k}} & \text{for } k < k_F \end{cases} \quad \hat{\gamma}^{\dagger}_{\downarrow -\mathbf{k}} \to \begin{cases} \hat{c}^{\dagger}_{\downarrow -\mathbf{k}} & \text{for } k > k_F \\ \hat{c}_{\uparrow \mathbf{k}} & \text{for } k < k_F \end{cases} \tag{C.4}$$

which means that the Bogoliubov quasiparticles behave as particles over the Fermi level, but as holes below, which explains why they are always associated with positive energy (relative to the ground state). The mean field ground state can be written

$$|GS\rangle = \prod_{\mathbf{k}} (u_{\mathbf{k}} + v_{\mathbf{k}} \hat{c}^{\dagger}_{\uparrow \mathbf{k}+\mathbf{q}/2} \hat{c}^{\dagger}_{\downarrow -\mathbf{k}+\mathbf{q}/2}) |0\rangle = \prod_{\mathbf{k}} \hat{\gamma}_{\uparrow \mathbf{k}} \hat{\gamma}_{\downarrow -\mathbf{k}} |0\rangle, \tag{C.5}$$

consistent with interpreting $\hat{\gamma}^{\dagger}$ as excitations.

# D Supercurrent and superflow

Dissipation is the result of a conversion of fluid kinetic energy to excitations. These excitations will, in turn, equilibrate with the surroundings (the lattice in the case of a superconductor), yielding a zero equilibrium flow.

In order to have a superflow, it is sufficient to require that no excitations occur spontaneously for some finite velocity $v$. This condition is referred to as the Landau criterion [143] which states that we have a stable superflow for velocities $v < v_c$ where $v_c$ is the Landau critical velocity defined by b

$$v_c = \min_{\mathbf{p}} \varepsilon(\mathbf{p})/\mathbf{p} \tag{D.1}$$

where $\epsilon(\mathbf{p})$ is the excitation spectra. One example which yields a finite $v_c$ is the roton-dispersion of Helium. For a fermionic system, superconductivity can remain above the critical velocity. This is due to the Pauli principle, which limits the available excitations. Thus for a superconductor, the current will be made up of two parts: one superfluid part and one back-propagating quasiparticle part.

## D.1 Supercurrents in superconductors, some phenomenology

In a charged superfluid, know as a superconductor, the above description (which describes the depairing current) is complemented with the fact that a magnetic field, which is generated by the current, suppresses the condensate. Therefore we expect that a charged superfluid could behave fundamentally differently. To quantify, in the charged superfluid, we have two lengths scales, the coherence length $\xi$ and the penetration depth $\lambda$, whereas we only have the coherence length for the uncharged fluid. The physics of the critical current will depend on the size of the sample $l$, compared to these two length-scales. Here we will consider some limiting behavior, assuming a type II superconductors, for which $\lambda \gtrsim \xi$.

**For small samples**, $l \ll \xi \lesssim \lambda$, where $l$ is the typical sample size the critical current will be given by the depairing current. $l \ll \lambda$ implies that the dynamics of the vector potential is frozen out, $\nabla \mathbf{A} = 0$, that is the sample is totally un-screened. Further $\xi \gg l$ means that magnitude variation of $\Delta$ is not favorable. From (2.2) we can then solve for the depairing current [92]

$$J_d = \frac{\phi_0}{3\sqrt{3}\pi\mu\lambda^2\xi} \tag{D.2}$$

where $\phi_0 = \frac{h}{2e}$ is the flux quantum.

**For large samples**, $\lambda \ll l$, the critical current will be determined by the induced magnetic field, which will penetrate the superconductor in the form of vortices. These vortices will drift, leading to dissipation (due to the interaction between the current and the magnetic field trapped in the vortex), unless they are pinned [92]. The critical current for a cylinder of radius $l$ equals the current that induces the lower critical field[1], $B_{c1}$, on the edge of the conductor [92]

$$B_{c1} = \mu \frac{J_{c1} l}{2}. \tag{D.3}$$

**For intermediate-sized samples** $\xi \ll l \ll \lambda$, the superconductor is sensitive to the formation of a vortex; however, it is still completely un-screened. It turns out that for $\xi \ll d_w \ll \lambda_P$, $d_t \sim \xi$ (with $d_w, d_t$ being the sample width and thickness) the onset of resistivity due to vortices is only slightly lower than the depairing current [145]

$$J_c = 0.83 J_d \tag{D.4}$$

and is caused by crossing of a single vortex.

**For thin samples**, $d_t \ll \lambda$, the penetration depth $\lambda$ should be replaced with the Pearl length $\lambda_P = \frac{2\lambda^2}{d_t}$ [146]. This results from constraining the current into a plane, while the electromagnetic field lives in 3D, which impedes the screening. In a pure 2D system, superconductivity only exits in a quasi long-range order sense, which is lost above the Kosterlitz–Thouless transition temperature, $T > T_{KT}$. This is due to the unbinding of vortex anti-vortex pairs. In these systems, resistivity occurs at any finite current [69].

Thus, even though the depairing current does not always yield the onset of resistance, it is still an essential property of a superconducting system, and it can be considered an upper estimate of the critical current. Further, for $J_c < J < J_d$, we expect superconducting correlations to exist still. In general, we expect the resistivity to increase above $J_c$, only to reach normal values at $J_d$.

[1]The vortex-interaction with the edges (zero current through surface yields attracting anti-vortex) delays the penetration of a vortex due to the so-called Bean-Livingston barrier [144], $B_b > B_{c1}$.

# E Bosonic occupation number

The bosonic occupation number can be written as

$$n_{\mathrm{B}} = -\mathrm{Tr}\, K \qquad K(z) = \frac{\partial}{\partial \mu} \ln(-L(z)). \tag{E.1}$$

Since $L$ is non-analytic (in $z$) along extended parts of the real axis we utilize the contour shown in Figure 1 to perform the Matsubara sum part of the Trace in (E.1)

$$\frac{1}{\beta} \sum_{i\Omega} K(i\Omega) = \frac{K(0)}{\beta} + \frac{1}{2\pi i} \int\limits_{C_1+C_2+\gamma_1+\gamma_2} f_B(z) K(z) \tag{E.2}$$

where $f_B(z) = \frac{1}{e^{\beta z}-1}$ is the Bose-Einstein distribution. ($K(z)$ is continuous at $z = 0$, which is guaranteed by the stability constraint: $\mathrm{Re}(-L^{-1}(\mathbf{k},0)) > 0, \mathrm{Im}(L^{-1}(\mathbf{k},0)) = 0$ [116, 147].) The contour does not include $i\Omega = 0$ so we have included it explicitly. After remembering the convergence factor[2] $e^{i\Omega 0^+}$ we conclude that the contours $C_1, C_2$ vanish. We proceed with calculating $\gamma_{1,2}$ by evaluating the integrand just above and below the real axis

$$\begin{aligned} &\frac{1}{\beta} \sum_{i\Omega} K(i\Omega) = \frac{K(0)}{\beta} + \\ &\frac{1}{2\pi i} \int\limits_{-\infty}^{\infty} \mathrm{d}x \left( f_B(x+i\eta) K(x+i\eta) - f_B(x-i\eta) K(x-i\eta) \right). \end{aligned} \tag{E.3}$$

Further, $f_B(z)$ is analytic across the real axis besides at $z = 0$ where the integral picks up a residue, which cancels the leading $K(0)/\beta$ term

$$\frac{1}{\beta} \sum_{i\Omega} K(i\Omega) = \frac{\mathscr{P}}{2\pi i} \int\limits_{-\infty}^{\infty} \mathrm{d}\omega\, f_B(\omega) \left( K(\omega + i0^+) - K(\omega - i0^+) \right). \tag{E.4}$$

The imaginary part of $L^{-1}$ jumps across the non-analytic regions of the real

[2] This can be seen as a residual factor coming from the time-ordering of the repeated insertion of the resolution of identity at different times in the coherent state path-integral. Basically, this corresponds to the normal ordering of operators, meaning that we are counting the number of particles, rather than antiparticles.

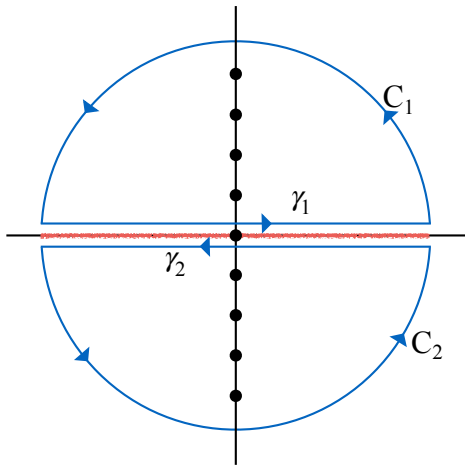


**Figure 1:** Contour used to evaluate (E.2).

axis, which yields a rather complicated behavior of $K^+ - K^-$. In the weak-coupling limit, $\mu = \varepsilon_F$ this quantity is small because of the vanishing effective mass $m_\mathrm{p}$. However, in the strong coupling limit, $\mu \to -E_b/2$, the branch cut and pole become increasingly separated. Thus, the low energy physics is well described by only keeping the, now freely propagating, bound state and (E.1) takes the form (see (7.11))

$$n_\mathrm{B} = -\frac{1}{\kappa}\frac{\partial r}{\partial \mu}\int_\mathbf{q} \frac{1}{\exp\left(\frac{q^2}{2m_\mathrm{p}}\right)-1} = 2\int_\mathbf{q} \frac{1}{\exp\left(\frac{q^2}{2m_\mathrm{p}}\right)-1} \tag{E.5}$$

which is the stated expression in (7.12).

# F Landau quantization — cyclotron orbits

Aligning a magnetic field in the (out-of plane) $z$-direction, particles follows the Landau solutions for cyclotron orbits. Using the Landau gauge $\mathbf{A} = (0, Bx, 0)$ the Hamiltonian in (8.12) can be diagonalized using $\varphi_{k_y,k_z,n}(\mathbf{x}) = e^{ik_z z}e^{ik_y y}f_n(x)$, for which the eigenvalue equation reads

$$\varepsilon_n(k_y,k_z)f_n(x) = \left(a\epsilon + \left[\frac{\hbar^2 k_z^2}{2m_{\mathrm{p},z}} + \frac{\hbar^2}{2m_{\mathrm{p},x}}\left(-\partial_x^2 + \frac{m_{\mathrm{p},x}^2\omega_c^2}{\hbar^2}(\hat{x}-x_0)^2\right)\right]\right)f_n(x). \tag{F.1}$$

Here we introduced $x_0 = \frac{\hbar k_y}{e^* B}$, and the cyclotron frequency $\omega_c = \frac{|e^* B|}{\sqrt{m_{\mathrm{p},x} m_{\mathrm{p},y}}}$. The residual part of the eigenfunctions, $f_n(x)$, are Hermite polynomials with eigenvalues $\hbar\omega_c(n+1/2)$. Thus,

$$\varepsilon_n(k_y, k_z) = \eta\epsilon + \frac{\hbar^2 k_z^2}{2m_{\mathrm{p},z}} + \hbar\omega_c(n+1/2)\,. \tag{F.2}$$

The energies are degenerate in $k_y = m\frac{2\pi}{L_y}$ where $m = 0, \pm 1, \pm 2...$ Thus $\Delta k_y = \frac{2\pi}{L_y}$ and $\Delta x_0 = \frac{\hbar}{e^* B}\Delta k_y$. The number of states that fits in $L_x$ is therefore

$$N_{\mathrm{Lan.}} = \frac{L_x}{\Delta x_0} = \frac{L_x L_y |e\,B|}{\pi\hbar}\,. \tag{F.3}$$

To express the current operator in the Landau basis we need the matrix elements of the kinetic momenta $\hat{\pi}_x = \hbar\hat{k}_x$ and $\hat{\pi}_y = \hbar\hat{k}_y - e^* B\hat{x}$, which are diagonal in $k_y, k_z$, but off-diagonal in the Landau basis. Using the ladder operators $\hat{x} - x_0 = \sqrt{\frac{\hbar}{2\omega_c m_{\mathrm{p},x}}}(a^\dagger + a)$, $\hbar\hat{k}_x = i\sqrt{\frac{\hbar\omega_c m_{\mathrm{p},x}}{2}}(a^\dagger - a)$ we find

$$\langle n'|\hat{\pi}_i|n\rangle = \begin{cases} i\sqrt{\frac{\hbar m_{\mathrm{p},x}\omega_c}{2}}(\sqrt{n+1}\delta_{n',n+1} - \sqrt{n}\delta_{n',n-1}) & i = x \\ \mathrm{sign}(B)\sqrt{\frac{\hbar m_{\mathrm{p},y}\omega_c}{2}}(\sqrt{n+1}\delta_{n',n+1} + \sqrt{n}\delta_{n',n-1}) & i = y\,. \end{cases} \tag{F.4}$$

## F.1 Landau-sums and the Digamma function

In (8.22) we considered the sum

$$\sum_{n=0} \frac{(n+1)(\varepsilon_{n+1} + \varepsilon_n)}{\varepsilon_n \varepsilon_{n+1} |\gamma\varepsilon_n + \gamma^* \varepsilon_{n+1}|^2} \tag{F.5}$$

by expanding in the imaginary part of $\gamma = \gamma' + i\gamma''$

$$\begin{aligned} &\frac{(\varepsilon_{n+1} + \varepsilon_n)}{\varepsilon_n \varepsilon_{n+1} |\gamma\varepsilon_n + \gamma^* \varepsilon_{n+1}|^2} = \frac{1}{\gamma'^2} \frac{1}{\varepsilon_n \varepsilon_{n+1}(\varepsilon_n + \varepsilon_{n+1})} \\ &- \frac{\gamma''^2}{\gamma'^4} \frac{(\varepsilon_n - \varepsilon_{n+1})^2}{\varepsilon_n \epsilon_{n+1}(\varepsilon_n + \varepsilon_{n+1})^3} + \mathcal{O}(\gamma''^4/\gamma'^4). \end{aligned} \tag{F.6}$$

The sum (F.5) can be evaluated in terms of the Digamma function, $\psi$, defined as the logarithmic derivative of the Gamma function. Expressed as an infinite sum

$$\psi(z) = -\gamma_{EM} + \sum_{n=0} \frac{z-1}{(n+1)(n+z)}\,, \tag{F.7}$$

where $\gamma_{EM}$ is the Euler–Mascheroni constant. This definition, together with the recurrence-relation $\psi(1+z)=\psi(z)+1/z$, can be used to perform the sum

$$\begin{aligned}
&\sum_{n=0}\frac{(n+1)(\varepsilon_{n+1}+\varepsilon_n)}{\varepsilon_n\varepsilon_{n+1}|\gamma\varepsilon_n+\gamma^*\varepsilon_{n+1}|^2}=\frac{2}{\gamma'^2\hbar^2\omega_c^2\eta\epsilon}\left(F_1\left(\frac{\epsilon}{2b}\right)-\upsilon^2F_2\left(\frac{\epsilon}{2b}\right)\right)+\mathcal{O}(\upsilon^4)\\
&F_1(x)=x^2\left(\psi\left(x+\frac{1}{2}\right)-\psi(x)-\frac{1}{2x}\right)\\
&F_2(x)=F_1(x)-\frac{2x\psi'(x)+x^2\psi''(x))}{8}
\end{aligned}\tag{F.8}$$

where $\upsilon=\gamma''/\gamma'$, $b=\frac{\hbar\omega_c}{2\eta}=B/B_{c2}$ with the upper critical field $B_{c2}=\frac{\hbar}{2e\xi_{0,x}\xi_{0,y}}$, $\xi_{0,(x,y)}=\frac{\hbar^2}{2m_{\mathrm{p},(x,y)}\eta}$.